Layer, cell-type and pathway-specific thalamocortical input to mouse somatosensory cortex

THÈSE N^{O} 9064 (2018)

PRÉSENTÉE LE 30 NOVEMBRE 2018

À LA FACULTÉ DES SCIENCES DE LA VIE

LABORATOIRE DE TRAITEMENT SENSORIEL

PROGRAMME DOCTORAL EN NEUROSCIENCES

ÉCOLE POLYTECHNIQUE FÉDÉRALE DE LAUSANNE

POUR L'OBTENTION DU GRADE DE DOCTEUR ÈS SCIENCES

PAR

Berat Semihcan SERMET

acceptée sur proposition du jury:

Prof. J. Gräff, président du jury
Prof. C. Petersen, directeur de thèse
Prof. D. Jabaudon, rapporteur
Prof. T. Karayannis, rapporteur
Dr G. Knott, rapporteur

ÉCOLE POLYTECHNIQUE
FÉDÉRALE DE LAUSANNE

Suisse
2018

Acknowledgements

First, I would like to thank my thesis supervisor, Prof. Carl Petersen. He gave me the opportunity to conduct a very exciting study in this scientifically stimulating atmosphere. I had the rewarding experience of performing challanging experiments while learning about the brain and neuroscience through those years. His passion and enthusiasm about science always kept me motivated to finish my PhD and continue my career in science.

Over the last 5 years, I was incredibly lucky to be in this highly multicultural place full of great scientists and individuals. Years with ups and downs, they made life easier and fun for me, both inside and outside of the lab. Therefore, I cannot thank enough to: Matthieu Auffret, Aaron Clarke, Sylvain Crochet, Berat Denizdurduran, Marie Eve Didier, Vahid Esmaeili, Célia Gasselin, Xander Houbert, Damien Huzard, Alexandros Kyriakatos, Marc Lauffs, Pierre Le Merre, Anastasiia Oryshchuk, Matt Pachai, Janir Ramos, Albulena Shaqiri, Miguel Sison, Jane Yi and Evi Zdrali.

I would especially like to thank two very talented individuals: Johannes M. Mayrhofer and Sami El-Boustani, who heavily contributed to this PhD work. I learned a lot from them about research and scientific thinking, and without their help, this work would not have been possible.

I would then like to thank my PhD Thesis examiners, Prof. Denis Jabaudon, Prof. Theofanis Karayannis and Prof. Graham Knott for their valuable and detailed feedback as well as Prof. Johannes Gräff, president of the jury committee.

Finally, I would like to thank my family, my brother Orcun and my parents, Aysu and Haldun, who always supported me no matter what. They were the ones who gave me the vision to continue my life doing science, even though it was not really supported where I grow up. I am really grateful for their constant support and care for my happiness both good and bad times.

Abstract

In the mouse whisker system, sensory information is relayed to the whisker somatosensory cortex by two major thalamic nuclei, the ventral posterior medial nucleus (VPM) and the posterior medial nucleus (POM). While the cortical axonal innervation pattern of these two nuclei has been studied anatomically in some detail, their synaptic input to distinct cell-types across different layers in barrel cortex is incompletely understood. I used the specificity of optogenetics to selectively stimulate axons from VPM or POM, and I measured the evoked excitatory postsynaptic potentials *in vitro* with whole-cell patch-clamp recordings in primary whisker somatosensory cortex (wS1). VPM or POM was infected *in vivo* with an adenoassociated virus (AAV) encoding the light-gated cation channel channelrhodopsin (ChR2). Synaptic input onto individual neurons of the barrel cortex was recorded in brain slices *in vitro* by activating the ChR2-expressing thalamic axons with blue light. I measured thalamic inputs onto excitatory and three distinct classes of GABAergic neurons, expressing Parvalbumin (PV), somatostatin (SST) or vasoactive intestinal peptide (VIP) neurons across all layers of the barrel cortex. In excitatory and PV neurons, I found that the biggest inputs appeared to largely colocalize with the anatomical innervation pattern Anatomically, VPM preferentially innervates layer4 (L4), deep L3 and the L5B/6A border, and, functionally, we found that the biggest input was observed in L4, followed by L3. Anatomically, POM innervates L5A and L1, and, functionally, I found the biggest input in L5A. SST neurons received very weak input from both thalamic nuclei. VIP neurons on the other hand received larger inputs than SST neurons, however, they were weaker than excitatory and PV neurons.

POM is considered to have both first-order and higher-order properties and I therefore began to investigate connectivity within sub-parts of POM. Taking advantage of a recently developed anterograde transsynaptic AAV injected into somatosensory brainstem nuclei, I defined first-order and higher-order sub-nuclei

of POM and investigated their functional connectivity with somatosensory cortex. Anatomically, first-order POM preferentially innervates L4 of secondary somatosensory cortex (wS2) and functionally, I found that neurons across many layers in wS2 received direct synaptic input from first-order POM. Higher-order POM innervates both wS2 and wS1, and I found that neurons in wS2 also receive direct synaptic input. The data suggest that first-order POM relays sensory information to wS2, apparently in a parallel signaling pathway to the classical VPM to wS1 sensory pathway. In contrast, higher order POM does not appear to receive direct sensory input from the brainstem

Our results begin to provide a more complete understanding of the distribution of thalamic input to specific cell-types across the layers of the mouse somatosensory cortex

Keywords

Optogenetics, Channelrhodopsin-2, adeno associated virus, whisker somatosensory cortex, thalamus, ventral posterior medial nucleus, posterior medial nucleus, postsynaptic potential, membrane potential

Résumé

Dans le système sensoriel des vibrisses de la souris, les informations sensorielles sont transmises au cortex somatosensoriel à tonneaux par deux noyaux thalamiques majeurs : le noyau médian ventral postérieur (VPM) et le noyau médian postérieur (POM). Si l'organisation anatomique de l'innervation corticale par ces deux noyaux a été étudiée en détail, leur contribution fonctionnelle à l'activité synaptique des différents types cellulaires localisés dans les diverses couches du cortex sensoriel à tonneaux reste incomprise. Durant ma thèse, j'ai utilisé la spécificité de l'optogénétique pour stimuler sélectivement les axones de VPM ou de POM et mesurer en retour les potentiels postsynaptiques excitateurs évoqués, grâce à des enregistrements de cellules en patch-clamp configuration entière dans le cortex somatosensoriel primaire (wS1) *in vitro*. VPM ou POM ont été infectés *in vivo* par un virus adéno-associé (AAV) codant pour la *canal-rhodopsine* 2 (ChR2), un canal cationique activé par la lumière. Les entrées synaptiques sur les neurones du cortex à tonneaux ont été enregistrées dans des tranches de cerveau *in vitro* en activant avec de la lumière bleue les axones thalamiques exprimant ChR2. J'ai alors mesuré les apports thalamiques sur les neurones excitateurs ainsi que sur trois classes distinctes de neurones GABAergiques exprimant respectivement la parvalbumine (PV), la somatostatine (SST) et le peptide vasoactif intestinal (VIP), dans toutes les couches du cortex. Dans les neurones excitateurs et PV, j'ai constaté que les entrées synaptiques les plus importantes semblaient en grande partie co-localiser avec le schéma anatomique d'innervation. En effet, anatomiquement, VPM innerve préférentiellement la couche 4 (L4), la L3 profonde et la frontière L5B / 6A, et fonctionnellement, les plus fortes réponses sont observées dans L4, suivi de L3. Du point de vue anatomique, POM innerve L5A et L1, fonctionnellement, j'ai pu enregistrer la plus grande réponse dans L5A. Les neurones SST reçoivent une très faible contribution des deux noyaux thalamiques. Les neurones VIP, quant à eux, reçoivent des entrées synaptiques plus importantes que les neurones SST, mais plus faibles que les neurones excitateurs et PV.

POM étant considéré comme ayant à la fois des propriétés de premier ordre et d'ordre supérieur, et j'ai commencé à étudier la connectivité des sous-parties de POM. Grâce à un AAV trans-synaptique antérograde récemment développé injecté dans des noyaux somatosensoriels du tronc cérébral, j'ai défini les sous-noyaux de POM de premier ordre et d'ordre supérieur et étudié leur connectivité fonctionnelle avec le cortex somatosensoriel. Du point de vue anatomique, le noyau du premier ordre de POM innerve de manière préférentielle la couche 4 du cortex somatosensoriel secondaire (wS2). Cependant, fonctionnellement, j'ai trouvé que les neurones de nombreuses couches de wS2 reçoivent une entrée synaptique directe du noyau du premier ordre de POM. Le noyau d'ordre supérieur de POM innerve à la fois wS2 et wS1, et j'ai constaté que les neurones de wS2 reçoivent également une entrée synaptique directe. Les données suggèrent que le noyau du premier ordre de POM relaie les informations sensorielles au WS2 dans une voie de signalisation parallèle à la voie sensorielle classique du VPM au WS1. En revanche, le noyau d'ordre supérieur de POM ne semble pas recevoir d'entrée sensorielle directe du tronc cérébral.

Nos résultats commencent à fournir une compréhension plus complète de la distribution des entrées thalamiques sur des types cellulaires spécifiques à travers les différentes couches du cortex somatosensoriel de la souris.

Mots-clés

Optogénétique, Channelrhodopsin-2, virus adéno-associé, cortex somatosensoriel des vibrisses, thalamus, noyau médial postérieur ventral, noyau médial postérieur, potentiel postsynaptique, potentiel membranaire

Contents

Chapter 1:

Introduction

We all perceive our world through gathering sensory information and making sense of it with our brains. We look around and see objects. We listen and hear sounds. We smell, we touch and we taste. These senses are collected by our sensory organs and relayed to our brain where everything is interpreted to create our perceived reality. Sensory perception is an active process. We actively gather sensory information with our sensors and the neuronal activity in our brains actively generates our sensory percepts. Since sensory percepts are internal constructs, they are subjective. The same sensory stimulus could be interpreted very differently by different individuals. In the case of some perceptual disorders, the outside world can be interpreted wrongly as an altered reality; therefore it is important to understand the underlying physical nature of sensation and perception.

Our sensory systems collect the peripheral sensory information and bring it ultimately to the neocortex. The neocortex is a complicated neuronal structure mainly responsible for higher brain functions such as sensory perception, learning and cognition (Lui et al., 2011; Herculano-Houzel, 2009; Rakic, 2009). Understanding the genuine function of the neocortex in perception is still a challenging issue. Investigating how neocortical circuits are involved in sensory signal processing can help address this issue by relating structure to function.

If the sensory percepts are mostly generated in the neocortex, it is important to know how the sensory information is relayed into it. As we mentioned, the neocortex is a complicated structure. It has specialized parts dedicated to different functions organized in anatomically and functionally distinct horizontal layers and vertical columns. These different parts consist of individual neurons which can also be subdivided according to their anatomy and function. Given this complicated structure of the neocortex, it is likely that sensory information must arrive in a very organized manner to be able to drive appropriate activity of this network of neurons and generate reasonable percepts.

From the periphery, sensory information reaches to the neocortex in several steps. For most of the sensory systems, the last stop for the sensory information before the neocortex is the thalamus. Thalamus is an egg-like structure in the middle of the brain and almost all of the neocortex is connected to it. Almost everything the neocortex knows about the outside world is through the thalamus. It is thus crucial

to know how sensory information relayed through the thalamus, in order to understand how sensory perception works.

The mouse whisker system is a useful system to study sensory processing. It has a very well-defined structure with its precise somatotopy in the neocortex. Sensory information collected by the whiskers reach ultimately the somatosensory cortex. There are two main stops until this information reaches to the cortex; first it arrives at the brain stem, and then to the thalamus and finally, it reaches to the cortex. This information transfer occurs via synapses and thalamus makes synapses with cortical neurons differently depending on the location and the type of its targets. In this thesis, we will explore how these thalamocortical inputs are distributed across different cell types in different locations of the mouse whisker somatosensory cortex. In the second chapter, we will map the distribution of inputs from the two main thalamic nuclei feeding the primary somatosensory barrel cortex (wS1). Then in the third chapter, we will further sub-divide these thalamic nuclei depending on their function and investigate their inputs to wS1 and the secondary somatosensory barrel cortex (wS2).

Sensory processing in the whisker system

The whisker system in rodents is a part of the somatosensory system. This system is responsible for relaying the tactile information from the external world to the brain and make sense out of it to create a reasonable percept for the animal. For the rodents, whiskers are really important to have a good understanding of their immediate surroundings. Rats and mice are nocturnal animals. In the dark, they use their whiskers to navigate, localize objects, identify surface textures (Hutson and Masterton, 1986; Gao et al., 2001; Chen et al., 2013). Whiskers of rodents are simply hairs attached to their snouts, working as tactile detectors. They "whisk" to scan the environment, moving their whiskers back and forth at 10 – 20 Hz (Gao et al., 2001; Berg and Kleinfeld, 2003).

When a whisker touches an object, the mechanogated ion channels located in the nerve endings that surround the base of the whisker follicle opens. Activation of these mechanogated ion channels causes a depolarization in the connected ganglion neurons which ultimately fire action potentials. Ganglion neurons relay this whisker information to the trigeminal nuclei of the brain stem. There are four trigeminal nuclei and three of them (nucleus principalis (PrV), interpolaris (SpVi) and caudalis (SpVc)) are organized in a way that vibrissal array is well represented in a structure called "barrelettes" (Veinante and Deschênes, 1999). Brain stem then sends the sensory information to the thalamus.

In a more simplified view, whisker somatosensory cortex is mainly driven by two pathways provided by PrV and SpVi. PrV driven pathway is called the lemniscal pathway and SpVi driven pathway is called the paralemniscal pathway (Figure 1.1). The lemniscal pathway innervates the ventral posterior medial nucleus of the thalamus (VPM). Similar to the well-organized barrelette structure of PrV, VPM also has a somatotopic representation of the whiskers in structures called "barreloids". The paralemniscal pathway, on the other hand, innervates the posterior medial nucleus of the thalamus (POM). Compared to VPM, POM has no anatomically well-defined structures like barreloids, however, there is a rough representation of whiskers with broader receptive fields (Diamond et al., 1992). VPM neurons innervate primary whisker somatosensory cortex (wS1). Like PrV and VPM, wS1 also has anatomically well-defined structures representing the vibrissae called

"barrels" (Woolsey and Van der Loos, 1970). VPM afferents mainly innervate those barrels in layer 4 and the layer 5B/6 border of wS1 (Killackey and Leshin, 1975; Pierret et al., 2000; Meyer et al., 2010). POM neurons innervate wS1 and secondary whisker somatosensory cortex (wS2). These afferents target L5A and L1 of wS1 and L5A, L4 and L1 of wS2 (Killackey and Leshin, 1975; Pierret et al., 2000; Meyer et al., 2010; Pouchelon et al., 2014). VPM neurons respond to whisker stimulation very reliably with short synaptic delays (Simons and Carvell, 1989; Diamond et al., 1992; Ahissar et al., 2001; Brecht and Sakmann, 2002). On the other hand, POM neurons respond to whisker stimulation in a weaker and more delayed manner (Diamond et al., 1992) due to their less precise somatotopy compared to VPM.

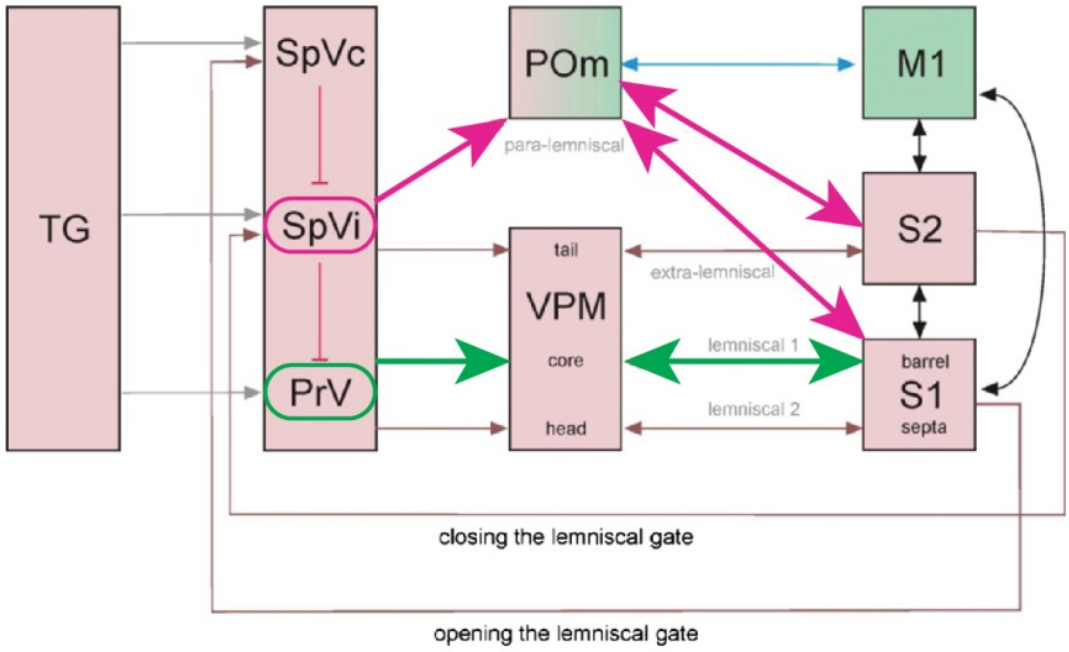

Figure 1.1 Lemniscal and paralemniscal sensory pathways of the mouse whisker system. Schematic showing the two main sensory pathways of the mouse whisker system. The sensory pathways starts with the trigeminal ganglion (TG) neurons bringing whisker sensory information to the brain stem trigeminal nuclei. The lemniscal pathway originates in PrV (circled in green) barrelettes and projects to VPM barreloids and ultimately to wS1. Paralemniscal pathway originates in SpVi (circled in magenta) and projects to POM and ultimately to wS1 and wS2. Green and magenta colors indicate lemniscal and paralemniscal pathways respectively (adapted from Feldmeyer et al., 2013).

The sensory information from the periphery enters the somatosensory cortex at multiple locations. In wS1, where the cortical sensory processing starts (Ferezou et al., 2007), single whisker information arrives mainly in L4 and L5/6 via lemniscal pathway (Constantinople and Bruno, 2013). VPM axons in L4 mainly target spiny stellate neurons (Brecht and Sakmann, 2002; Staiger et al., 2004). These spiny stellate neurons innervate and target L2/3 pyramidal neurons (Petersen and Sakmann, 2001; Lefort et al., 2009). Information from L2/3 pyramidal neurons spread to L5A, L5B and superficial L6 (Feldmeyer et al., 2005; Lefort et al., 2009). This activation is not restricted in a single column. There are neurons in specific layers that could transfer sensory information across neighboring barrel columns. Pyramidal neurons in L2/3 mainly and L5, innervate other columns horizontally in the same layer (Larsen and Callaway, 2006; Bruno et al., 2009; Adesnik and Scanziani, 2010) and can activate them in order to integrate the multi-whisker information.

The sensory information in the barrel field then travels to different cortices. L2/3 pyramidal neurons, send long-range projections to wS2 and primary motor cortex (wM1) and also to contralateral wS1 (Petreanu et al., 2007; Aronoff et al., 2010; Chen et al., 2013; Yamashita et al., 2013, 2018). L5A slender-tufted pyramidal neurons also send projections to wS2 and wM1 (Mao et al., 2011). Besides being connected to different cortices, these L5A neurons send projections to the dorsal striatum (Mercier et al., 1990; Wright et al., 1999; Sippy et al., 2015). L5B pyramidal neurons target subcortical regions. They project the to trigeminal nucleus, the superior colliculus, the pons and POM (Welker et al., 1988; Mercier et al., 1990; Bourassa et al., 1995; Wright et al., 1999; Larsen et al., 2007). L6 neurons target mainly other cortical regions or sensory thalamus. Superficial L6 neurons send projections to both VPM and POM and also the reticular nucleus of the thalamus (TRN) (Bourassa et al., 1995; Landisman and Connors, 2007; Kim et al., 2014). Deep L6 neurons on the other hand, send projections to POM (Killackey and Sherman, 2003; Hoerder-Suabedissen et al., 2018).

Cell types of the somatosensory cortex

As we mentioned, the neocortex is a complicated structure divided into different parts anatomically and functionally. These different parts contain different types of neurons with distinct electrical properties, morphologies, and function.

The neuronal population in the neocortex consists of two main groups: glutamatergic excitatory neurons and GABAergic inhibitory neurons. Excitatory neurons comprise approximately 85% of the neuronal population whereas GABAergic neurons make up ~15% (DeFelipe et al., 2002; Lefort et al., 2009). All cortical areas show a layer structured appearance that is caused by the organized clustering of different type of excitatory and inhibitory neurons.

The excitatory neurons use glutamate as their neurotransmitter and they can be classified into different subtypes based on their locations in different layers (Figure 1.2). Every layer contains pyramidal neurons, however, only in L4 of wS1 there are two additional cell types in contrast to other layers; spiny stellate neurons and star pyramids (Staiger et al., 2004). L2/3 neurons form cortico-cortical connections in ipsi and contralateral hemispheres. L4 spiny stellate neurons project locally within the cortical column. L6 neurons mostly project to thalamus and L5 neurons project to other cortices, basal ganglia, midbrain, hindbrain and spinal cord.

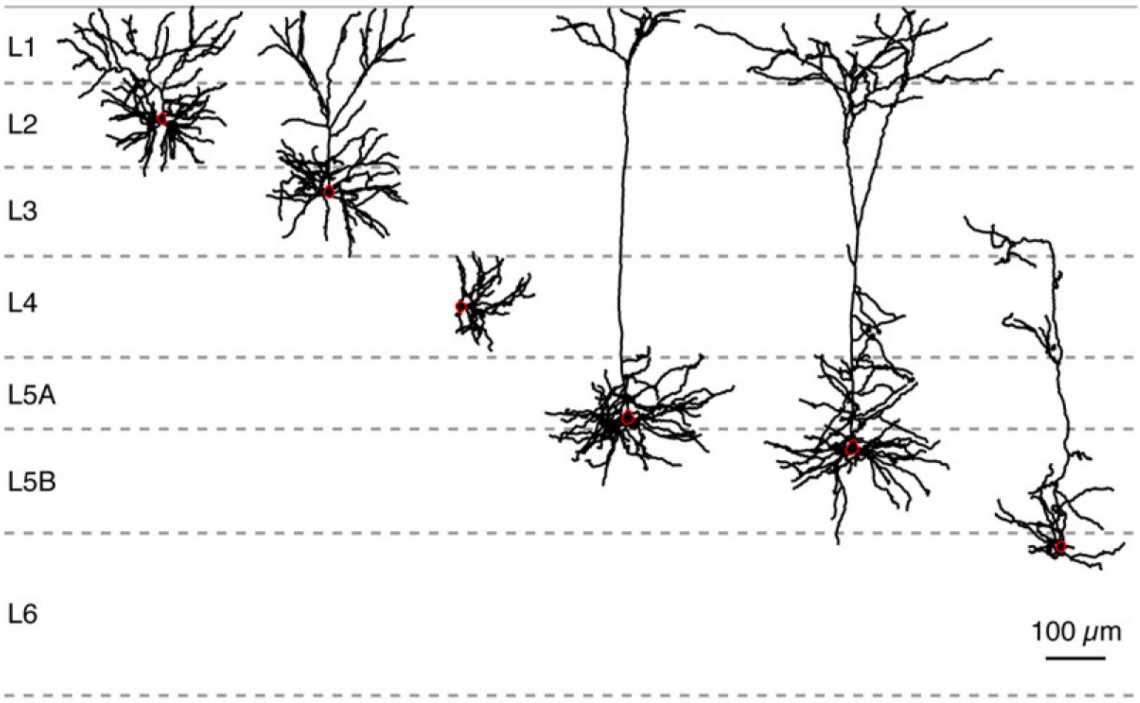

Figure 1.2 Excitatory neuron morphologies of the mouse wS1. Digitally reconstructed excitatory neurons demonstrating different somato-dendritic morphologies across layers of wS1 (from Lefort et al., 2009)

The inhibitory GABAergic population of the neocortex is much sparser than the excitatory population; however, they are highly diverse. This high diversity has made inhibitory neuron classification quite complicated. Every layer of the somatosensory cortex contains inhibitory neurons, and they are classified based on their morphology, electrophysiological properties, and their gene expression patterns (Cauli et al., 1997; Burkhalter, 2008; Gentet, 2012).

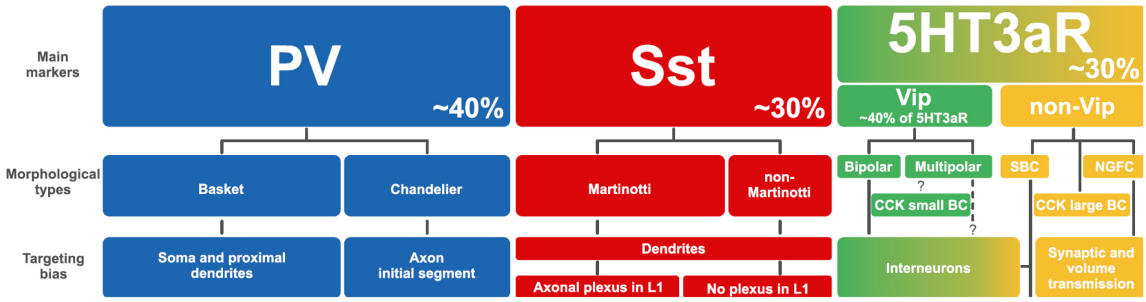

Figure 1.3 Inhibitory neuron classification based on their gene expression, morphology and targets in the neocortex (Tremblay et al., 2016)

Almost all neocortical interneurons express one of the main three largely-non-overlapping markers: parvalbumin (PV), somatostatin (SST) and the ionotropic serotonin receptor 5HT3a (5HT3aR) (Rudy et al., 2011; Tremblay et al., 2016). The inhibitory neuron population can be sub-divided based on these marker expressions (Figure 1.3).

PV neurons make up approximately 40% of the cortical GABAergic population (Tremblay et al., 2016). Consisting of morphologically distinct basket and chandelier cells, PV cells strongly inhibit one another and also excitatory neurons (Packer and Yuste, 2011; Pfeffer et al., 2013), making GABAergic synapses with the perisomatic region of postsynaptic pyramidal cells (Chattopadhyaya et al., 2004). They exhibit a very characteristic fast-spiking behavior.

SST neurons make up around 30% of GABAergic population and they consist of morphologically different Martinotti and non-Martinotti cells (Tremblay et al., 2016). These neurons typically target distal dendrites of excitatory neurons for inhibition (Wang et al., 2004; Fino and Yuste, 2011). Martinotti cells send axons to L1 which branch out horizontally, inhibiting distal dendrites of pyramidal neurons. Non-Martinotti cells, on the other hand, have more local axonal arborizations.

As the third class or inhibitory neurons, 5HT3aR neurons accounting for approximately 30% of the GABAergic neurons (Tremblay et al., 2016). These cells show higher diversity than PV and SST neuron populations. A subset of this group (~40%) is vasointestinal peptide (VIP) expressing cells which comprises nearly half of 5HT3aR population (Lee et al., 2010). Morphologically, VIP neurons are divided as

bipolar and multipolar cells (Prönneke et al., 2015). These cells mainly target SST expressing neurons (Pfeffer et al., 2013). Since SST neurons inhibit pyramidal neurons, inhibition of SST neurons via VIP neurons can cause disinhibition in the cortical network.

First-order and higher-order thalamic input somatosensory cortex

As mentioned, VPM and POM are the two main sensory input sources to the somatosensory cortex. As considered to be the main sensory input to wS1, VPM is a first-order thalamic nucleus which is driven mainly by the periphery and relays that information to wS1 (Diamond et al., 1992). It innervates strongly wS1 at L4 and the L5B/6 border (Figure 1.4) and receives cortical feedback only from wS1. On the other hand, POM is driven by the periphery as well as the cortical feedbacks from both sensory and motor areas (Diamond et al., 1992; Groh et al., 2014; Urbain et al., 2015). POM innervates wS1 at L5A and L1 (Figure 1.4) and wS2 at L4 and L1 (Pouchelon et al., 2014). POM neurons have broadly tuned receptive fields in contrast to the sharp tuning of VPM (Diamond et al., 1992). Receiving sensory input with cortical feedback from multiple areas suggest that POM could be a higher-order thalamic nucleus, processing contextual information and modulating sensory input to the cortex. Both of these nuclei innervate specific layers of the somatosensory cortex and drive different networks (Bruno and Simons, 2002; Bruno and Sakmann, 2006; Petreanu et al., 2009; Cruikshank et al., 2007, 2010; Constantinople and Bruno, 2013; Audette et al., 2018), however, how distinct cell-types in different cortical layers are affected by these inputs is not completely understood. In the thesis, we will take advantage of optogenetics to investigate the inputs from these two nuclei to somatosensory cortex separately.

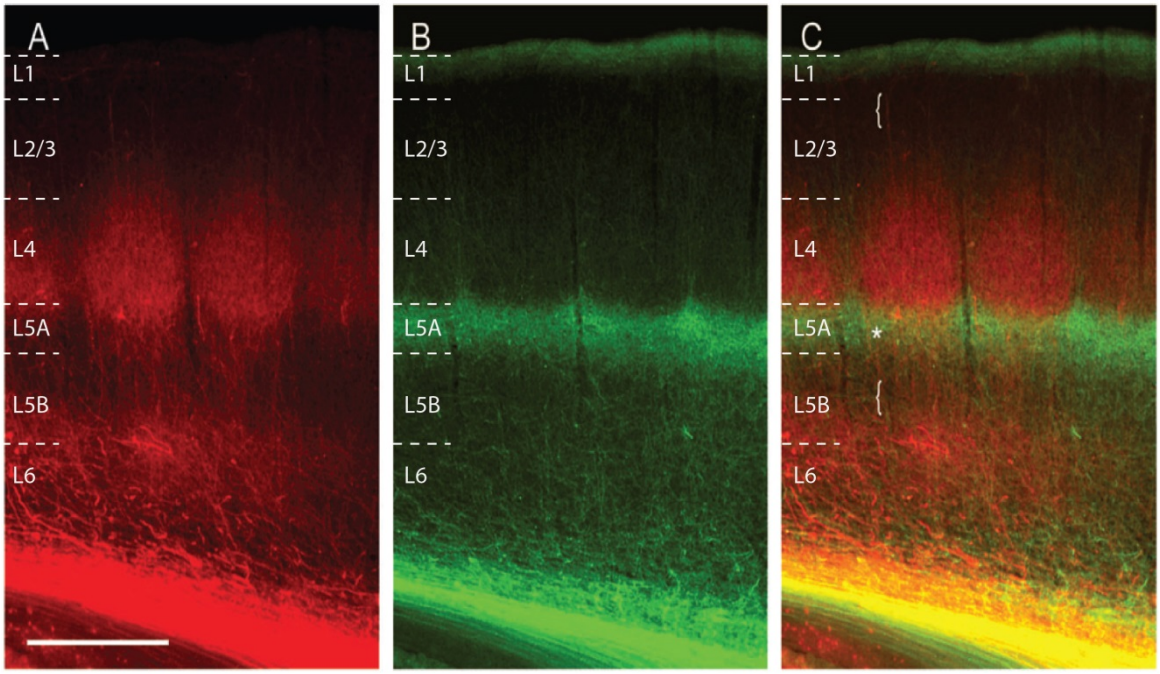

Figure 1.4 Visualization of VPM and POM innervations in rat wS1 (A) VPM afferents innervating mainly L4 and the border of L5B/6 of wS1 (red). **(B)** POM afferents innvervating mainly L5A and L1 of wS1 (green) **(C)** Merge of A and B illustrating complementary innervation of VPM and POM. (adapted from Wimmer et al., 2010)

Optogenetics and long range connectivity

As we described, sensory information travels to the neocortex in a very organized manner; passing through different regions of the brain with distinct functions and targets, and ultimately reaches to the cortex in different layers onto different types of neurons. In this highly organized system with diverse subunits, achieving the highest specificity is crucial for investigations.

Over the last decade, a revolutionary method has been developed in neuroscience: optogenetics. Optogenetics enables us to deal with causal interventions in the brain through genetically expressing actuators that control neuronal activity and having those actuators under optical control. Channelrhodopsin-2 (ChR2) is a light-activated cation channel, cloned from the green algae *Chlamydomonas reinhardtii* (Nagel et al., 2003). It is a transmembrane ion channel with a molecule called retinal which is a derivative of Vitamin A. Retinal is the part of ChR2 which interacts with the light. During light exposure, retinal absorbs a photon and changes its

confirmation. This confirmation change increases the open probability of the channel protein. ChR2 is a non-selective cation channel permeable to potassium (K^+), sodium (Na^+) and calcium (Ca^{2+}). Under physiological conditions the major conductance is an inward sodium and calcium current that has a reversal potential of 0 mV. Typically, neurons have a resting membrane potential around -70 mV and activation of ChR2 in these neurons will depolarize these cells and ultimately they will fire action potentials.

ChR2 was expressed in neurons first time in hippocampal culture neurons (Boyden et al., 2005). These ChR2 expressing neurons were light sensitive and brief pulses of blue light were driving action potential firing with millisecond temporal precision. Given the genetic access and high temporal precision, ChR2 is an important tool to investigate neural networks with high spatial and temporal specificity.

In this thesis, we will focus on thalamocortical networks. In order to understand how the sensory information is distributed across different layers of the somatosensory cortex, we need to activate specific thalamocortical afferents. As we mentioned, the somatosensory cortex receives thalamocortical input from different thalamic nuclei. Early studies before optogenetics used electrical activation of the thalamus to evoke responses in the cortex (Agmon and Connors, 1991, 1992; Beierlein et al., 2002). In living brain slices, they sent brief current pulses through stimulation electrodes to activate the neurons nearby. This method indeed activates the region of interest, however, it could also activate other neighboring thalamic nuclei or other axons connected to other brain regions, which limit the overall specificity. Instead of using stimulation electrodes, with optogenetics it is possible to achieve much higher specificity. One of the first studies investigating long-range connectivity with optogenetics was by Petreanu et al. (2009). They expressed ChR2 in different brain regions and recorded neurons in wS1. They were able to activate axonal terminals in wS1 and evoke postsynaptic potentials, even though the cell bodies of these axons were not intact. This made the investigation of long range connectivity possible with high specificity. Following this approach, some thalamocortical connectivity studies used optogenetics successfully to isolate specific inputs and measured responses in different cell types (Petreanu et al., 2009; Cruikshank et al., 2010; Audette et al., 2018). However, these studies have never

investigated separate contributions of VPM or POM inputs onto a subset of the GABAergic population in every cortical layer.

General aims of the PhD thesis

The general aim of the PhD thesis is to provide a complete understanding of how thalamic input is distributed to specific cell-types across the layers of the somatosensory cortex and further characterize first-order and higher-order properties.

In chapter 2 of the thesis, we will focus on VPM and POM inputs to wS1. We will use optogenetics to selectively activate either VPM or POM and measure their inputs in excitatory, PV, SST and VIP neurons across all layers of wS1.

In chapter 3, we will explore different parallel thalamocortical pathways and investigate their functional inputs to both wS1 and wS2. We will subdivide POM using anterograde transsynaptic virus and characterize its sensory and higher-order sub-nuclei and compare it with the PrV-driven VPM pathway.

Chapter 2:

Layer, cell-type and pathway-specific thalamocortical input to mouse primary somatosensory barrel cortex

In collaboration with Johannes M. Mayrhofer, Matthieu Auffret, Tess B. Oram and Ofer Yizhar

Introduction

Several studies have investigated the thalamus-cortex relationship both *in vivo* and *in vitro*. It has been shown that, the axons coming from VPM neurons innervate L4 and 5B/6 border of the respective barrel column in the wS1 (Bureau et al., 2006; Cruikshank et al., 2010; Oberlaender et al., 2012) whereas the POM neurons target L1 and L5A (Herkenham, 1980; Chmielowska et al., 1989; Lu and Lin, 1993; Wimmer et al., 2010; Bureau et al., 2006; Jouhanneau et al., 2014). wS1 receives thalamic input from either VPM or POM in its every layer.

The strongest axonal innervations of VPM are in L4 (Jensen and Killackey, 1987; Bernardo and Woolsey, 1987; Chmielowska et al., 1989; Senft and Woolsey, 1991; Pierret et al., 2000; Wimmer et al., 2010; Oberlaender et al., 2012; Poulet et al., 2012). When we look at the thalamocortical connections to excitatory neurons, the majority of VPM innervations make synapses with excitatory neurons because they outnumber the L4 interneurons. (Bruno and Simons, 2002; Cruikshank et al., 2010). VPM afferents strongly target L4 spiny stellate cells, star pyramids, and L4 pyramidal neurons (Bruno and Sakmann, 2006; Oberlaender et al., 2012). Additionally, it is important to emphasize that VPM doesn't just excite L4, in fact, it makes just as big an impact on L5/6 neurons (Constantinople and Bruno, 2013). POM has the strongest innervations in L5A and L1. Excitatory neurons in every layer receive input from POM, however, the biggest inputs are in L5A pyramidal neurons, which are nearly 5 fold bigger compared to other layers (Audette et al., 2018).

In GABAergic population, fast-spiking PV neurons receive a strong input from the thalamus. The fast-spiking interneuron response to thalamocortical input is stronger than the excitatory neurons' response, triggering powerful feedforward inhibition (Cruikshank et al., 2007, 2010; Audette et al., 2018). On the other hand, somatostatin-expressing neurons have much weaker responses to thalamocortical input compared to excitatory and fast-spiking neurons (Cruikshank et al., 2010; Audette et al., 2018). 5HT3aR-expressing neurons receive weak and heterogeneous responses from the thalamus in the main input layers (Ji et al., 2016; Audette et al., 2018). The cited studies investigated the inputs from either both VPM and POM combined, or one of the nuclei looking at a subset of layers. The separate contributions of VPM or POM inputs onto specific subsets of the GABAergic

population in every cortical layer have never been investigated. Today, having different mouse lines for different cell types enables us to label different subsets of excitatory and GABAergic cells. With the combination of optogenetics and the different mouse lines, it is possible to achieve a higher level of specificity than previous investigations. In this chapter, we will explore the VPM and POM inputs to excitatory, Parvalbumin (PV) expressing, Somatostatin (SST) expressing and Vasoactice Intestinal Peptide (VIP) expressing neurons across all layers of wS1.

Materials and Methods

All experiments were performed in accordance with the Swiss Federal Veterinary Office, under authorization 1889 issued by the 'Service de la consommation et des affaires vétérinaires' of the Canton de Vaud.

ChR2 virus injection in the thalamus

An AAV2/5 expressing ChR2 fused to EYFP (AAV2/5.DIO.EF1α.hChR2(H134R).EYFP by Penn Vector Core, AAV-hSyn-DFO-ChR2-eYFP by Tess Oram and Ofer Yizhar (collaborators in this study) of the Weizmann Institute, AAV5.hSyn.hChR2 (H134R)-eYFP.WRPE.hGH by Addgene) was used to express the light-gated cation channel, Channelrhodopsin-2 (ChR2), in either VPM or POM nucleus of the thalamus of GPR26-Cre, PV-Cre x LSL-tdTomato, SST-Cre x LSL-tdTomato, VIP-Cre x LSL-tdTomato animals (4 – 5 weeks old). Injections were targeted VPM or POM at the stereotaxic co-ordinate 1.6 mm posterior and 2.0 mm lateral, 2.0 mm posterior and 1.25 lateral to Bregma, respectively. We did a small craniotomy (approximately 1 mm in diameter) and left the dura intact. We used an injection pipette (internal tip diameter 20 – 30 μm) and filled its tip with the virus solution and lowered into the brain. We carried out injections (50 nl) at two different depths (3.25 mm for VPM and 2.8 mm for POM, below the pia) to infect cells in two thalamic nuclei. We kept the pipette remaining in the brain for 5 minutes before retracting it slowly in approximately 5 minutes. We allowed the virus to express 4 – 8 weeks before starting experiments.

Brain slicing

We anesthetized mice using a mixture of Ketamine (25 mg/ml) and Xylazine (2mg/ml) and perfused them with dissection buffer containing (in mM): 87 NaCl, 25 $NaHCO_3$, 25 D-glucose, 2.5 KCl, 1.25 NaH_2PO_4, 0.5 $CaCl_2$, 7 $MgCl_2$, 75 Sucrose, aerated with 95% O_2 + 5% CO_2. We cut parasagittal (35° away from vertical) acute slices with the same ice-cold dissection buffer in 300-µm-thick sections on a vibratome (Leica; VT1200). After slicing, we transeferred the tissue to a chamber with the same solution at room temperature for 25 min. We then transferred the slices to a chamber with standard ACSF containing (in mM): 125 NaCl, 25 $NaHCO_3$, 25 D-glucose, 2.5 KCl, 1.25 NaH_2PO_4, 2 $CaCl_2$, 1 $MgCl_2$, aerated with 95% O_2 + 5% CO_2 at room temperature and maintained them there for at least 1 hour prior to use.

In vitro whole-cell recordings

We recorded membrane potentials of 758 neurons (n=70 mice) in the whole-cell patch-clamp configuration in primary somatosensory barrel cortex (wS1) in the animals at the age of postnatal day 50 to 84 in both sexes. Patch-clamp recordings of EPSPs were obtained from neurons in the presence of TTX (1 µM), 4-AP (100 µM) and PTX (50 µM). We visualized neurons with a 40x/0.80NA W objective under video microscopy (Olympus BX51WI) coupled with infrared gradient contrast. Patch pipettes with a resistance of 5-7 MΩ were used. The pipettes were filled with the intracellular solution containing (in mM): 135 K-gluconate, 4 KCl, 4 Mg-ATP, 10 Na_2-phosphocreatine, 0.3 Na-GTP, and 10 HEPES (pH 7.3, 280 mOsmol/l). We added biocytin to the intracellular solution to give a final concentration of 3-4 mg/ml. We used an Ag/AgCl wire attached to the head-stage, as the recording electrode. We filled the pipettes with internal solution, fixed onto the head stage and lowered into the recording chamber which was superfused with artificial cerebrospinal fluid (ACSF). Another Ag/AgCl electrode connected to the head-stage was dipped into the recording chamber and used as the reference electrode. We applied positive pressure (200 mbar) and lowered the pipette until it touches the slice surface. Then with the same positive pressure, the pipette was advanced to a selected cell. When we touched the cell, we applied negative pressure to allow the formation of a gigaohm seal. Once the gigaohm seal is formed, we applied brief pulses of suction to break into the cell. We carried out all recordings in current clamp mode. The

membrane potential was sampled at 20 kHz in blocks of 2 seconds. Signals were digitized and recorded on an ITC-18 (Instrutech) analog to digital converter board, using custom written routines implemented in IgorPro. Liquid junction potential was not corrected.

Optogenetic stimulation

We used a fiber-optic cable (Thorlabs; NA 0.48; 1 mm) coupled to a 470 nm blue LED (Thorlabs) to deliver the optogenetic stimulus. One end of the fiber was plugged into the LED source and the other end of the fiber was mounted on a manipulator (Luigs and Neumann), and was lowered towards the cortex in the brain slice until the tip of the fiber-optic cable just touched the slice. The light stimulus was a single 1 ms pulse and it was delivered every 5 seconds. The peak light power, below the fiber, was approximately 30 mW.

Histology and cell visualization

At the end of the recording session, we fixed the slices with 4% PFA overnight at 4°C. We incubated the slices in blocking solution containing 5% normal goat serum and 0.3% Triton X for 1 hour. Then we transferred them to the staining solution containing 0.3% Triton X and 1:2000 of Streptavidin conjugated to Alexa 647 (Life Technologies). We incubated the slices for 2-3 hours and then washed them in PBS at RT. We used DAPI as a counterstain. We then mounted the slices and imaged them under a confocal microscope (Leica SP8). All the recovered neurons could be identified and matched to the recording. We measured the cell depth vertically from the pial surface of the slice to the cell body. In the cases where the cell could not be recovered, the manipulator reading was taken as the depth. In the cases where the cell was recovered, we measured it on the fixed slice.

Estimation of layer boundaries

Using the combination of DAPI stained sections containing axons with ChR2/YFP expression, wS1 layer boundaries are defined by the experimenter.

Analysis of PSP amplitudes

We aligned the membrane potential traces to the onset of the 1 ms ChR2 stimulus of the thalamocortical axons in S1. We averaged individual traces of 20 consecutive

sweeps to obtain an average membrane potential trace. Mean EPSP amplitudes were calculated by taking the average peak and subtracting the baseline pre-stimulus membrane potential. The latency of the EPSP was calculated by taking the time at 1% of its maximum peak value. All PSP amplitudes were measured from the resting membrane potentials of the neurons (Table 2.12).

Analysis of passive membrane properties

We calculated the resting membrane potentials of each cell during the recordings of light-evoked postsynaptic potentials. We averaged 100 ms of each trace prior to light stimulation. The final resting membrane potential of the cell is computed as an average across 20 consecutive sweeps. The membrane time constant is calculated from each trace by applying a hyperpolarizing current step and fitting an exponential decay curve to the initial portion of a hyperpolarizing potential. The input resistance is computed by calculating the slope in the plots of applied current vs voltage relationship of the traces.

Statistical analysis

Data are presented as mean ± SD and median. For each analysis as described throughout in this chapter, values were measured from average responses of 20 consecutive sweeps. To statistically assess the differences between groups, one-way ANOVA combined with Tukey-Kramer posthoc test was used (Matlab implementation).

Results

Anatomical separation of in VPM and POM

To map the VPM and POM inputs in the barrel cortex, it is crucial to activate the axons of these nuclei separately. Since these two nuclei are located very close to each other, it is almost impossible to activate either one of the nuclei using electrical stimulation. That is why we took advantage of optogenetics and mouse genetics to enhance the specificity of our investigations.

In order to have a separated Channelrhodopsin-2 (ChR2) (Nagel et al., 2003) infection in either VPM or POM, first we need to label them separately using genetic tools. To achieve that, we used a transgenic mouse line expressing Cre-recombinase under the control of the GPR26 promoter (Figure 2.1A). GPR26 is a protein expressed specifically in POM and some other neighboring nuclei of the thalamus except VPM (Gerfen et al., 2013). Using an adeno-associated virus (AAV) whose transgene expression is activated by Cre allowed us to have a specific infection of POM and no spillover infection in VPM (Figure 2.1B,C). To be able to infect VPM, we used an AAV which is inactivated by Cre (DFO) (Tess Oram and Ofer Yizhar), thus we observed an expression only in VPM, not in POM (Figure 2.1B,C).

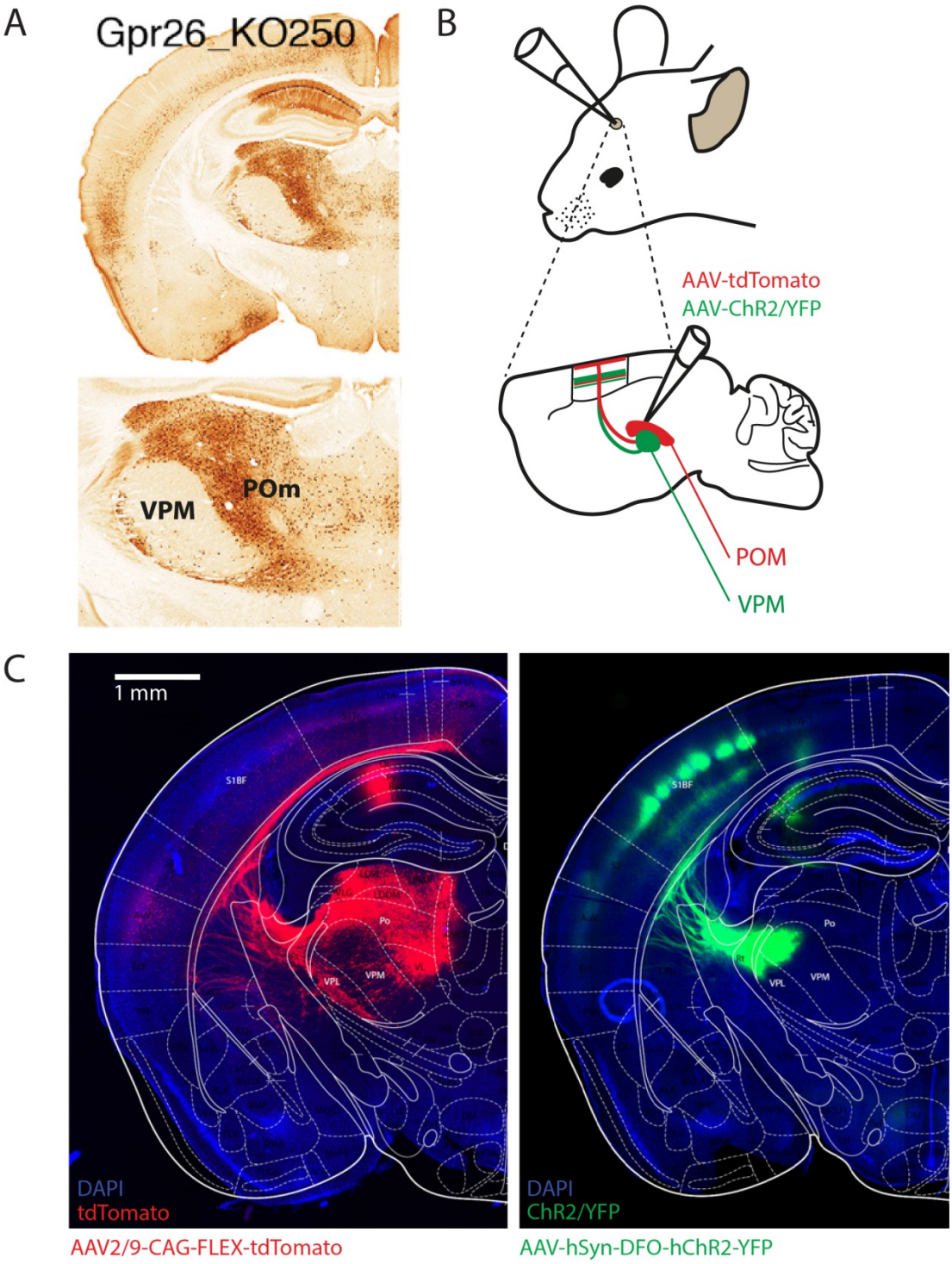

Figure 2.1 Anatomically separated labeling of VPM and POM nuclei. (A) Cre expression in POM in GPR26-Cre mouse (adapted from Gerfen et al., 2013) **(B)** Schematic drawing showing the strategy used to infect two thalamic nuclei separately. tdTomato expressing Cre-dependent AAV was injected into POM and ChR2/YFP expressing AAV-DFO was injected into VPM. **(C)** Coronal sections at the level of S1 showing the expression of the tdTomato in POM (left) and ChR2/YFP in VPM (right).

After having this clear anatomical separation of VPM and POM nuclei with genetic tools, we then expressed two different fluorescent proteins in VPM and POM axons in the same animal by injecting these two viruses into VPM and POM respectively to visualize the dual thalamocortical projections more clearly in wS1. These two different fluorescent proteins expressed in VPM and POM (tdTomato and eYFP; POM axons in red, VPM axons in green) allowed us to visualize both VPM and POM innervation patterns within wS1 (Fig 2.2B)

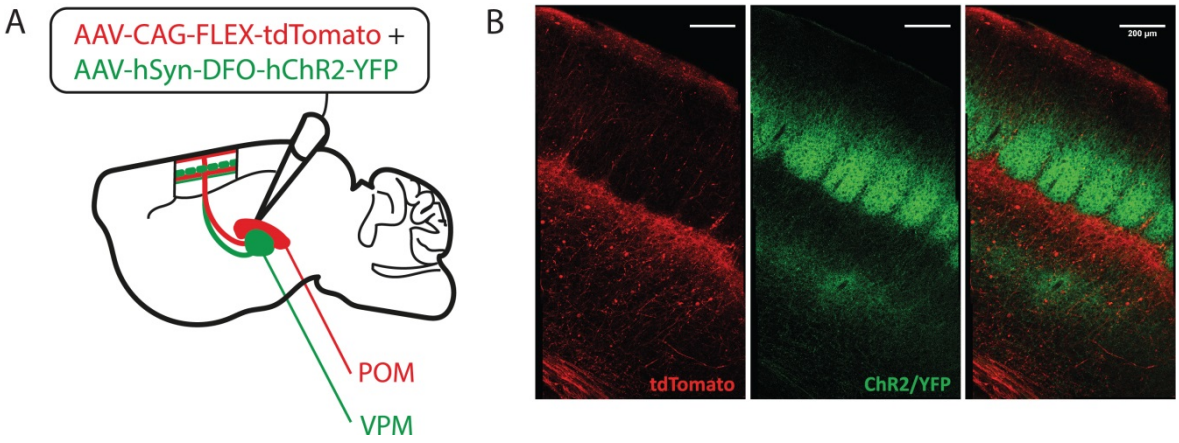

Figure 2.2 Expression of two different fluorescent proteins in VPM and POM. (A) Schematic drawing showing the strategy used to label two thalamic nuclei separately in the same animal. tdTomato expressing Cre-dependent AAV and ChR2/YFP expressing AAV-DFO was injected together into the thalamus. **(B)** POM projections (tdTomato; red) (left), VPM projections (ChR2/YFP; green) (middle) and merge of POM and VPM images (right), illustrating the non-overlapping, complementary axonal innervation in S1 barrel field in a parasagittal slice. Scale bar 200 µm.

ChR2 expression in VPM and POM

After establishing clean and separated labeling of VPM and POM we then injected ChR2 into these two nuclei separately (Figure 2.3A,B). As described in the introduction chapter, ChR2 is a light-gated cation channel that can be expressed in specific parts of the brain, activating neurons by blue light with high temporal precision (Nagel et al., 2003; Boyden et al., 2005; Arenkiel et al., 2007; Gradinaru et al., 2007; Petreanu et al., 2007; Cardin et al., 2009).

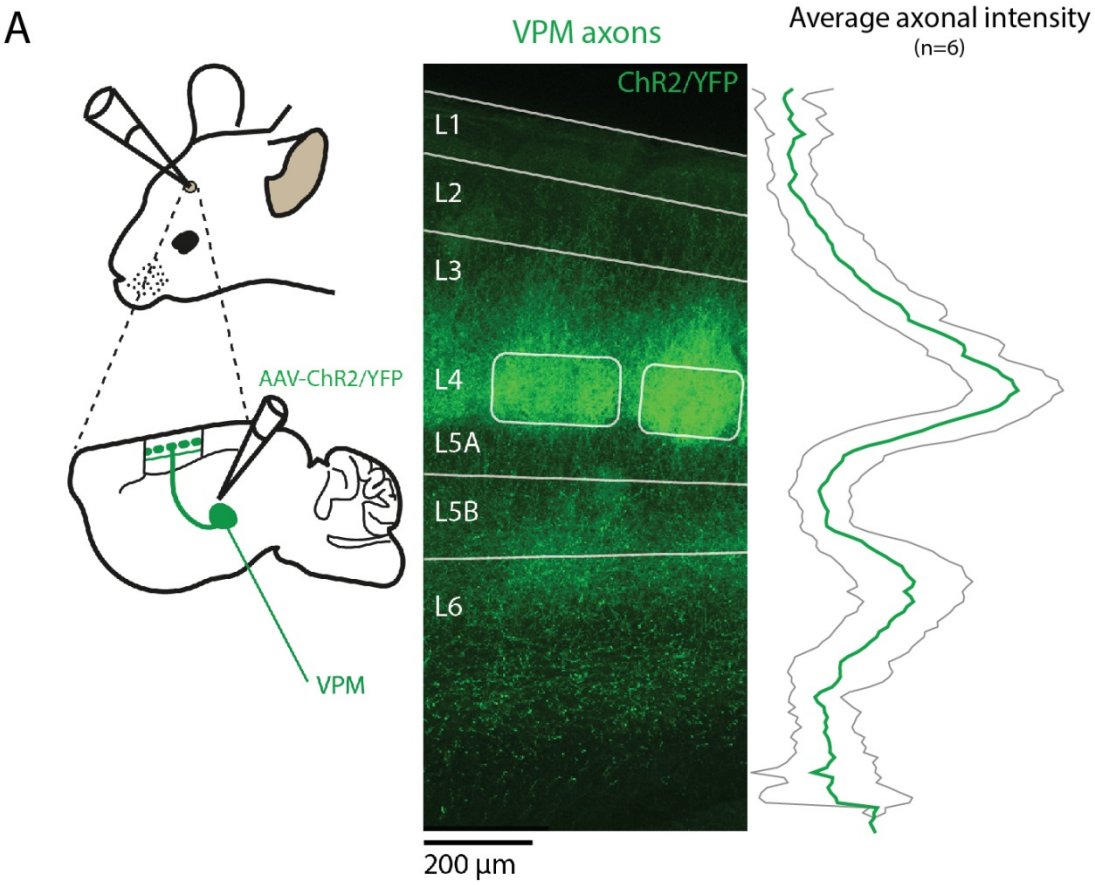
A
VPM axons
Average axonal intensity
(n=6)
ChR2/YFP
L1
L2
L3
L4
L5A
L5B
L6
AAV-ChR2/YFP
VPM
200 µm
B
POM axons
Average axonal intensity
(n=6)
L1
L2
L3
L4
L5A
L5B
L6
AAV-ChR2/YFP
POM
200 µm

Figure 2.3 Cre dependent AAV injections into POM and VPM of GPR26-Cre mice produced ChR2/YFP expression in thalamocortical axons. (A) Schematic showing the strategy used to inject ChR2 in VPM (left). Image from parasagittal slice after fixation with the expression of ChR2/YFP in the VPM axons in S1 (middle). The average VPM axonal intensity profile is shown in green (right) (n=6 mice, grey lines indicate ±SD). **(B)** Schematic drawing showing the strategy used to inject ChR2 in POM (left). Image from parasagittal slice after fixation with the expression of ChR2/YFP in the POM axons in S1 (middle). The average POM axonal intensity profile is shown in green (right) (n=6 mice, grey lines are ±SD)

After the ChR2 expression in the thalamocortical axons, we can then investigate their postsynaptic inputs onto different cells. Even though the connections from thalamus to the S1 barrel cortex are cut due to the parasagittal slicing, ChR2-expressing axons are intact with somato-dendritic zones of postsynaptic cells and we can activate the VPM or POM axons selectively. The neurons will be recorded in wS1 and VPM or POM afferents will be activated to evoke postsynaptic potentials.

ChR2-mediated optical excitation

To be able to map the thalamic input onto distinct cell-types across all layers of the primary whisker somatosensory cortex (wS1) of the mouse, we performed experiments combining *in vitro* whole-cell patch-clamp recordings with optogenetic activation of thalamocortical axonal terminals. We used an *in vitro* approach to enhance the accessibility to all layers of the cortex and increase the number of neurons recorded in order to have a detailed comparison between different layers and cell-types.

When we infect the thalamocortical cell bodies with ChR2, their axons also express the same protein. This allows us to evoke glutamate release in a specific pathway in a brain slice, even if the cell bodies are not connected to the axons. Since ChR2 is expressed in the axons, blue light exposure will let the synaptic terminals to release glutamate and this will lead to evoke a postsynaptic potential in the recorded cell.

We cut a parasagittal brain slice after the ChR2 expression in the thalamus (Figure 2.4). Then we place a 1 mm optic fiber on the cortical column selected to perform

whole-cell patch-clamp recordings (Figure 2.4). 1 mm optic fiber is used to activate the thalamocortical axons in every layer of the cortex.

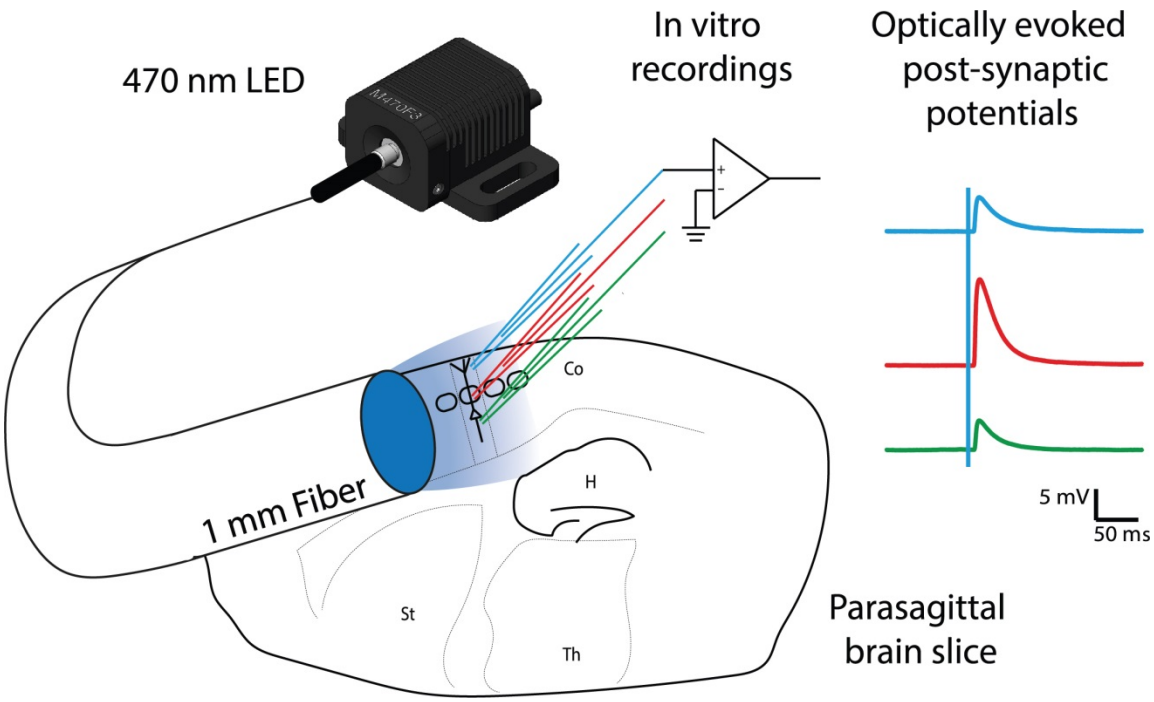

Figure 2.4 Design of the thalamocortical mapping experiment. Schematic drawing showing the method used to activate thalamocortical axons expressing ChR2 to evoke postsynaptic potentials in the barrel cortex. 470 nm wavelength light was delivered with a LED light source coupled with a 1 mm optic fiber onto wS1 (left). Then *in vitro* whole-cell patch-clamp recordings were performed to record PSPs evoked by the blue light.

Evoking monosynaptic PSPs using TTX + 4-AP

To isolate direct thalamocortical responses in recorded neurons, we applied the voltage-gated sodium channel antagonist tetrodotoxin (TTX) to prevent polysynaptic activity along with 100 µM 4-aminopyridine (4-AP) to help axonal depolarization and neurotransmitter release (Petreanu et al., 2007).

TTX application blocks action potential (AP) firing; therefore the polysynaptic activity would not exist when we activate the ChR2 in the axonal terminals. However, during ChR2 activation, the voltage-gated potassium channels actively repolarize the axonal terminals which make it difficult to achieve depolarization in

the synaptic terminals of the axons. In order to release glutamate, the axonal terminals should reach a certain depolarized membrane potential. To achieve that, we used the voltage-gated potassium channel antagonist 4-AP. With the combination of TTX and 4-AP, we can evoke ChR2-mediated monosynaptic light evoked postsynaptic potentials (Figure 2.5).

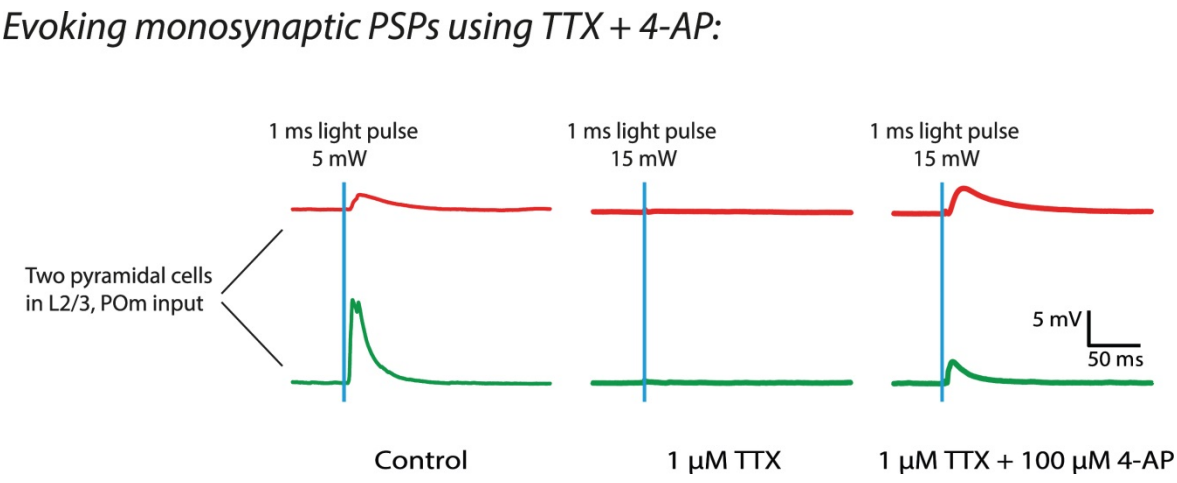

Figure 2.5 Evoking monosynaptic PSPs with the combination of TTX and 4-AP. Two example pyramidal cells simultaneously recorded in L2/3 of wS1. In control case cell shown as red trace receives light-evoked PSP in a monosynaptic manner, however, cell shown as green trace receives multiple synaptic inputs having multiple PSP peaks. Application of 1µM TTX diminishes the light-evoked PSPs. Addition of 100 µM 4-AP recovers light-evoked responses.

Thalamic input onto excitatory neurons

We then started to investigate the VPM and POM input distribution onto excitatory neurons in wS1 across different layers. Prior studies showed that VPM and POM stimulation can evoke excitatory postsynaptic potentials in some cortical neurons (Bureau et al., 2006; Petreanu et al., 2007; Viaene et al., 2011; Constantinople and Bruno, 2013; Gambino et al., 2014; Jouhanneau et al., 2014) and input strength onto excitatory cells correlates with where the axonal innervations are in the cortex (Audette et al., 2018; Cruikshank et al., 2010), however, how these responses are distributed across different cell types in every cortical layer has not been fully

investigated. To address that we started recording excitatory neurons in every layer in the same barrel column and activated VPM and POM axons separately.

First, we started recordings of VPM and POM inputs in the presence of TTX, 4-AP, and PTX for excitatory neurons across different layers of the cortical column in a single slice. Blue light illumination of ChR2 afferents with a 1 ms light pulse elicited EPSPs in excitatory neurons (Fig 2.7A,B). We always kept the optic fiber position and the stimulation strength stable throughout the whole experiment, in order to have an accurate comparison across layers.

Light-evoked responses were eliminated in the presence of AMPA receptor antagonist CNQX and NMDA receptor antagonist AP5, indicating that thalamocortical inputs were glutamatergic (n=2 cells) (Fig 2.6A). We also tested the stability of ChR2 to see if there was a PSP rundown because of a long duration of experiments. We recorded membrane potentials of two cells in whole-cell patch-clamp mode, activating the ChR2 expressing VPM fibers every 10 seconds for two hours (Figure 2.6B). There was no sign of PSP rundown in the recorded neurons (n=2 cells), however, there was a slight increase in PSP amplitudes after two hours.

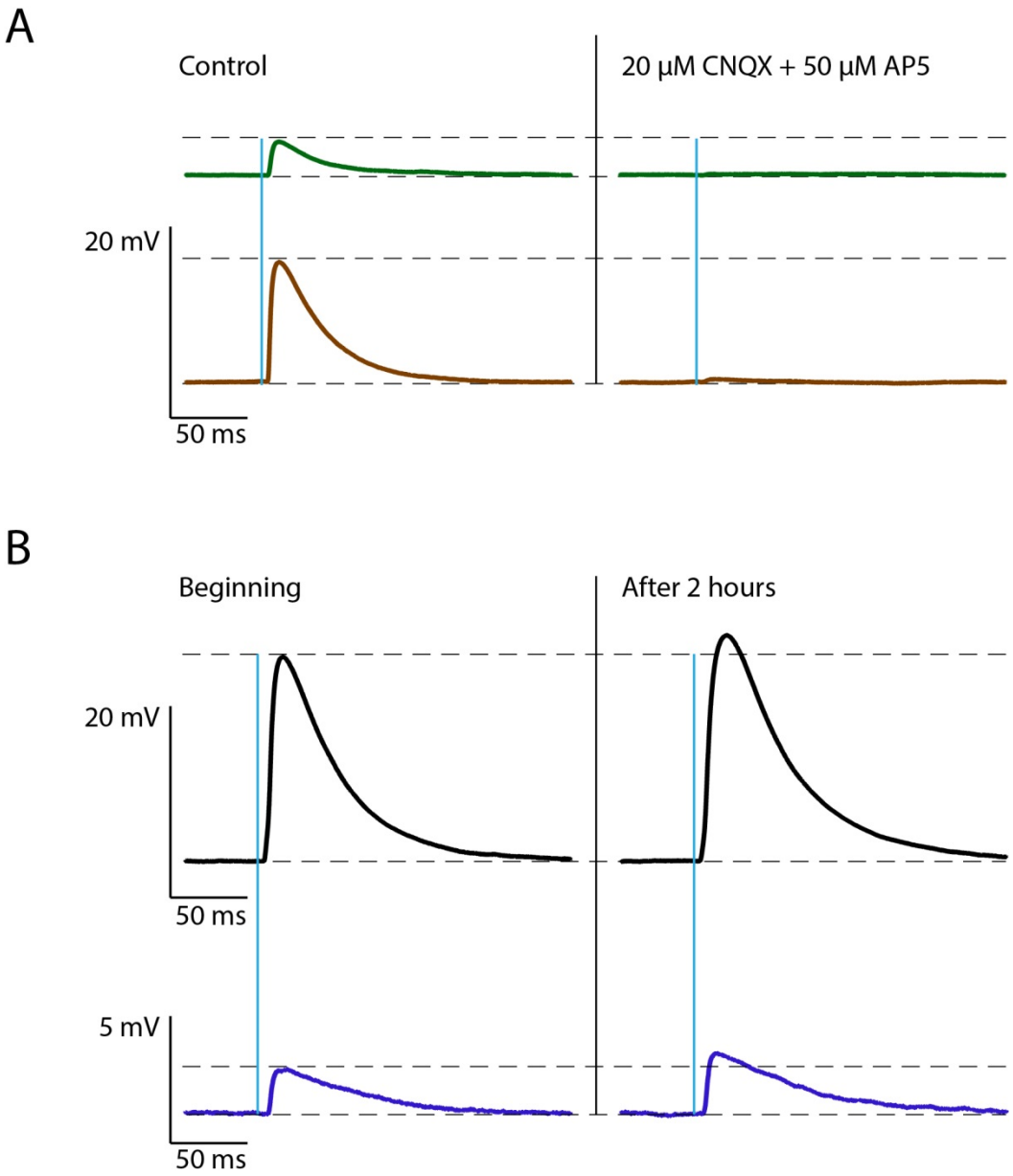

Figure 2.6 Glutamatergic thalamocortical inputs and ChR2 stability. (A) Simultaneous membrane potential recordings in whole-cell patch-clamp configuration of two excitatory neurons in L4 responding to ChR2 expressing VPM fiber activation by light (1ms) (left). Application of CNQX and AP5 eliminated the evoked PSPs (right). Traces are averages of 20 trials. **(B)** Simultaneous membrane potential recordings in whole-cell patch-clamp mode of two excitatory neurons in L4 responding to ChR2 expressing VPM fiber activation by light (1ms). Neurons were recorded for 2 hours. Traces on the left are the membrane potential averages of the responses to first 10 light pulses. Traces on the right are the membrane potential averages of the responses to 10 light pulses after 2 hours.

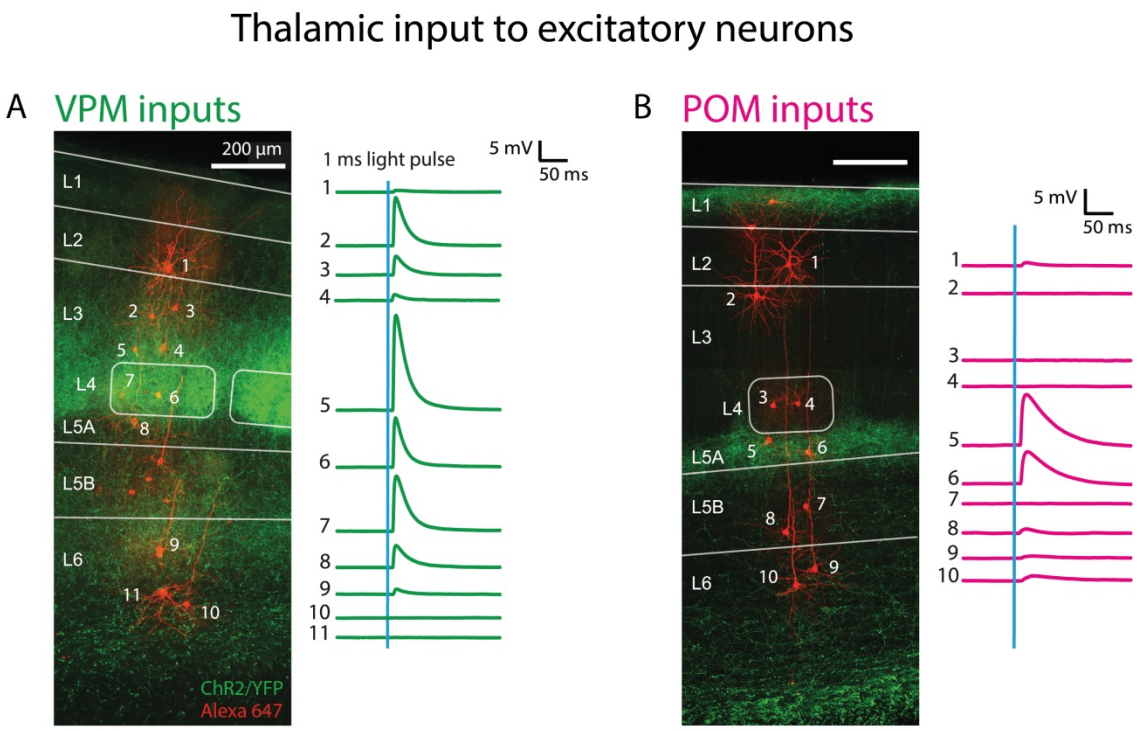

Figure 2.7 Optically evoked postsynaptic potentials in excitatory neurons. (A) VPM input to excitatory neurons across different layers of barrel cortex. Confocal image of a parasagittal slice after fixation with the expression of ChR2/YFP (green) in the VPM axons and recorded neurons with Alexa 647 (red) in wS1 (left). Light-evoked postsynaptic potentials from the recorded neurons after 1 ms blue light pulse (right). **(B)** POM input onto excitatory neurons across different layers of barrel cortex. Confocal image of a parasagittal slice after fixation with the expression of ChR2/YFP (green) in the POM axons and recorded neurons with Alexa 647 (red) in wS1 (left). Light-evoked postsynaptic potentials from the recorded neurons after 1 ms light pulse (right). Numbers on the left of the PSP traces indicate the recorded neurons in the confocal image.

To be able to compare optically-evoked thalamocortical input strength across different layers of the barrel column, we recorded excitatory neurons in every layer in current-clamp recordings. We mostly recorded from two nearby neurons simultaneously. VPM and POM axonal activation evoked the biggest amplitude responses mostly in L4 and L5A respectively (Figure 2.8).

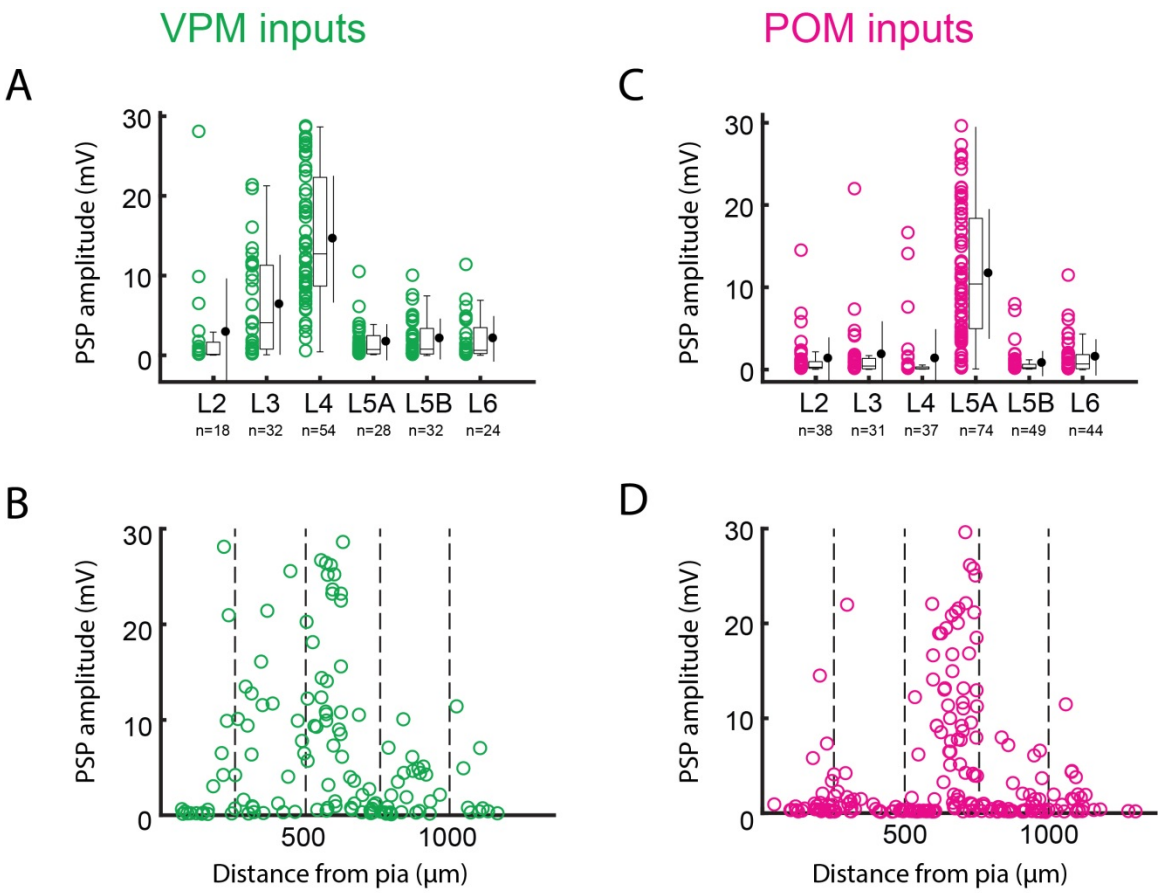

Figure 2.8 Population data of thalamocortical input to excitatory neurons. (A) VPM-evoked postsynaptic potentials in all recorded excitatory neurons across different layers. **(B)** VPM-evoked postsynaptic potentials in excitatory neurons plotted by depth from pia surface. **(C)** POM-evoked postsynaptic potentials in all recorded excitatory neurons across different layers. **(D)** POM-evoked postsynaptic potentials in excitatory neurons plotted by depth from pia surface.

We observed VPM-evoked postsynaptic potentials in excitatory neurons in every layer of the cortical column. In our experiments, we used three different light powers per recording to see responses at different stimulation strengths. Here we present responses having a maximum of 30 mV PSP amplitude in L4 excitatory neurons. Maximum mean response was in L4 (14.6 ± 7.9 mV (median: 12.7mV) , mean ± SD; L4 vs. L2: $p < 0.0001$, L4 vs L3: $p < 0.0001$, L4 vs L5A: $p < 0.0001$, L4 vs L5B: $p < 0.0001$, L4 vs L6: $p < 0.0001$) and it was followed by L3 (6.3 ± 6.3 mV (median: 4.1), mean ± SD) (Figure 2.8A). Neurons whose cell bodies located in other layers had smaller inputs (Table 2.1). As mentioned, we mostly performed paired

simulatenous recordings and we observed that some neurons located in the same layer responded very differently to VPM activation (pairs of 2 & 3, 4 & 5 in Figure2.7A).

POM evoked direct postsynaptic potentials in excitatory neurons were also observed in every layer of the cortical column. We present responses having a maximum of 30 mV PSP amplitude in L5A excitatory neurons. Maximum mean response was in L5A (11.63 ± 7.9 mV (median: 10.41 mV), mean ± SD; L5A vs. L2: $p < 0.0001$, L5A vs L3: $p < 0.0001$, L5A vs L4: $p < 0.0001$, L5A vs L5B: $p < 0.0001$, L5A vs L6: $p < 0.0001$) (Figure 2.8 C). Neurons whose cell bodies located in other layers on average had nearly 10 fold smaller inputs than L5A (Table 2.2) which shows the very precise targeting of POM axons to L5A neurons.

Given the nature of the experiments, the expression level of ChR2 could be different among animals. Therefore, in order to compare the input strengths more accurately, responses across layers were normalized to the mean strength of L4 for VPM and L5A for POM (Figure 2.9).

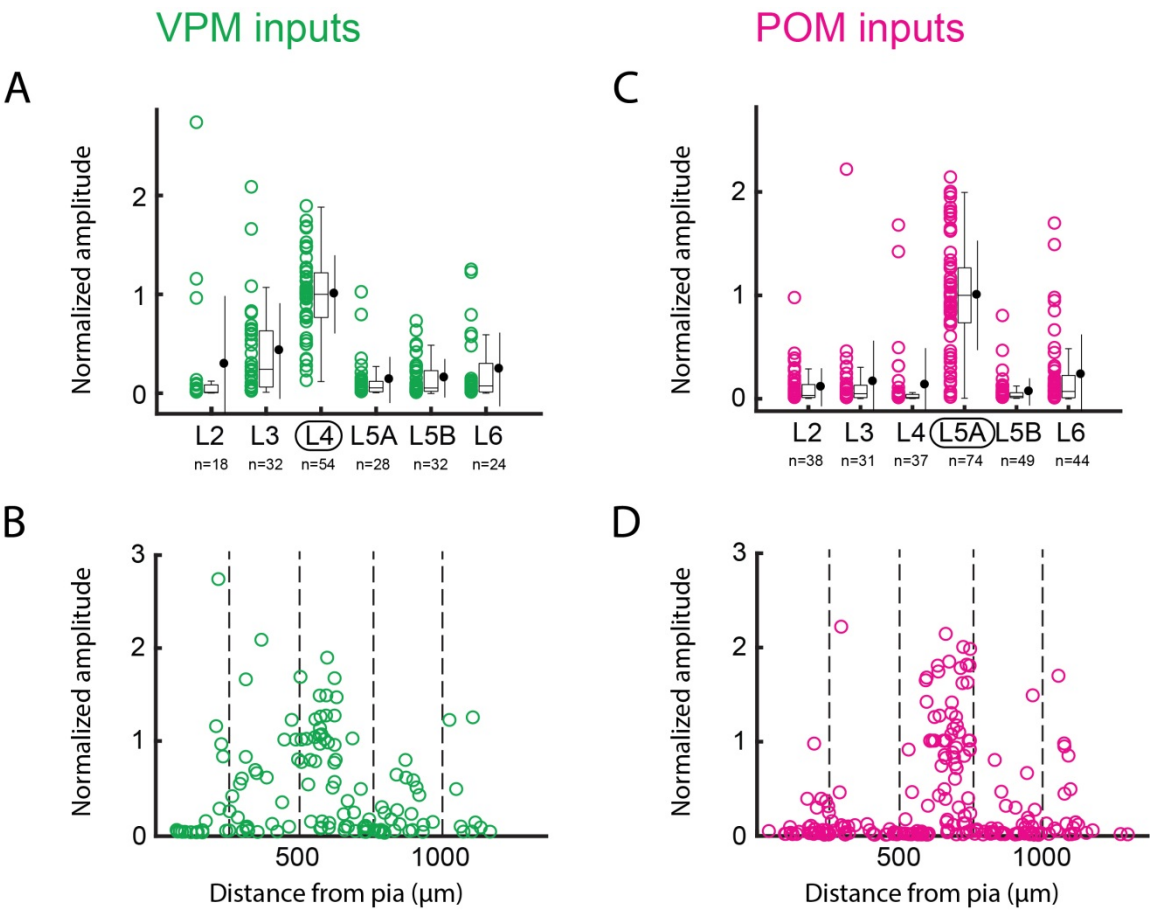

Figure 2.9 Normalized thalamocortical input to excitatory neurons. (A) VPM-evoked postsynaptic potentials in all recorded excitatory neurons across different layers, normalized to the average of inputs to L4 neurons in the same slice per experiment. **(B)** VPM-evoked postsynaptic potentials in excitatory neurons plotted by depth from pia surface, normalized to the average of inputs to L4 neurons in the same slice per experiment. **(C)** POM-evoked postsynaptic potentials in all recorded excitatory neurons across different layers, normalized to average of inputs to L5A neurons in the same slice per experiment.. **(D)** POM-evoked postsynaptic potentials in excitatory neurons plotted by depth from pia surface, normalized to the average strength of input to L5A neurons in the same slice per experiment.

Normalized data also gave a very similar result. For VPM, within the same slice, normalized mean PSP amplitude was maximum in L4 (1 ± 0.39 (median: 1), L4 vs. L2: $p < 0.0001$, L4 vs L3: $p < 0.0001$, L4 vs L5A: $p < 0.0001$, L4 vs L5B: $p < 0.0001$, L4 vs L6: $p < 0.0001$, mean ± SD) and followed by L3 (0.4 ± 0.48 (median: 0.24), mean ±

SD) (Figure 2.9A). Neurons whose cell bodies located in other layers had smaller inputs (Table 2.1).

POM normalized mean PSP amplitude within the same slice was maximum in L5A (1 ± 0.53 (median: 1), L5A vs. L2: $p < 0.0001$, L5A vs L3: $p < 0.0001$, L5A vs L4: $p < 0.0001$, L5A vs L5B: $p < 0.0001$, L5A vs L6: $p < 0.0001$, mean ± SD). Neurons whose cell bodies resided in other layers had almost 10 folds smaller inputs than L5A (Table 2.2).

We found that the thalamic input to excitatory neurons tends to correlate well with thalamocortical axonal innervation pattern. This result is in agreement with predictions from prior studies (Petreanu et al., 2007; Meyer et al., 2010; Cruikshank et al., 2010; Audette et al., 2018). VPM axons innervate heavily L4 and L3 and less strongly in L5B/L6 border (Fig 2.3) and they evoke the maximum mean responses in L4 and L3 (Fig 2.10). POM axons, on the other hand, innervate mainly L5A and L1 (Fig 2.3) and they evoke the maximum mean responses in L5A (Fig 2.10).

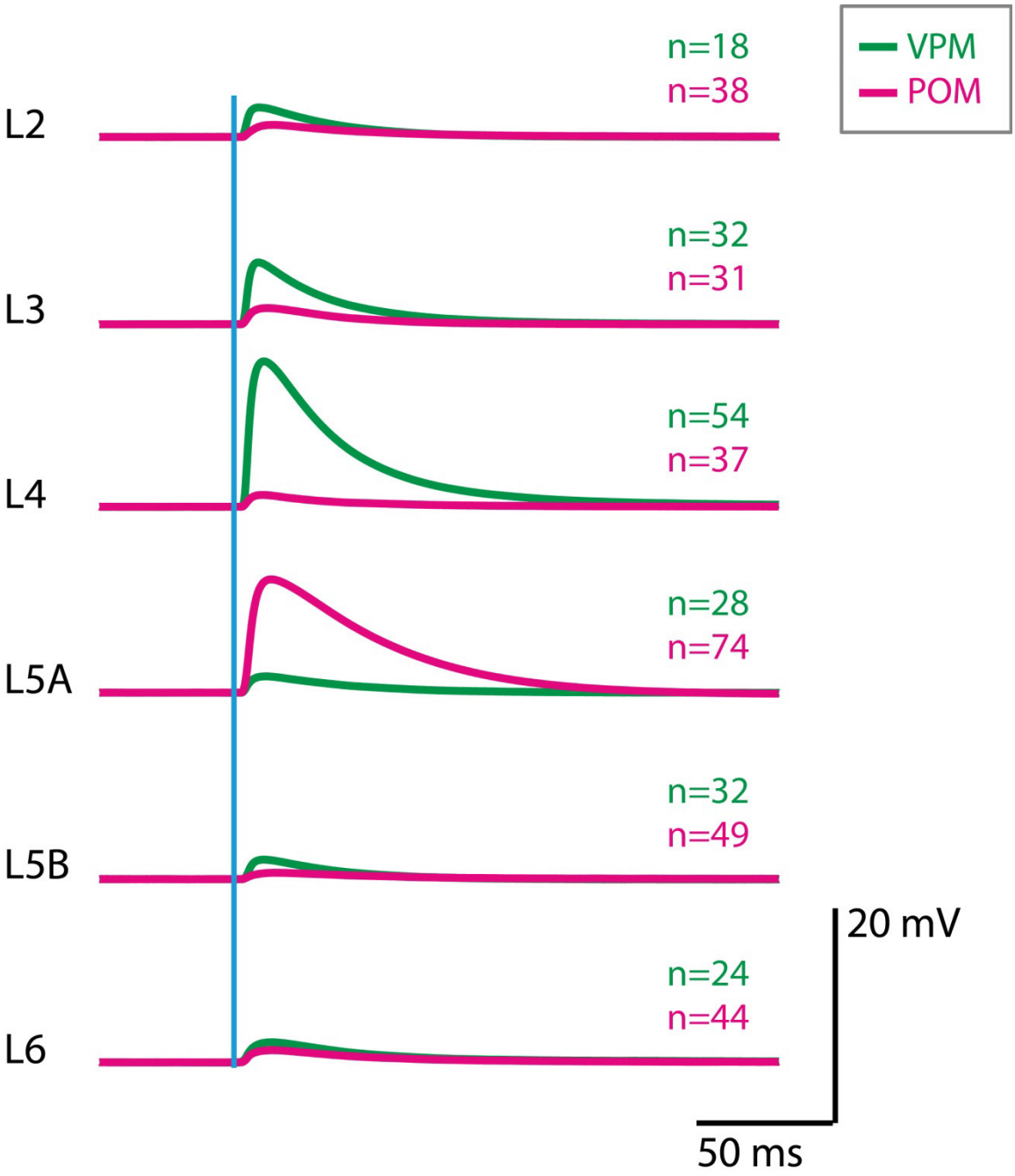

Figure 2.10 Grand averages of VPM and POM evoked responses across all layers of wS1. Mean PSPs evoked by VPM and POM afferents. VPM activation generated the largest amplitude response in L4, whereas for POM-activation largest amplitude response was in L5A.

Thalamic input to GABAergic neurons

We were then interested in investigating the thalamic input to GABAergic neurons. We used the same methodology used for investigating thalamic input to excitatory neurons except we were not able to use GPR26-Cre driver line of transgenic mice because Cre driver lines were instead used to define classes of GABAergic neurons. We took advantage of different transgenic mouse lines to label 3 non-overlapping major subsets of inhibitory neurons; Parvalbumin (PV), Somatostatin (SST) and Vasoactive Intestinal Peptide (VIP) expressing neurons (Gong et al., 2007; Taniguchi et al., 2011). For PV expressing neurons, we used PV-Cre x LSL-tdTomato, for SST expressing neurons we used SST-Cre x LSL-tdTomato and for VIP expressing neurons we used VIP-Cre x LSL-tdTomato transgenic mouse lines. We injected non-Cre dependent ChR2 expressing AAV in VPM and POM in adult mice (3-4 weeks old) and confirmed the targeting by looking at the typical pattern of axonal innervation concentrated L4 and L5B/6 border for VPM and L5A and L1 for POM. In case of injection site overlap, VPM and POM axons were both presents in wS1 and we discarded those experiments from the analysis.

Thalamic input onto Parvalbumin expressing neurons

To investigate the thalamic input onto PV neurons, we used PV-Cre x LSL-tdTomato transgenic mice. With tdTomato expression, we were able to target PV neurons for whole-cell patch-clamp recordings.

Similar to the thalamic input to excitatory neurons experiments, we again recorded cells across all layers within the same slice (Figure 2.11, 2.12). We used three different light powers per recording to see responses in different stimulation strengths. We typically recorded from two nearby neurons simultaneously. To be able to compare light-evoked VPM and POM input distribution in the cortical column, we recorded excitatory neurons in each layer. Here we present responses having a maximum of 30 mV PSP amplitude in L4 excitatory neurons for VPM, L5A excitatory neurons for POM inputs. VPM and POM activation evoked the largest amplitude responses in L4 and L5A respectively (Figure 2.13). As mentioned before, the expression level of ChR2 could be different among animals. Therefore, to

compare the input strengths more accurately, responses across layers were normalized to the mean strength of excitatory neurons in L4 for VPM and L5A for POM (Figure 2.13B,D).

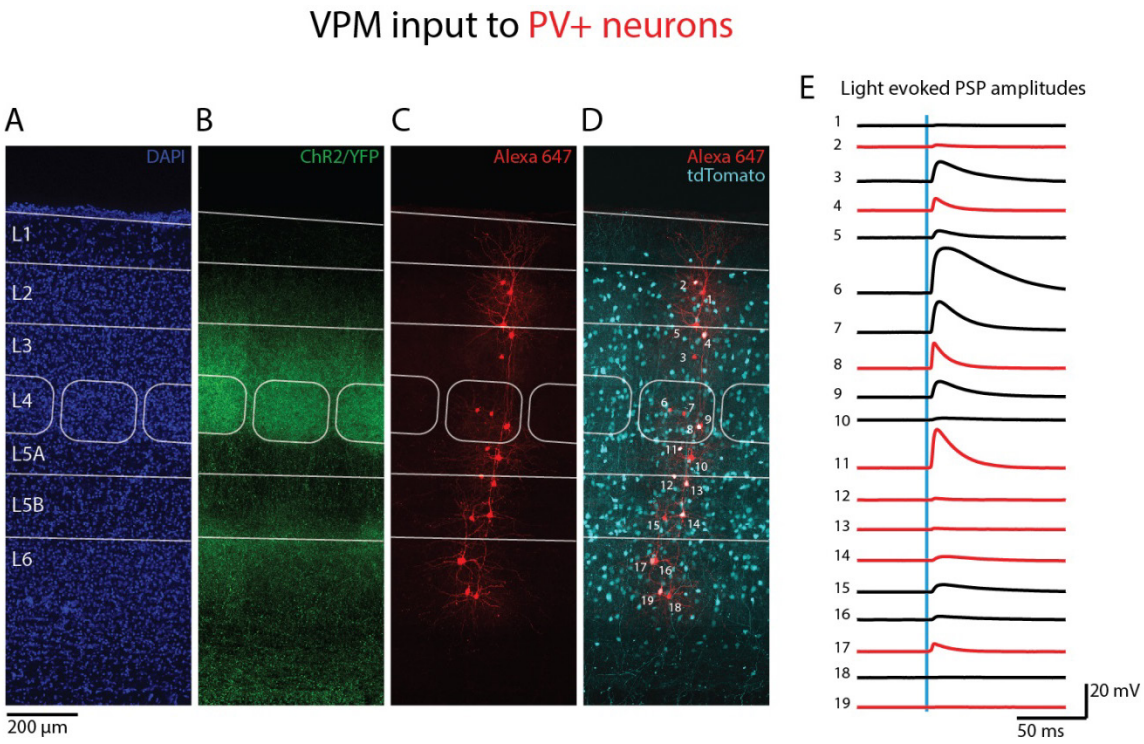

Figure 2.11 VPM input to PV expressing neurons. Confocal images of a parasagittal slice of wS1 after fixation. Images are maximum intensity projections of a confocal z-stack **(A)** DAPI staining (blue). **(B)** Expression of ChR2/YFP (green) in the VPM axons. **(C)** Recorded neurons with Alexa647 (red). **(D)** PV neurons with tdTomato reporter (cyan) and recorded neurons with Alexa647 (red). Targeted PV neurons are shown in white in the overlay of cyan and red fluorescence. **(E)** Light-evoked postsynaptic potentials from the recorded neurons after 1 ms blue light pulse. Numbers on the left of the PSP traces indicate the recorded neurons in the confocal image.

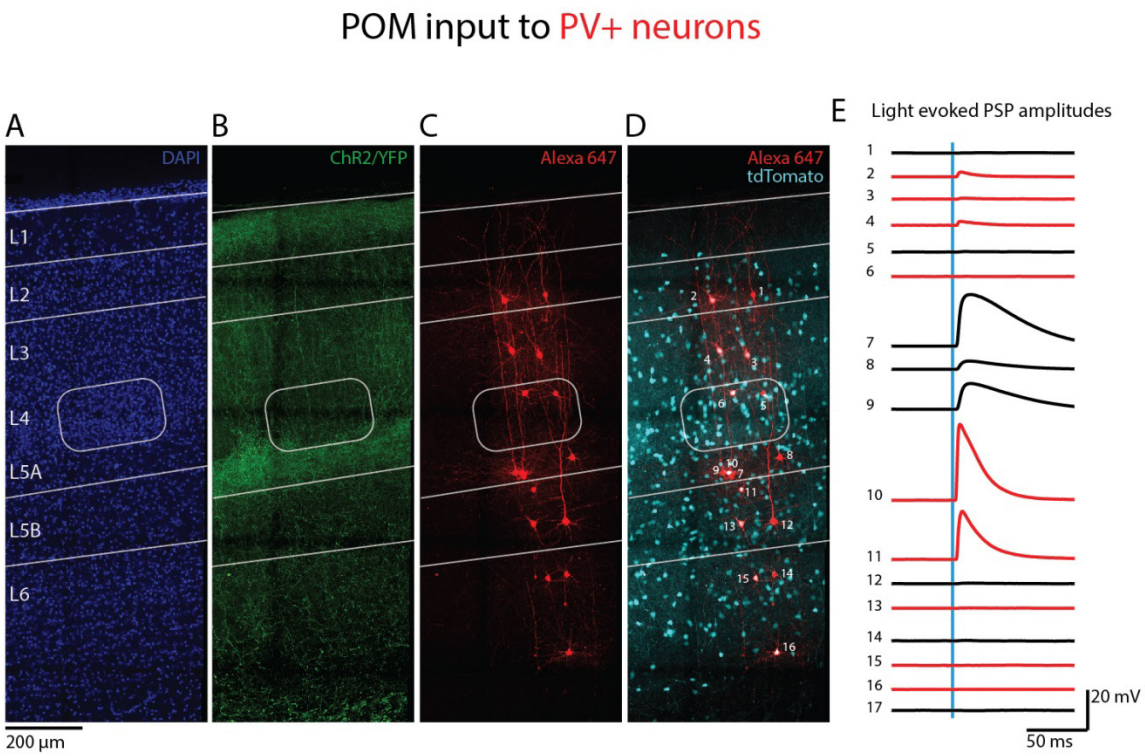

Figure 2.12 POM input to PV expressing neurons. Confocal images of a parasagittal slice of wS1 after fixation. Images are maximum intensity projections of a confocal z-stack **(A)** DAPI staining (blue). **(B)** Expression of ChR2/YFP (green) in the VPM axons. **(C)** Recorded neurons with Alexa647 (red). **(D)** PV neurons with tdTomato reporter (cyan) and recorded neurons with Alexa647 (red). Targeted PV neurons are shown in white in the overlay of cyan and red fluorescence. **(E)** Light-evoked postsynaptic potentials from the recorded excitatory (black) and PV (red) neurons after 1 ms blue light pulse. Numbers on the left of the PSP traces indicate the recorded neurons in the confocal image.

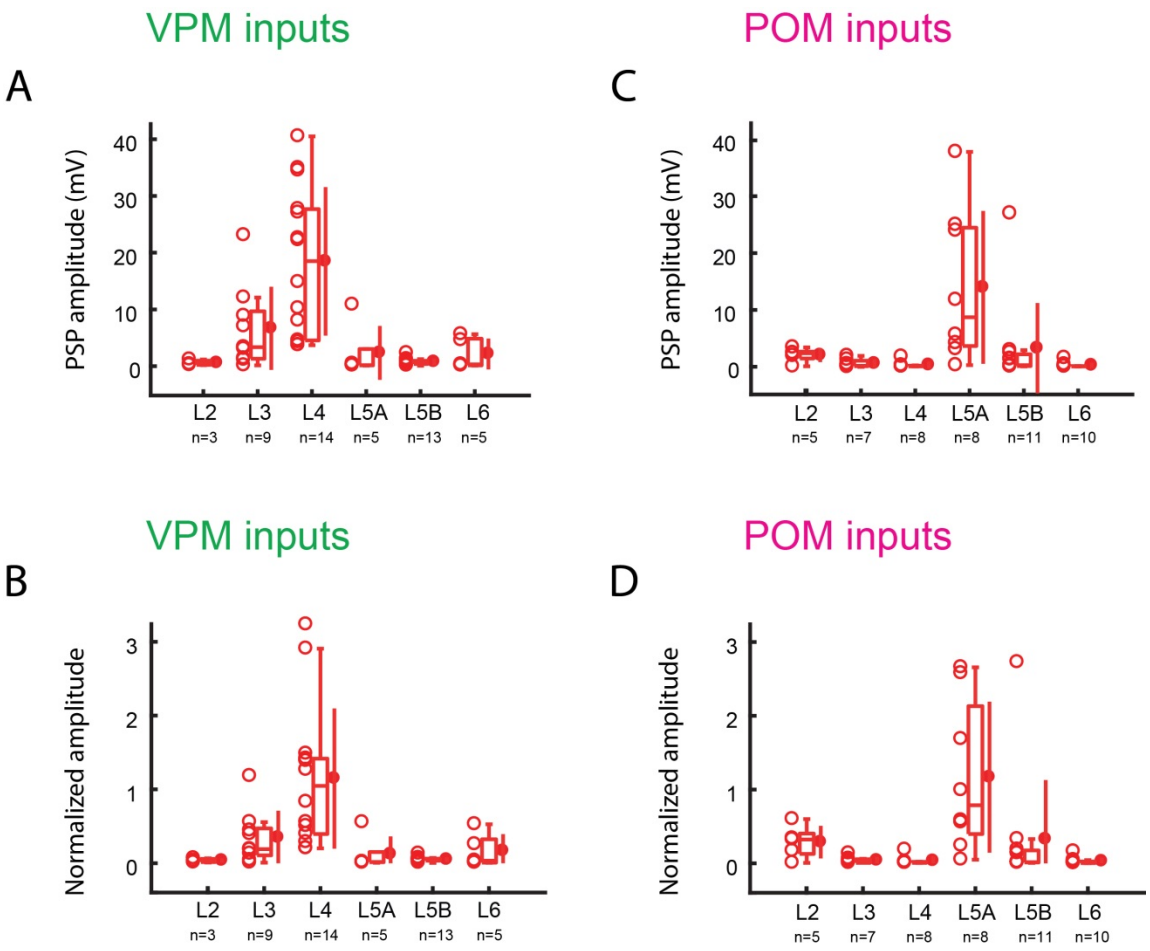

Figure 2.13 Population data of thalamocortical input to PV expressing neurons. (A) VPM-evoked postsynaptic potentials in PV neurons across different layers. **(B)** VPM-evoked postsynaptic potentials in PV neurons across different layers, normalized to the average of inputs to L4 excitatory neurons in the same slice per experiment **(C)** POM-evoked postsynaptic potentials in PV neurons across different layers. **(D)** POM-evoked postsynaptic potentials in PV neurons across different layers, normalized to the average of inputs to L5A excitatory neurons in the same slice per experiment.

We observed VPM-evoked postsynaptic potentials in PV neurons in every layer of the cortical column. We present responses having a maximum of 30 mV PSP amplitude in L4 excitatory neurons. Maximum mean response was in L4 (18.47 ± 13.09 mV (median: 18.51 mV), mean ± SD; L4 vs. L2: $p = 0.0131$, L4 vs L3: $p = 0.0157$, L4 vs L5A: $p = 0.0049$, L4 vs L5B: $p < 0.0001$, L4 vs L6: $p = 0.0043$) and it was followed by L3 (6.67 ± 7.32 mV (median: 3.34), mean ± SD) (Figure 2.13A). Neurons whose cell bodies resided in other layers had smaller inputs (Table 2.3).

Responses across layers were normalized to the average input to L4 excitatory neurons. Within the same slice, normalized mean PSP amplitude was maximum in L4 (1.15 ± 0.95 (median: 1.05), mean ± SD; L4 vs. L2: $p = 0.0332$, L4 vs L3: $p = 0.0184$, L4 vs L5A: $p = 0.0115$, L4 vs L5B: $p < 0.0001$, L4 vs L6: $p = 0.0175$) and followed by L3 (0.35 ± 0.36 (median: 0.19), mean ± SD) (Figure 2.9A). Neurons whose cell bodies resided in other layers had smaller inputs (Table 2.3).

POM activation evoked postsynaptic potentials in PV neurons in every layer of the cortical column. Here we present responses having maxium of 30 mV PSP amplitude in L5A excitatory neurons. Maxiumum mean response was in L5A (13.97 ± 13.43 mV (median: 8.71 mV), mean ± SD; L5A vs. L2: $p = 0.0338$, L5A vs L3: $p = 0.0044$, L5A vs L4: $p = 0.0023$, L5A vs L5B: $p = 0.0147$, L5A vs L6: $p = 0.0011$) (Figure 2.8 C). Neurons located in other layers had almost 10 folds smaller inputs than L5A, except L2 (2.05 ± 1.23 mV (median: 2.4), mean ± SD) (Table 2.4). Normalized data also gave a very similar input distribution across layers. Responses across layers were normalized to the mean strength of L5A excitatory neurons. Within the same slice, normalized mean PSP amplitude was maximum in L5A (1.17 ± 1.02 (median: 0.79), mean ± SD; L5A vs. L2: $p = 0.0338$, L5A vs L3: $p = 0.0044$, L5A vs L4: $p = 0.0023$, L5A vs L5B: $p = 0.0147$, L5A vs L6: $p = 0.0011$).

In summary, PV expressing neurons received a similar pattern of thalamic input distribution in excitatory neurons. Thalamocortical afferents seem to give strong inputs to PV neurons in their innervation zones.

Thalamic input onto Somatostatin expressing neurons

To investigate the thalamic input onto SST neurons, we used SST-Cre x LSL-tdTomato transgenic mice. With tdTomato expression, we were able to target SST neurons for whole-cell patch-clamp recordings.

We recorded cells across all layers within the same slice (Figure 2.14, 2.15). We used three different light powers per recording to see responses in different stimulation strengths. We typically recorded from two nearby neurons simultaneously. We again used excitatory neurons as references, therefore we recorded excitatory neurons in every layer for our current-clamp recordings. In contrast to strong input to PV neurons, VPM and POM fiber activation evoked very weak postsynaptic potentials in SST neurons, even though there was a very strong input into their neighboring excitatory neurons (Figure 2.14D,E). VPM inputs were maximum in L4 and L3 (Figure 2.16). POM inputs were maximum in L5A (Figure 2.16). We then normalized the PSP responses per slice. Responses across layers were normalized to the mean response strength of excitatory neurons in L4 for VPM and L5A for POM (Figure 2.16B,D).

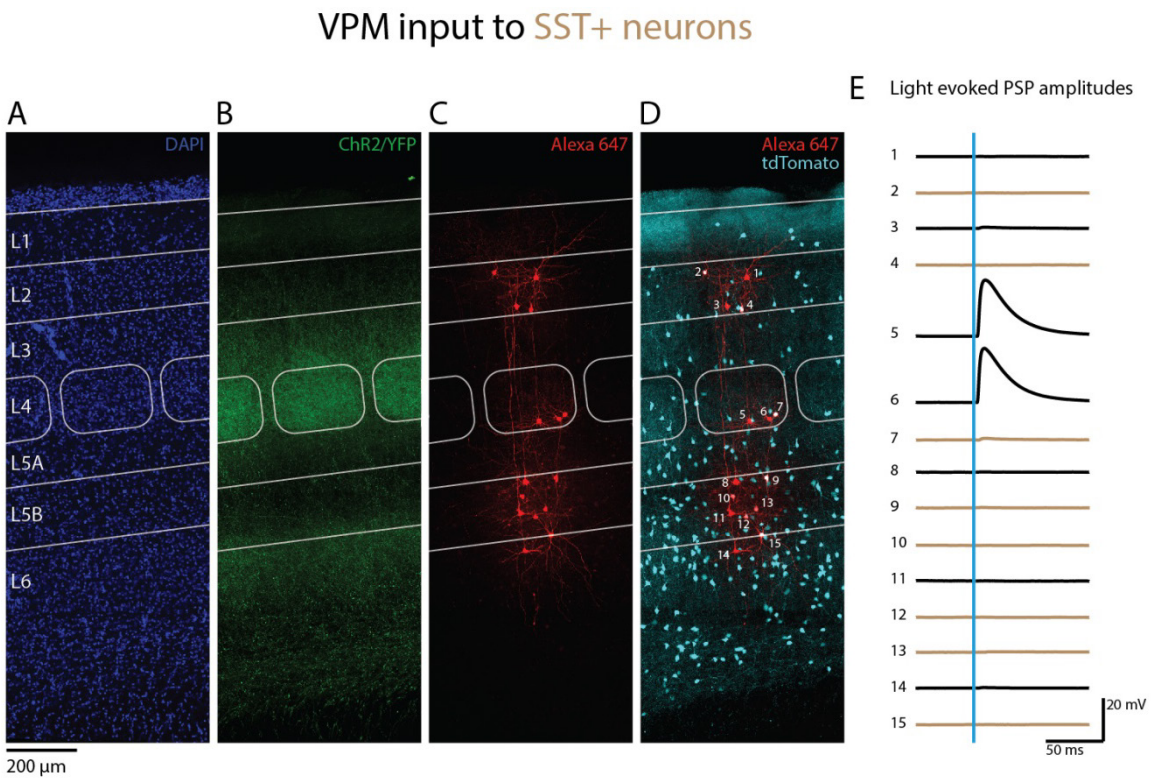

Figure 2.14 VPM input to SST expressing neurons. Confocal images of a parasagittal slice of wS1 after fixation. Images are maximum intensity projections of a confocal z-stack **(A)** DAPI staining (blue). **(B)** Expression of ChR2/YFP (green) in the VPM axons. **(C)** Recorded neurons with Alexa647 (red). **(D)** SST neurons with tdTomato reporter (cyan) and recorded neurons with Alexa647 (red). Targeted SST neurons are shown in white in the overlay of cyan and red fluorescence. **(E)** Light-evoked postsynaptic potentials from the recorded excitatory (black) and SST (brown) neurons after 1 ms blue light pulse. Numbers on the left of the PSP traces indicate the recorded neurons in the confocal image.

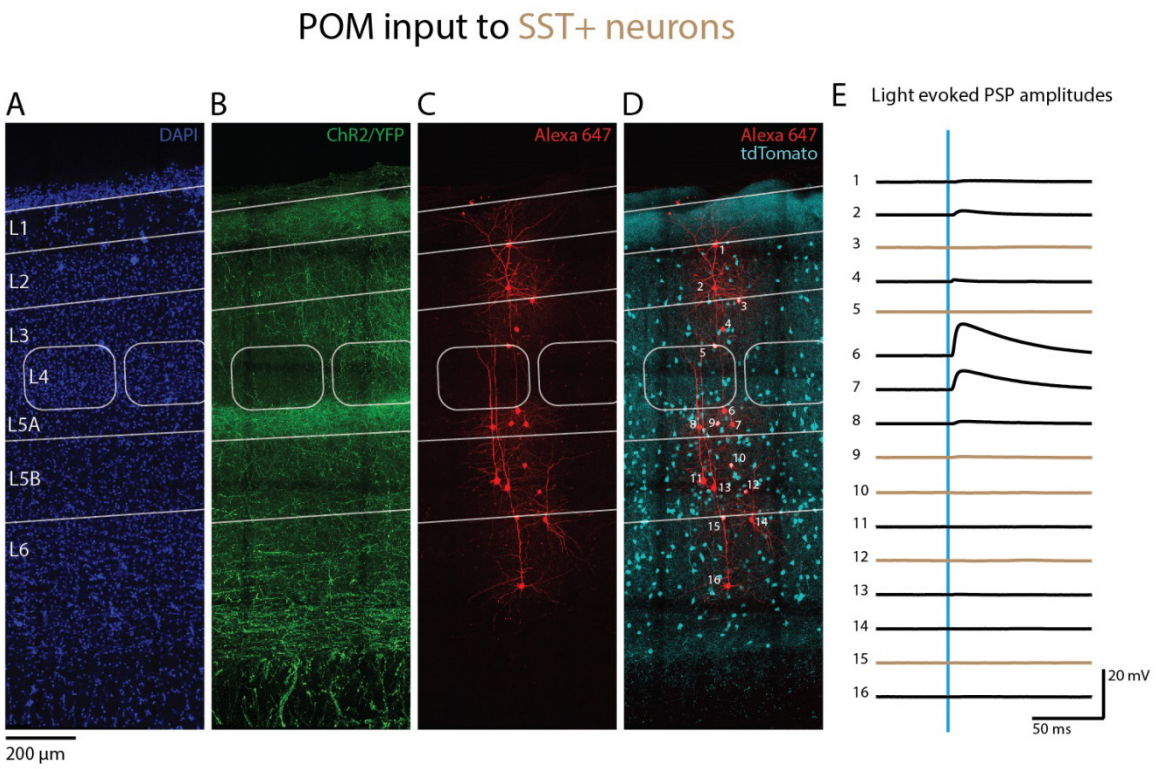

Figure 2.15 POM input to SST expressing neurons. Confocal images of a parasagittal slice of wS1 after fixation. Images are maximum intensity projections of a confocal z-stack **(A)** DAPI staining (blue). **(B)** Expression of ChR2/YFP (green) in the POM axons. **(C)** Recorded neurons with Alexa647 (red). **(D)** SST neurons with tdTomato reporter (cyan) and recorded neurons with Alexa647 (red). Targeted SST neurons are shown in white in the overlay of cyan and red fluorescence. **(E)** Light-evoked postsynaptic potentials from the recorded excitatory (black) and SST (brown) neurons after 1 ms blue light pulse. Numbers on the left of the PSP traces indicate the recorded neurons in the confocal image.

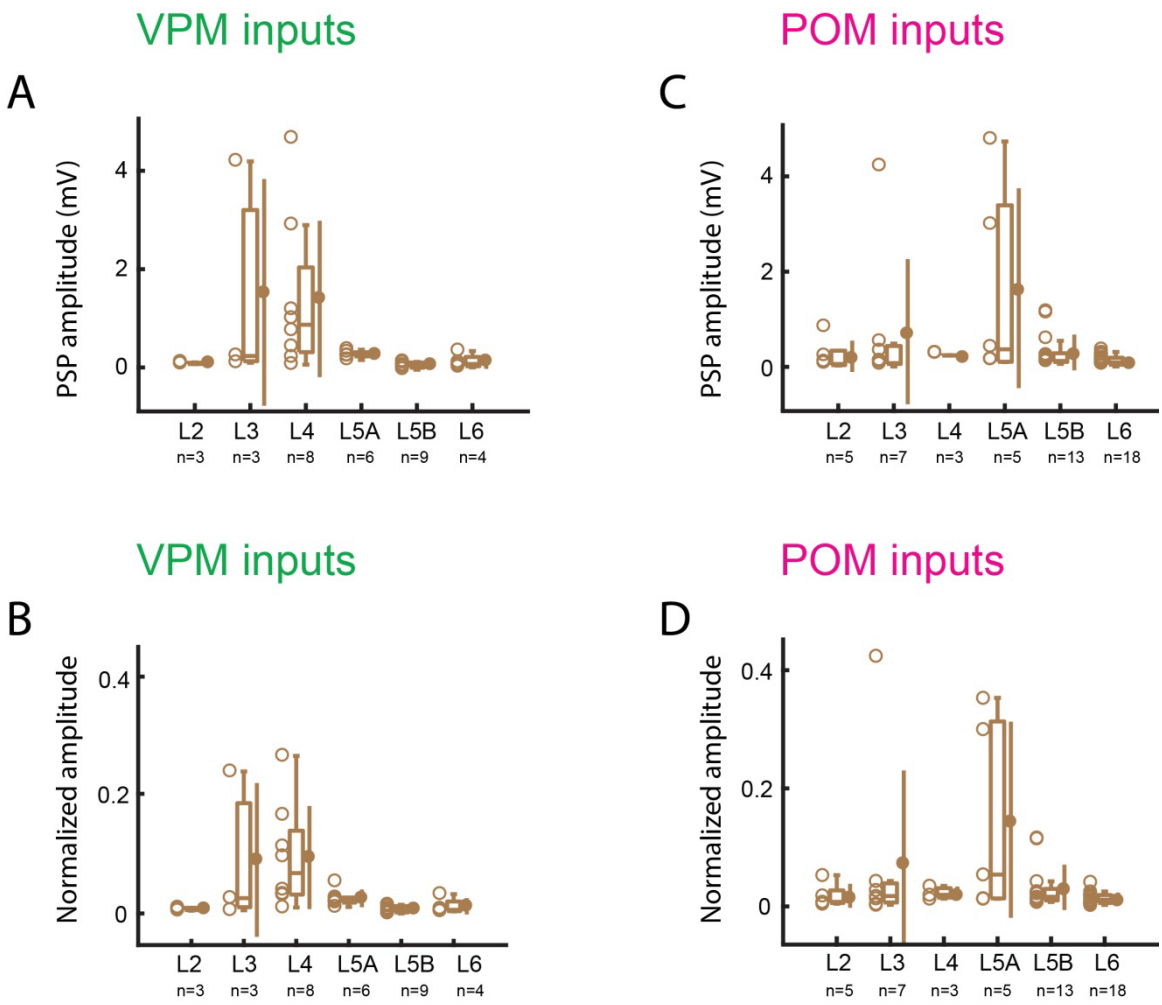

Figure 2.16 Population data of thalamocortical input to SST expressing neurons. (A) VPM-evoked postsynaptic potentials in SST neurons across different layers. **(B)** VPM-evoked postsynaptic potentials in SST neurons across different layers, normalized to the average input of inputs to L4 excitatory neurons in the same slice per experiment **(C)** POM-evoked postsynaptic potentials in SST neurons across different layers. **(D)** POM-evoked postsynaptic potentials in SST neurons across different layers, normalized to the average of inputs to L5A excitatory neurons in the same slice per experiment.

We observed VPM-evoked postsynaptic potentials in SST neurons in every layer of the cortical column, even though the responses were very weak compared to PV and excitatory neurons. We present responses having maxium of 30 mV PSP amplitude in L4 excitatory neurons. Maxiumum mean response was in L4 however, it was not significantly different from other layers (1.44 ± 1.59 mV (median: 0.91 mV), mean ± SD; ; L4 vs. L2: p = 0.4355, L4 vs L3: p = 1, L4 vs L5A: p = 0.3422, L4 vs L5B: p =

0.190, L4 vs L6: p = 0.3578) (Figure 2.16A, Table 2.5). Normalized data also gave a slightly different input distribution across layers. Normalized mean PSP amplitude was maximum in L4 (0.09 ± 0.09 (median: 0.07), mean ± SD), however, it was not significantly different than other layers except L5B (L4 vs. L2: p = 0.2531, L4 vs L3: p = 1, L4 vs L5A: p = 0.2589, L4 vs L5B: p = 0.0429, L4 vs L6: p = 0.2103) (Figure 2.16B, Table 2.5).

We found that POM-evoked postsynaptic potentials in SST neurons were present in every layer of the cortical column, however, input strength was again much weaker than PV and excitatory neurons, as we observed for VPM inputs. Here we present responses having a maximum of 30 mV PSP amplitude in L5A excitatory neurons. Maximum mean response was in L5A (1.66 ± 2.09 mV (median: 0.38 mV), mean ± SD; L5A vs. L2: p = 0.1164, L5A vs L3: p = 0.4763, L5A vs L4: p = 0.2449, L5A vs L5B: p = 0.0521, L5A vs L6: p = 0.0122) (Figure 2.16C,D). Neurons whose cell bodies located in L6 had smaller inputs than L5A (Table 2.6). We observed a similar input distribution across layers in the normalized data as well. Maximum normalized mean PSP amplitude was in L5A (0.15 ± 0.17 (median: 0.05), mean ± SD), however, it was not significantly different from other layers except L6 (L5A vs. L2: p = 0.1158, L5A vs L3: p = 0.6372, L5A vs L4: p = 0.2667, L5A vs L5B: p = 0.0778, L5A vs L6: p = 0.0177).

In summary, SST neurons seemed to have a similar pattern of thalamic input distribution across layers in excitatory neurons, however, the amplitudes were much smaller, almost non-existent compared to excitatory neurons. Our results are in agreement with prior studies (Cruikshank et al., 2007; Tan et al., 2008; Hu and Agmon, 2016; Audette et al., 2018).

Thalamic input onto Vasoactive Instestinal Peptide expressing neurons

To investigate the thalamic input onto VIP neurons, we used VIP-Cre/LSL-tdTomato transgenic mice. Having tdTomato expression in VIP neurons allowed us to target them for whole-cell patch-clamp recordings.

We recorded cells across all layers within the same slice (Figure 2.17, 2.18). We used three different light powers per recording to see responses in different stimulation strengths. We mostly recorded from two nearby neurons simultaneously. To be able to map VPM and POM input distribution of the entire column, we again recorded excitatory neurons in every layer. VPM or POM fiber activation generated postsynaptic potentials in VIP neurons. VPM activation evoked the largest response in L3 and it was followed by L4 (Figure 2.16). On the other hand, POM activation created the largest PSPs in L5A (Figure 2.19). We normalized the responses across layers to the mean strength of excitatory neurons in L4 for VPM and L5A for POM to have an accurate comparison between experiments (Figure 2.19B,D).

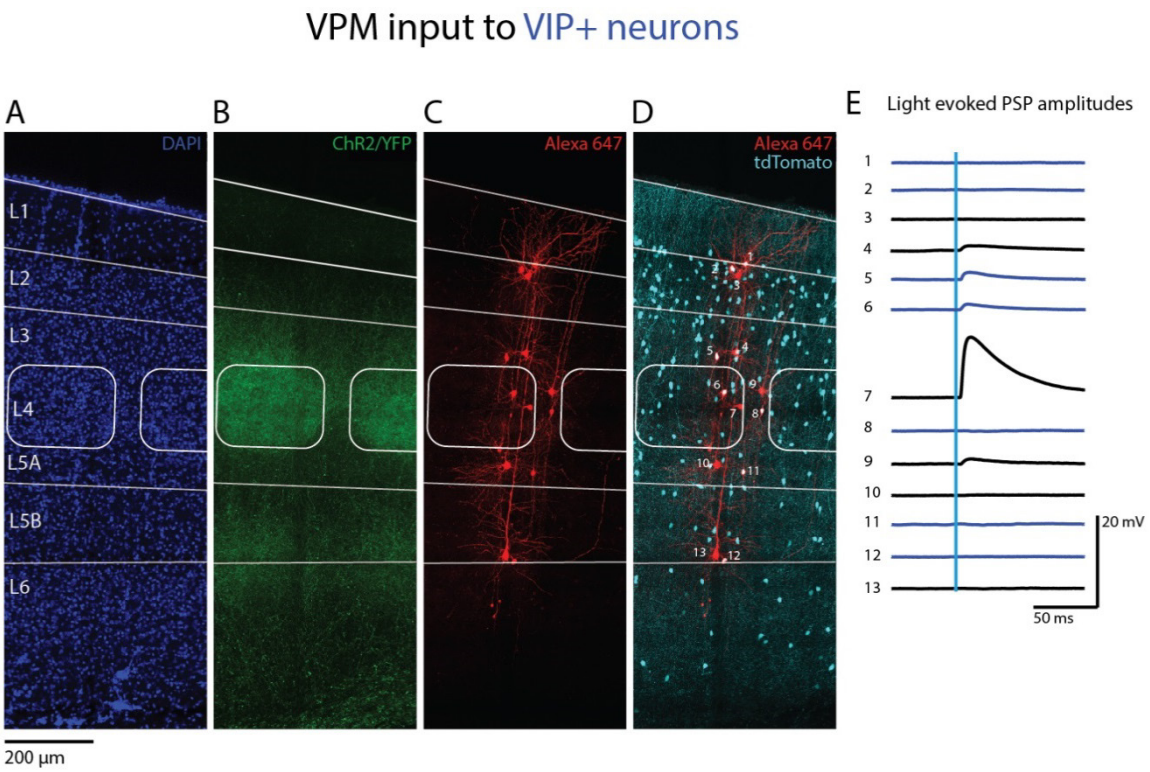

Figure 2.17 VPM input to VIP expressing neurons. Confocal images of a parasagittal slice of wS1 after fixation. Images are maximum intensity projections of a confocal z-stack **(A)** DAPI staining (blue). **(B)** Expression of ChR2/YFP (green) in the VPM axons. **(C)** Recorded neurons with Alexa647 (red). **(D)** VIP neurons with tdTomato reporter (cyan) and recorded neurons with Alexa647 (red). Targeted VIP neurons are shown in white in the overlay of cyan and red fluorescence. **(E)** Light-evoked postsynaptic potentials from the recorded excitatory (black) and VIP (blue) neurons after 1 ms blue light pulse. Numbers on the left of the PSP traces indicate the recorded neurons in the confocal image.

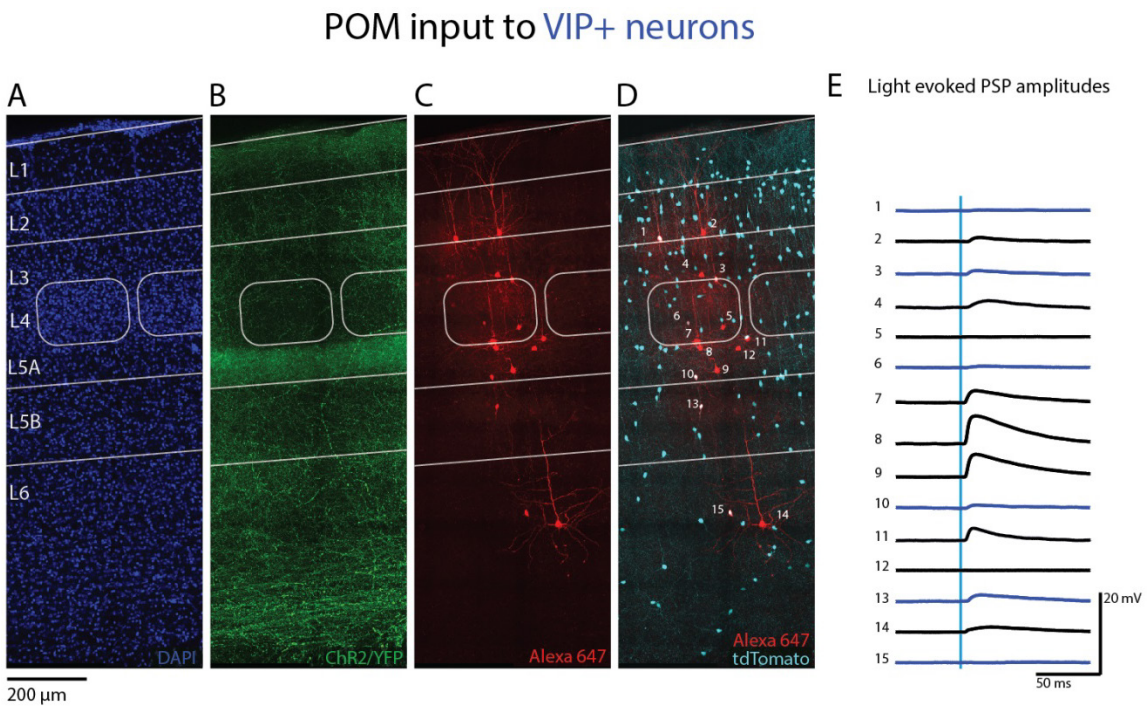

Figure 2.18 POM input to VIP expressing neurons. Confocal images of a parasagittal slice of wS1 after fixation. Images are maximum intensity projections of a confocal z-stack **(A)** DAPI staining (blue). **(B)** Expression of ChR2/YFP (green) in the POM axons. **(C)** Recorded neurons with Alexa647 (red). **(D)** VIP neurons with tdTomato reporter (cyan) and recorded neurons with Alexa647 (red). Targeted VIP neurons are shown in white in the overlay of cyan and red fluorescence. **(E)** Light-evoked postsynaptic potentials from the recorded excitatory (black) and VIP (blue) neurons after 1 ms blue light pulse. Numbers on the left of the PSP traces indicate the recorded neurons in the confocal image.

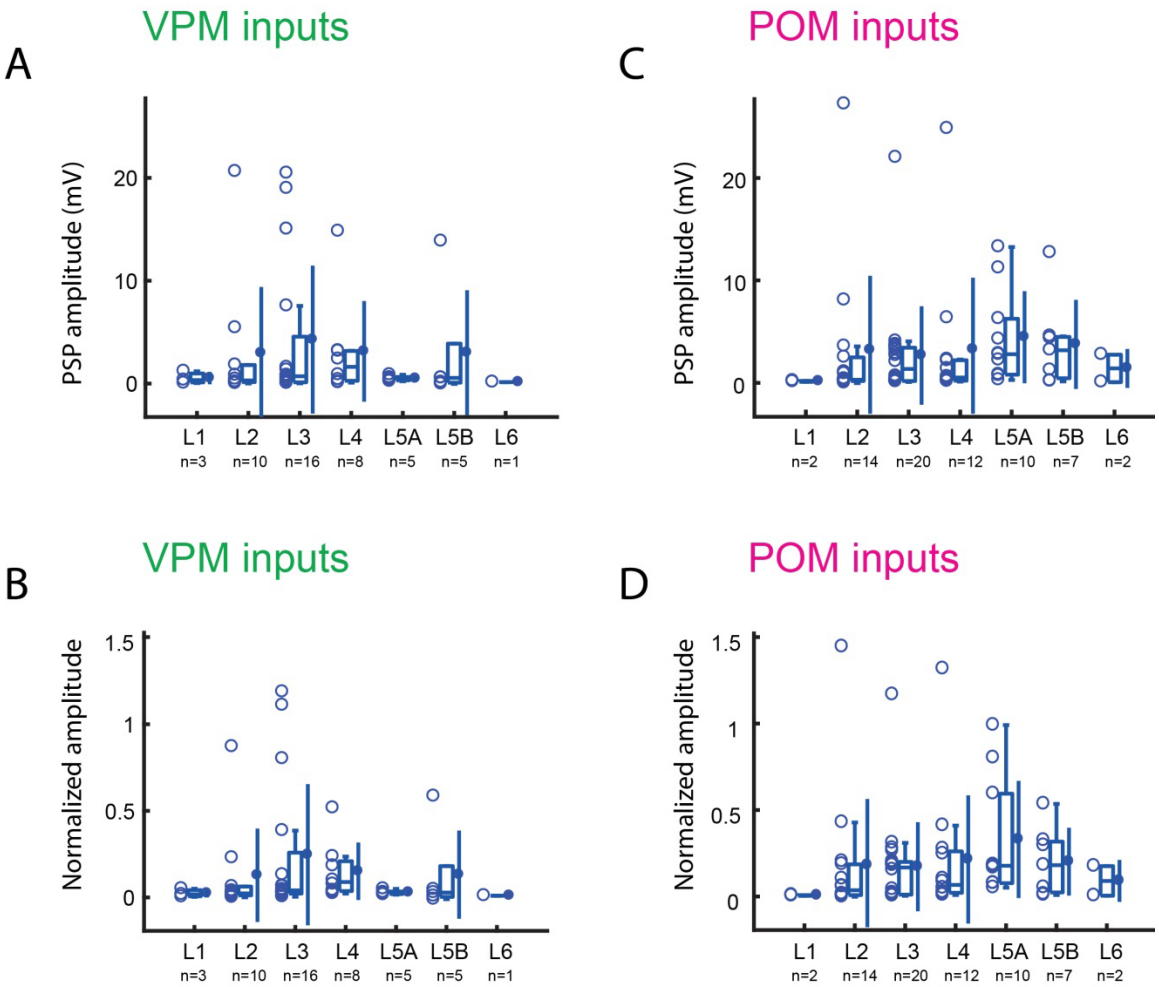

Figure 2.19 Population data of thalamocortical input to VIP neurons. (A) VPM-evoked postsynaptic potentials in VIP neurons across different layers. **(B)** VPM-evoked postsynaptic potentials in VIP neurons across different layers, normalized to the average of inputs to L4 excitatory neurons in the same slice per experiment **(C)** POM-evoked postsynaptic potentials in VIP neurons across different layers. **(D)** POM-evoked postsynaptic potentials in VIP neurons across different layers, normalized to the average of inputs to L5A excitatory neurons in the same slice per experiment.

We observed VPM-evoked postsynaptic potentials in VIP neurons in every layer of the cortical column. We present responses having a maximum of 30 mV PSP amplitude in L4 excitatory neurons. In addition, we also recorded VIP positive neurons in L1 and VPM fiber activation evoked direct postsynaptic potentials (Figure 2.19). Unlike excitatory, PV and SST neurons, for VIP neurons maximum mean response was in L3 (4.28 ± 7.18 mV (median: 0.7 mV), mean ± SD) and

followed by L4 (3.13 ± 4.90 mV (median: 1.62), mean ± SD) (Figure 2.19A). We did not find any significant difference between layers (L4 vs L1: p = 0.9948, L4 vs. L2: p = 1, L4 vs L3: p = 0.9994, L4 vs L5A: p = 0.9858, L4 vs L5B: p = 1, L4 vs L6: p = 0.9991). Neurons whose cell bodies located in other layers had smaller inputs (Table 2.7). Normalized data also gave a similar input distribution across layers. In the same slice, maximum average PSP amplitude was observed in L3 (0.25 ± 0.41 (median: 0.04), mean ± SD) and followed by L4 (0.15 ± 0.17 (median: 0.24), mean ± SD) (Figure 2.19B, Table 2.7), however, we again did not find any significant difference between layers (L4 vs L1: p = 0.9952, L4 vs. L2: p = 1, L4 vs L3: p = 0.9889, L4 vs L5A: p = 0.9902, L4 vs L5B: p = 1, L4 vs L6: p = 0.9993).

POM-evoked postsynaptic potentials in VIP neurons were also observed in every layer of the cortical column. We present responses having maxium of 30 mV PSP amplitude in L5A excitatory neurons. As we observed for VPM inputs, POM-evoked PSP amplitudes of VIP neurons were larger than SST neurons, however smaller than PV and excitatory neurons. Maxiumum mean response was in L5A (4.45 ± 4.49 mV (median: 2.79 mV), mean ± SD) (Figure 2.16C,D, Table 2.8), however, we did not find any significant difference between layers (L5A vs L1: p = 0.9578, L5A vs. L2: p = 0.9982, L5A vs L3: p = 0.9837, L5A vs L4: p = 0.9989, L5A vs L5B: p = 1, L5A vs L6: p = 0.9929). Normalized data also gave a very similar input distribution. Normalized mean PSP was maximum in L5A (0.33 ± 0.34 (median: 0.18), mean ± SD), however, it was not significantly different from other layers (L5A vs L1: p = 0.8362, L5A vs. L2: p = 0.9131, L5A vs L3: p = 0.8522, L5A vs L4: p = 0.9774, L5A vs L5B: p = 0.9813, L5A vs L6: p = 0.9560).

VPM and POM activation generated PSP amplitudes in VIP cells and these inputs were larger than what we observed in SST neurons, however, mostly smaller than PV and excitatory neurons. We did not observe any significant difference in input strength among layers.

Comparison of thalamic input to different cell types

After measuring all the thalamic inputs to different cell types across different layers of wS1, we found that on average, excitatory and PV cells received the strongest mean input, especially in the input layers (L4 and L5A) (Figure 2.20). SST neurons received very weak inputs compared to the other cell types (Figure 2.20). VIP neurons did not necessarily receive the strongest inputs in the main input layers (L4 and L5A) (Figure 2.20) and inputs were heterogeneous within layers.

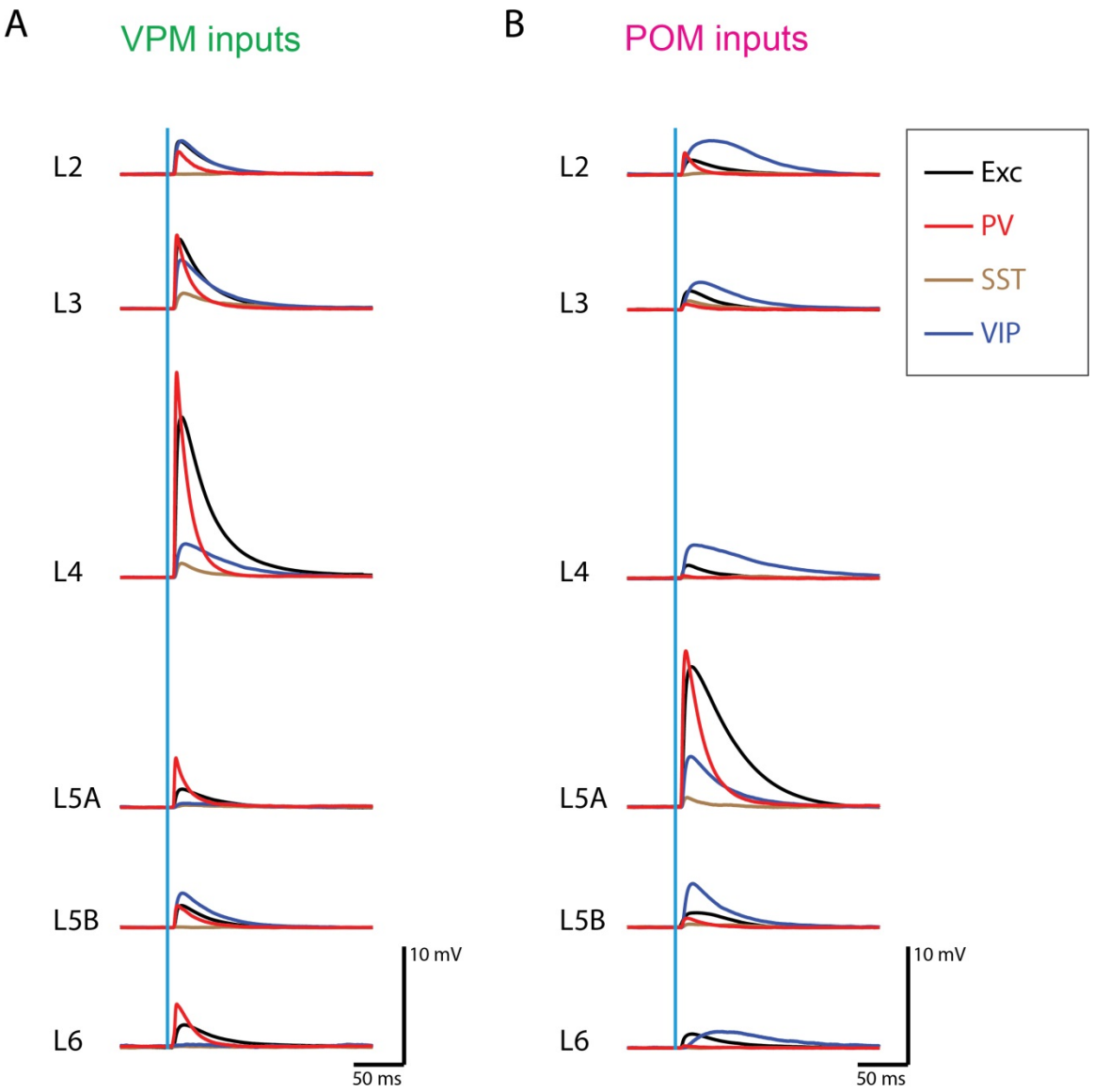

Figure 2.20 Grand averages of VPM and POM evoked responses in different cell types across all layers of wS1. Mean PSPs evoked by VPM and POM afferents. **(A)** VPM fiber activation and light-evoked postsynaptic potentials in excitatory (black), PV (red), SST

(brown) and VIP (blue) neurons across all layers of wS1. **(B)** POM fiber activation and light-evoked postsynaptic potentials in excitatory (black), PV (red), SST (brown) and VIP (blue) neurons across all layers of wS1.

In the normalized data for VPM inputs, excitatory neurons in L4 showed significantly higher mean PSP response compared to all other groups except L4 PV and L6 VIP neurons (Figure 2.21A) (L4 excitatory vs other groups: maximum $p < 0.026$ except L4 excitatory vs L4 PV: $p = 1$ & L4 excitatory vs L6 VIP: $p= 0.737$). We saw the same result for L4 PV neurons (L4 PV vs other groups: maximum $p<0.007$ except L4 PV vs L4 excitatory: $p = 1$ & L4 PV vs L6 VIP: $p = 0.502$).

Among the normalized POM inputs, excitatory neurons in L5A showed significantly larger mean PSP response compared to all other groups except L5A PV and L6 VIP neurons (Figure 2.21B) (L5A excitatory vs other groups: maximum $p < 0.044$ except L5A excitatory vs L5A PV: $p = 1$ & L5A excitatory vs L6 VIP: $p = 0.118$). We saw the same result for L4 PV neurons (L4 PV vs other groups: maximum $p < 0.020$ except L5A PV vs L5A excitatory: $p = 1$ & L5A PV vs L6 VIP: $p = 0.055$).

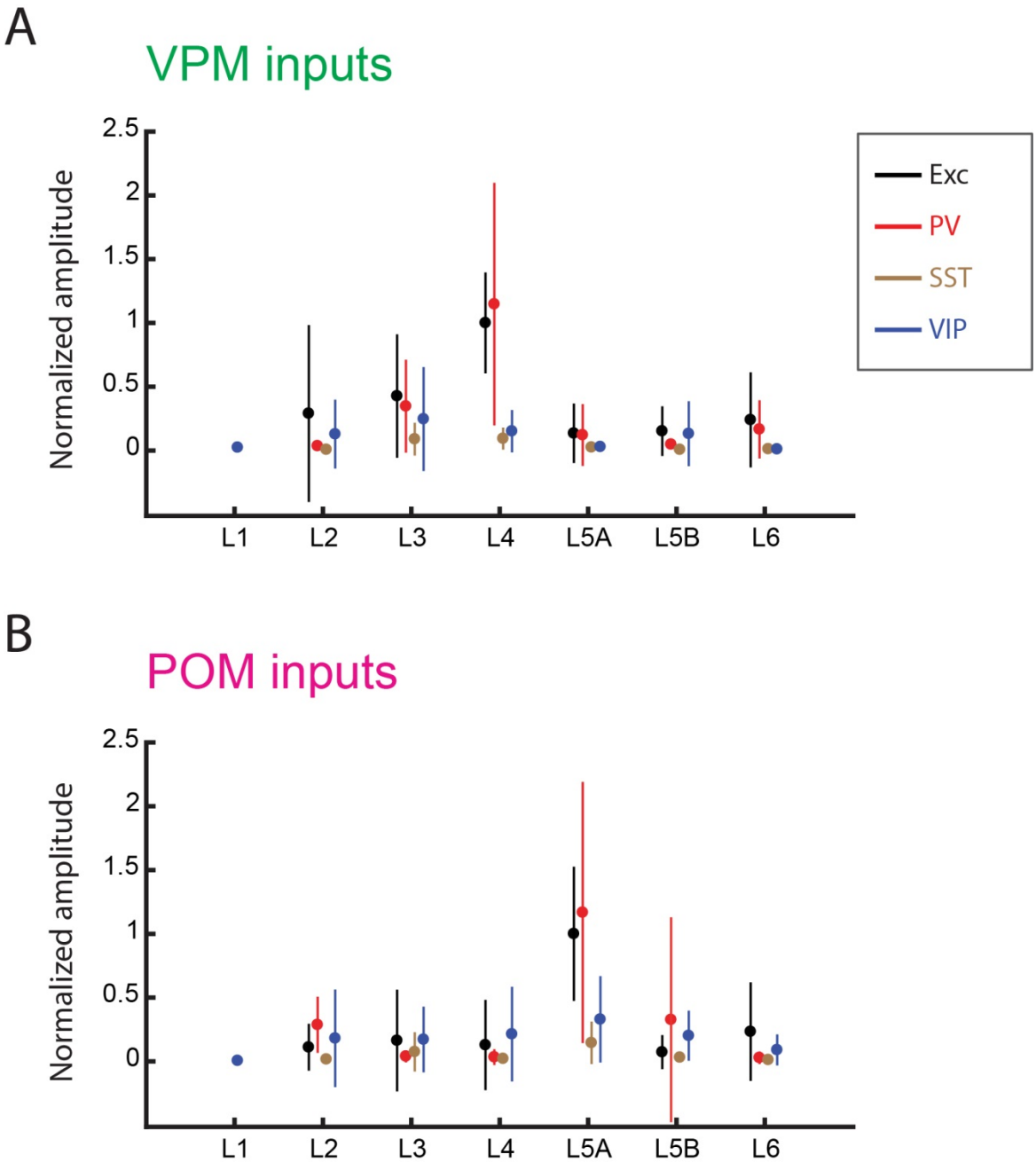

Figure 2.21 Normalized mean responses of different cell types to VPM and POM stimulation across all layers of wS1. Normalized mean PSPs evoked by VPM and POM afferents. **(A)** VPM-evoked postsynaptic potentials in excitatory, PV, SST and VIP neurons across different layers, normalized to the average of inputs to L4 excitatory neurons in the same slice per experiment. **(B)** POM-evoked postsynaptic potentials in excitatory, PV, SST and VIP neurons across different layers, normalized to the average of inputs to L5A excitatory neurons in the same slice per experiment.

Discussion

In this chapter, we used electrophysiological methods to isolate thalamocortical inputs to different cell types in different layers of wS1. We showed that responses in excitatory neurons tend to correlate with the axonal innervation pattern. PV neurons showed a similar pattern to excitatory neurons with similar PSP amplitudes. SST neurons received direct inputs with similar layer distribution as excitatory and PV neurons, however, their response amplitudes were much smaller. VIP neurons also received direct thalamic inputs in every layer, however, input distribution was not similar to the excitatory, PV and SST neurons.

Thalamic input onto excitatory neurons seem to correlate with the axonal innervation

We found that the synaptic input from VPM and POM onto excitatory neurons have a tendency to correlate with their innervation pattern. Some prior studies suggested that this could be thalamocortical input pattern for sensory systems (Petreanu et al., 2007; Meyer et al., 2010; Cruikshank et al., 2010).

For VPM, even though the axons are the densest in L4, we observed strong responses in L3, in some cases larger than L4; however, we found the biggest mean response in L4. It has been shown that VPM activates deep layers of the barrel cortex as strong as L4 (Constantinople and Bruno, 2013). We did not observe the same input strength between L4 and deeper layers; however, we confirmed that there were direct synaptic inputs to deep layers. Moreover, taking advantage of dual patch recordings, we were able to monitor two cells simultaneously during VPM fiber activation. We found that, the same cell types located in the same layer could give very different responses, mostly in L2 and 3. This shows that the VPM axons could be highly selective even among the same cell types. Same cell types in the same layer receiving very different input might suggest that maybe these cells are different types according to their projection patterns.

For POM, we observed that these axons are targeting L5A pyramidal neurons specifically. Direct synaptic inputs were observed in every layer; however, L5A inputs to pyramidal neurons were mostly 10 folds greater than other layers.

PV neurons receive the same pattern of thalamic input as excitatory neurons

We found that thalamocortical axons seem to activate PV neurons whenever they are targeting adjacent excitatory cells. Input distribution pattern across layers was very similar to excitatory neurons. Input strength was not always stronger than the neighboring excitatory cells as shown before in prior studies (Cruikshank et al., 2010; Audette et al., 2018). This might be due to using different preparations. We used a 1 mm fiber to activate thalamocortical afferents. Our experiments were in the presence of TTX, 4-AP, and PTX and we used parasagittal slices. In their study, Cruikshank et al. (2010) used standard ACSF without any pharmacological agents which keeps the feedforward inhibiton intact. This could decrease the PSP responses in excitatory cells dramatically. In the study from Audette et al. (2018), they measured light-evoked EPSCs with and without TTX and 4-AP. In case of no drugs, PV and excitatory neurons' response strength was almost the same. With TTX and 4-AP, PV neurons responded two folds bigger than excitatory neurons. Since they have done voltage-clamp recordings, our results from current-clamp recordings cannot be compared easily, since we are not clamping any properties of neurons in our recordings. In summary, we observed that PV neurons, on average, received inputs as strong as excitatory neurons from thalamus.

SST neurons are not preferred by the thalamus

One prior anatomical study suggests that thalamus targets SST neurons in somatosensory cortex (Wall et al., 2016) and found that SST neurons received direct input from both VPM and POM in every layer; however, the inputs we found were very weak compared to the other cell types investigated. This result is in agreement with previous studies (Staiger et al., 1996; Porter et al., 2001; Swadlow and Gusev, 2002; Cruikshank et al., 2007; Tan et al., 2008; Hu and Agmon, 2016; Audette et al., 2018). These neurons are mostly more depolarized and more excitable from the

other neuron types (Table 2.12), yet, the evoked PSPs were feeble. This also demonstrates the weakness of thalamocortical synaptic strength to SST neurons.

In our experimental conditions using TTX and 4-AP, we might be undercounting the thalamic synaptic strength onto SST neurons. It has been shown that thalamocortical axons are strongly facilitating (Tan et al., 2008; Hu and Agmon, 2016). We were using single 1 ms light pulses, and the glutamate release was not mediated by an action potential. The release was purely depended on ChR2 kinetics. It is possible that burst activity *in vivo* might enhance the weak VPM and POM inputs to SST neurons. It is a possibility that these state-dependent enhancements could not be detected in our assay.

VIP neurons receive a different thalamic input pattern from the other cell types

The thalamic input to VIP neurons was not necessarily correlated with the thalamocortical innervation pattern.

For VPM, we observed the biggest mean response in L3 VIP neurons, in contrast to all the other cell types. We found some VPM inputs to L1 VIP neurons which were not expected since the VPM innervation in this layer is the weakest. It seemed that there was a tendency to activate not only L4 but also L2/3 and even 1.

For POM, we observed the biggest mean input response in L5A VIP neurons. We found also strong POM inputs to L4 VIP neurons. In L4, all the other cell types receive weak or no input from POM, in contrast to VIP neurons. L2/3 cells were also targeted by POM.

These results suggest that thalamocortical input activate the VIP neurons in their main input layers (L4 and L5A); however, they also activate the neurons in L2/3. VIP neurons are known to inhibit SST neurons (Lee et al., 2013; Pfeffer et al., 2013). Since SST neurons target mostly distal dendrites of excitatory neurons, silencing them can evoke disinhibition and the overall potentiation of the cortex. Thalamocortical targeting of VIP cells might be related to amplification of their input.

Tables

VPM evoked EPSPs	L2	L3	L4	L5A	L5B	L6
Amplitude (mV)	**n=18**	**n=32**	**n=54**	**n=28**	**n=32**	**n=24**
mean ± SD	2.86 ± 6.79	6.33 ± 6.26	14.57 ± 7.94	1.65 ± 2.27	2.05 ± 2.56	2.07 ± 2.85
median	0.12	4.09	12.73	0.74	0.78	0.64
interquartile range	1.65 - 0.08	11.31 - 0.78	22.33 - 8.69	2.48 - 0.19	3.38 - 0.17	3.48 - 0.23
Norm amplitude	**n=18**	**n=32**	**n=54**	**n=28**	**n=32**	**n=24**
mean ± SD	0.29 ± 0.69	0.4 ± 0.48	1 ± 0.39	0.14 ± 0.23	0.15 ± 0.19	0.24 ± 0.37
median	0.01	0.24	1	0.054	0.054	0.074
interquartile range	0.08 - 0.01	0.63 - 0.06	1.22 - 0.77	0.12 - 0.02	0.23 - 0.02	0.30 - 0.01

Table 2.1 VPM-evoked EPSPs in excitatory neurons

POM evoked EPSPs	L2	L3	L4	L5A	L5B	L6
Amplitude (mV)	**n=38**	**n=31**	**n=37**	**n=74**	**n=49**	**n=44**
mean ± SD	1.26 ± 2.65	1.78 ± 4.08	1.29 ± 3.63	11.63 ± 7.89	0.732 ± 1.53	1.49 ± 2.20
median	0.29	0.43	0.11	10.41	0.22	0.68
interquartile range	0.96 - 0.15	1.36 - 0.09	0.31 - 0.08	18.38 - 4.97	0.64 - 0.10	1.83 - 0.10
Norm amplitude	**n=38**	**n=31**	**n=37**	**n=74**	**n=49**	**n=44**
mean ± SD	0.11 ± 0.18	0.16 ± 0.39	0.13 ± 0.36	1 ± 0.53	0.07 ± 0.13	0.23 ± 0.39
median	0.03	0.05	0.01	1	0.02	0.07
interquartile range	0.14 - 0.01	0.13 - 0.01	0.04 - 0.01	1.26 - 0.73	0.06 - 0.01	0.23 - 0.01

Table 2.2 POM-evoked EPSPs in excitatory neurons

VPM evoked EPSPs (PV)	L2	L3	L4	L5A	L5B	L6
Amplitude (mV)	**n=3**	**n=9**	**n=14**	**n=5**	**n=13**	**n=5**
mean ± SD	0.56 ± 0.54	6.67 ± 7.32	18.47 ± 13.09	2.33 ± 4.75	0.75 ± 0.58	2.15 ± 2.71
median	0.34	3.34	18.51	0.18	0.65	0.31
interquartile range	0.97 - 0.21	9.67 - 1.30	27.69 - 4.53	3.02 - 0.13	0.95 - 0.37	4.84 - 0.13
Norm amplitude	**n=3**	**n=9**	**n=14**	**n=5**	**n=13**	**n=5**
mean ± SD	0.04 ± 0.03	0.35 ± 0.36	1.15 ± 0.95	0.12 ± 0.24	0.05 ± 0.03	0.16 ± 0.22
median	0.03	0.19	1.05	0.02	0.05	0.03
interquartile range	0.06 - 0.01	0.47 - 0.11	1.42 - 0.39	0.15 - 0.01	0.06 - 0.03	0.32 - 0.01

Table 2.3 VPM-evoked EPSPs in PV neurons

POM evoked EPSPs (PV)	L2	L3	L4	L5A	L5B	L6
Amplitude (mV)	**n=5**	**n=7**	**n=8**	**n=8**	**n=11**	**n=10**
mean ± SD	2.05 ± 1.23	0.58 ± 0.72	0.33 ± 0.59	13.97 ± 13.43	3.27 ± 7.93	0.27 ± 0.47
median	2.4	0.17	0.12	8.71	0.29	0.09
interquartile range	2.68 - 1.46	1.07 - 0.11	0.19 - 0.08	24.46 - 3.65	2.21 - 0.13	0.14 - 0.07
Norm amplitude	**n=5**	**n=7**	**n=8**	**n=8**	**n=10**	**n=10**
mean ± SD	0.29 ± 0.22	0.04 ± 0.05	0.03 ± 0.06	1.17 ± 1.02	0.33 ± 0.80	0.03 ± 0.05
median	0.32	0.03	0.01	0.79	0.02	0.01
interquartile range	0.40 - 0.13	0.06 - 0.01	0.02 - 0.01	2.13 - 0.39	0.18 - 0.01	0.03 - 0.00

Table 2.4 POM-evoked EPSPs in PV neurons

VPM evoked EPSPs (SST)	L2	L3	L4	L5A	L5B	L6
Amplitude (mV)	**n=3**	**n=3**	**n=8**	**n=6**	**n=9**	**n=4**
mean ± SD	0.13 ± 0.01	1.55 ± 2.32	1.44 ± 1.59	0.29 ± 0.07	0.09 ± 0.06	0.16 ± 0.15
median	0.12	0.28	0.91	0.28	0.08	0.11
interquartile range	0.14 - 0.11	3.24 - 0.17	2.08 - 0.35	0.35 - 0.27	0.14 - 0.04	0.26 - 0.07
Norm amplitude	**n=3**	**n=3**	**n=8**	**n=6**	**n=9**	**n=4**
mean ± SD	0.01 ± 0.00	0.09 ± 0.13	0.09 ± 0.09	0.03 ± 0.01	0.01 ± 0.01	0.01 ± 0.01
median	0.01	0.03	0.07	0.02	0.01	0.01
interquartile range	0.01 - 0.01	0.18 - 0.01	0.14 - 0.03	0.03 - 0.02	0.01 - 0.00	0.02 - 0.00

Table 2.5 VPM-evoked EPSPs in SST neurons

POM evoked EPSPs (SST)	L2	L3	L4	L5A	L5B	L6
Amplitude (mV)	**n=5**	**n=7**	**n=3**	**n=5**	**n=13**	**n=18**
mean ± SD	0.23 ± 0.33	0.78 ± 1.52	0.25 ± 0.00	1.66 ± 2.09	0.31 ± 0.38	0.12 ± 0.88
median	0.07	0.09	0.25	0.38	0.14	0.1
interquartile range	0.35 - 0.05	0.45 - 0.07	0.25 - 0.25	3.40 - 0.12	0.29 - 0.11	0.20 - 0.06
Norm amplitude	**n=5**	**n=7**	**n=3**	**n=5**	**n=13**	**n=18**
mean ± SD	0.02 ± 0.02	0.07 ± 0.15	0.02 ± 0.01	0.15 ± 0.17	0.03 ± 0.04	0.01 ± 0.01
median	0.01	0.02	0.02	0.05	0.02	0.01
interquartile range	0.03 - 0.00	0.04 - 0.01	0.03 - 0.01	0.31 - 0.01	0.03 - 0.01	0.02 - 0.00

Table 2.6 POM-evoked EPSPs in SST neurons

VPM evoked EPSPs (VIP)	L1	L2	L3	L4	L5A	L5B	L6
Amplitude (mV)	**n=3**	**n=10**	**n=16**	**n=8**	**n=5**	**n=5**	**n=1**
mean ± SD	0.53 ± 0.60	2.97 ± 6.42	4.28 ± 7.18	3.13 ± 4.90	0.48 ± 0.25	3.01 ± 6.06	0.14
median	0.34	0.3	0.7	1.62	0.41	0.55	0.14
interquartile range	0.96 - 0.12	1.81 - 0.15	4.57 - 0.13	3.18 - 0.28	0.65 - 0.31	3.88 - 0.09	N/A
Norm amplitude	**n=3**	**n=10**	**n=16**	**n=8**	**n=5**	**n=5**	**n=1**
mean ± SD	0.02 ± 0.02	0.13 ± 0.27	0.25 ± 0.41	0.15 ± 0.17	0.03 ± 0.01	0.13 ± 0.25	0.01
median	0.02	0.02	0.04	0.09	0.03	0.03	0.01
interquartile range	0.04 - 0.01	0.06 - 0.01	0.26 - 0.02	0.21 - 0.04	0.03 - 0.02	0.18 - 0.00	N/A

Table 2.7 VPM-evoked EPSPs in VIP neurons

POM evoked EPSPs (VIP)	L1	L2	L3	L4	L5A	L5B	L6
Amplitude (mV)	**n=2**	**n=14**	**n=20**	**n=12**	**n=10**	**n=7**	**n=2**
mean ± SD	0.14 ± 0.07	3.19 ± 7.25	2.67 ± 4.79	3.25 ± 7.01	4.45 ± 4.49	3.76 ± 4.34	1.41 ± 1.90
median	0.14	0.31	1.36	0.52	2.79	3.19	1.41
interquartile range	0.19 - 0.09	2.49 - 0.19	3.44 - 0.18	2.21 - 0.21	6.25 - 0.80	4.49 - 0.45	2.75 - 0.07
Norm amplitude	**n=2**	**n=14**	**n=20**	**n=12**	**n=10**	**n=7**	**n=2**
mean ± SD	0.01 ± 0.00	0.18 ± 0.38	0.17 ± 0.26	0.21 ± 0.37	0.33 ± 0.34	0.20 ± 0.19	0.09 ± 0.12
median	0.01	0.04	0.17	0.07	0.18	0.18	0.09
interquartile range	0.01 - 0.00	0.19 - 0.01	0.20 - 0.01	0.26 - 0.02	0.59 - 0.08	0.32 - 0.24	0.18 - 0.00

Table 2.8 POM-evoked EPSPs in VIP neurons

VPM-evoked PSP properties (EXC)	L2	L3	L4	L5A	L5B	L6
Synaptic delay (ms)	**n=5**	**n=21**	**n=53**	**n=12**	**n=14**	**n=10**
median	2.85	3.45	3.55	3.05	3.6	3.58
interquartile range	3.1 - 2.67	3.7 - 3.09	3.71 - 3.23	3.78 - 2.58	3.9 - 3.2	3.85 - 3
PSP half-width (ms)	**n=5**	**n=21**	**n=53**	**n=12**	**n=14**	**n=10**
median	21.7	23.68	26.2	32.4	28	31.25
interquartile range	29.11 - 19.49	28.95 - 16.7	31.63 - 20.79	38.4 - 26.88	34 - 19.1	41.95 - 22.5

VPM-evoked PSP properties (PV)	L2	L3	L4	L5A	L5B	L6
Synaptic delay (ms)		**n=7**	**n=14**	**n=1**	**n=3**	**n=2**
median		3.35	3.05	2.85	2.9	1.65
interquartile range		3.54 - 3.05	3.3 - 3	N/A	4.18 - 1.89	1.85 - 1.5
PSP half-width (ms)	**n=1**	**n=8**	**n=14**	**n=1**	**n=3**	**n=2**
median	13.7	11	10.95	9	13.15	15.85
interquartile range	N/A	18.98 - 9.37	14.05 - 8.05	N/A	24.25 - 8.09	20.8 - 10.9

VPM-evoked PSP properties (SST)	L2	L3	L4	L5A	L5B	L6
Synaptic delay (ms)		**n=1**	**n=4**			
median		4.15	4.03			
interquartile range		N/A	4.5 - 3.63			
PSP half-width (ms)			**n=4**			
median			20.13			
interquartile range			24.58 - 18.8			

VPM-evoked PSP properties (VIP)	L2	L3	L4	L5A	L5B	L6
Synaptic delay (ms)	**n=3**	**n=6**	**n=4**		**n=1**	
median	3.05	3.85	3.83		3.05	
interquartile range	3.69 - 3.01	3.95 - 3.3	4 - 2.95		N/A	
PSP half-width (ms)	**n=3**	**n=6**	**n=4**		**n=1**	
median	23.7	31.98	47.68		32.6	
interquartile range	28.01 - 21.75	37.35 - 25.45	52.42 - 34.18		N/A	

Table 2.9 VPM-evoked PSP properties

POM-evoked PSP properties (EXC)	L2	L3	L4	L5A	L5B	L6
Synaptic delay (ms)	**n=9**	**n=9**	**n=5**	**n=68**	**n=8**	**n=17**
median	3.4	3.45	3.05	3.75	3.8	3.85
interquartile range	4.16 - 3.08	3.73 - 3.14	3.56 - 2.85	4.1 - 3.28	4.1 - 3.2	4.71 - 3.41
PSP half-width (ms)	**n=9**	**n=11**	**n=6**	**n=69**	**n=9**	**n=20**
median	33.6	25.25	22.63	41.4	40.5	28.68
interquartile range	39.02 - 22.11	39.96 - 22.28	40.95 - 20.95	49.41 - 33.36	53.14 - 29.33	40 - 24.65
POM-evoked PSP properties (PV)	**L2**	**L3**	**L4**	**L5A**	**L5B**	**L6**
Synaptic delay (ms)	**n=4**	**n=2**	**n=1**	**n=7**	**n=5**	**n=1**
median	3.83	3.35	3.1	3.55	3.15	3.65
interquartile range	4.08 - 3.58	3.9 - 3.65	N/A	3.72 - 3.16	4.03 - 2.83	N/A
PSP half-width (ms)	**n=4**	**n=2**	**n=1**	**n=7**	**n=5**	**n=1**
median	10.63	16.88	9.85	17.5	16.35	10.05
interquartile range	12.17 - 8.53	17.2 - 16.55	N/A	18.28 - 15.99	21.69 - 14.12	N/A
POM-evoked PSP properties (SST)	**L2**	**L3**	**L4**	**L5A**	**L5B**	**L6**
Synaptic delay (ms)		**n=1**		**n=2**	**n=2**	
median		3.65		3.73	5	
interquartile range		N/A		3.75 - 3.7	5.75 - 4.25	
PSP half-width (ms)		**n=1**		**n=2**	**n=2**	
median		22.95		25.55	35.8	
interquartile range		N/A		36.3 - 14.8	41.65 - 29.95	
POM-evoked PSP properties (VIP)	**L2**	**L3**	**L4**	**L5A**	**L5B**	**L6**
Synaptic delay (ms)	**n=4**	**n=7**	**n=5**	**n=7**	**n=4**	
median	4.1	4.3	4.5	4.25	4.6	
interquartile range	4.8 - 2.85	5.2 - 3.95	4.52 - 4	4.33 - 3.81	4.93 - 4.33	
PSP half-width (ms)	**n=4**	**n=10**	**n=5**	**n=7**	**n=5**	
median	52.65	31.8	44.75	31.6	30.4	
interquartile range	69.33 - 32.12	50.75 - 27.9	59.19 - 33.89	38.84 - 27.13	45 - 27.38	

Table 2.11 POM-evoked PSP properties

Passive membrane properties (EXC)	L1	L2	L3	L4	L5A	L5B	L6
Membrane potential (mV)		**n=55**	**n=63**	**n=92**	**n=103**	**n=83**	**n=71**
mean ± SD		-73.7 ± 8.7	-74.3 ± 5.3	-72.7 ± 5.3	-69.7 ± 5.6	-69 ± 5.8	-71.6 ± 6.85
Membrane resistance (MΩ)		**n=35**	**n=28**	**n=41**	**n=49**	**n=46**	**n=48**
mean ± SD		122.2 ± 78.2	91 ± 62	130.6 ± 121.6	101.5 ± 58.6	103.3 ± 72.8	114.5 ± 67.4
Membrane time constant (ms)		**n=35**	**n=28**	**n=41**	**n=49**	**n=46**	**n=48**
mean ± SD		11 ± 2.3	13.1 ± 14.1	14.5 ± 35.5	16.9 ± 14.2	16.8 ± 34.8	13.1 ± 7.8
Passive membrane properties (PV)	**L1**	**L2**	**L3**	**L4**	**L5A**	**L5B**	**L6**
Membrane potential (mV)		**n=8**	**n=16**	**n=22**	**n=13**	**n=24**	**n=15**
mean ± SD		-70.7 ± 6.87	-69.4 ± 4.2	-69.5 ± 3.4	-73.1 ± 3.9	-70.2 ± 4.4	-71.6 ± 4.35
Membrane resistance (MΩ)				**n=3**	**n=5**	**n=5**	**n=2**
mean ± SD				83.3 ± 15.1	129.8 ± 21.9	110.9 ± 38.1	101.7 ± 22.6
Membrane time constant (ms)				**n=3**	**n=5**	**n=5**	**n=2**
mean ± SD				6.9 ± 9	9 ± 1.1	11.1 ± 13.1	12.4 ± 4.7
Passive membrane properties (SST)	**L1**	**L2**	**L3**	**L4**	**L5A**	**L5B**	**L6**
Membrane potential (mV)		**n=8**	**n=10**	**n=11**	**n=11**	**n=22**	**n=22**
mean ± SD		-66.4 ± 7.16	-67.4 ± 4.4	-68.2 ± 4	-70.2 ± 4.61	-67.5 ± 6.1	-68.9 ± 4.93
Membrane resistance (MΩ)		**n=4**	**n=5**	**n=4**	**n=5**	**n=3**	**n=8**
mean ± SD		223.8 ± 63.4	130.9 ± 71.8	153.2 ± 41.2	203.8 ± 57.5	300.4 ± 53.2	236 ± 134.2
Membrane time constant (ms)		**n=4**	**n=5**	**n=4**	**n=5**	**n=3**	**n=8**
mean ± SD		14.4 ± 6.3	11.1 ± 5.9	8.7 ± 2.9	14.9 ± 3.4	29.1 ± 5.2	18.9 ± 11
Passive membrane properties (VIP)	**L1**	**L2**	**L3**	**L4**	**L5A**	**L5B**	**L6**
Membrane potential (mV)	**n=5**	**n=24**	**n=36**	**n=20**	**n=15**	**n=12**	**n=3**
mean ± SD	-68.2 ± 4	-66.4 ± 6	-67.7 ± 5.8	-68.4 ± 5.9	-68.6 ± 5.9	-68.9 ± 6.7	-74.9 ± 1.3
Membrane resistance (MΩ)		**n=10**	**n=10**	**n=3**	**n=4**	**n=5**	**n=1**
mean ± SD		428.7 ± 172.5	248.9 ± 62.3	361.6 ± 81.5	320.2 ± 108.5	234.5± 335.4	270.7
Membrane time constant (ms)		**n=4**	**n=5**	**n=4**	**n=5**	**n=3**	**n=8**
mean ± SD		13.2 ± 5.24	10.3 ± 3.8	9.5 ± 2.5	11.4 ± 8.9	9.4 ± 35.8	7.5

Table 2.12 Membrane properties

***Chapter 3**:*

Parallel thalamocortical pathways to mouse somatosensory cortices

In collaboration with Sami El-Boustani and Johannes M. Mayrhofer

Introduction

In the mouse whisker system, sensory information is relayed to the primary somatosensory barrel cortex (wS1) by two major thalamic nuclei, the ventral posterior medial nucleus (VPM) and the posterior medial nucleus (POM). These two thalamic nuclei have their own parallel pathways. Sensory information coming to wS1 through VPM is called the lemniscal pathway. Trigeminal neurons bring the information first to the principal nucleus (PrV). Then these PrV neurons project to the VPM nucleus of the thalamus, which is organized into somatotopic regions called "barreloids" (Hoogland et al., 1987; Land et al., 1995; Ahissar et al., 2001; Varga et al., 2002). As we have shown in the previous chapter, axons from VPM neurons innervate layer 4 and layer 5B/6 border (Bureau et al., 2006; Cruikshank et al., 2010; Oberlaender et al., 2012).

The other main input pathway, however, does not only innervate wS1. Trigeminal neurons bring the whisker information to another nucleus which is called interpolaris nucleus (SpVi) which forms the beginning of the paralemniscal pathway, projecting to the POM nucleus of the thalamus (Lavallée et al., 2005). POM afferents project to both wS1 and secondary somatosensory cortex (wS2) (Pouchelon et al., 2014). Unlike VPM neurons, POM neurons have complex receptive fields. They are activated by peripheral sensory input via SpVi; however, they are also strongly driven by feedback from the motor and sensory cortices (Diamond et al., 1992)

Having both first-order and higher-order properties, we hypothesized that, the POM nucleus might have sub-compartments dedicated to first-order and higher-order functions separately. Specifically, we propose two subdivisions of POM: a sensory POM and a higher-order POM. To test that hypothesis, we took advantage of a recently developed transsynaptic adeno-associated virus (AAV) (Zingg et al., 2017). This virus allowed us to label the different parts of the thalamus based on their presynaptic inputs from different brainstem nuclei.

In this chapter, we will explore different parallel thalamocortical pathways and investigate their functional inputs to wS2. We will subdivide POM using anterograde

transsynaptic virus and characterize sensory and higher-order sub-nuclei and compare it with the PrV-driven VPM pathway.

Materials and Methods

All experiments were performed in accordance with the Swiss Federal Veterinary Office, under authorization 1889 issued by the 'Service de la consommation et des affaires vétérinaires' of the Canton de Vaud.

Virus injections in the thalamus

An AAV1 transsynaptic virus expressing Cre-recombinase (AAV1.CaMKII0.4.Cre.SV40 by Penn Vector Core) and an AAV2/5 virus expressing humanized ChR2 (histidine 134 converted to arginine) fused to EYFP under the control of the EF1α promoter (AAV2/5.DIO.EF1α.hChR2(H134R).eYFP by Penn Vector Core, AAV-hSyn-DFO-ChR2-eYFP (DFO) by Tess Oram and Ofer Yizhar (collaborators in this study) of the Weizmann Institute) and an AAV9 expressing tdTomato (AAV9.CAG.FLEX.tdTomato) was used in wild-type (C57BL/6) and GPR26-Cre animals. A small craniotomy was made (approximately 1 mm in diameter) the dura was left intact. We used an injection pipette (internal tip diameter 20 – 30 μm) and filled its tip with the virus solution and lowered into the brain. To label different sub-nuclei of POM, 100 nl of AAV1 transsynaptic virus was injected in SpVi with stereotaxic coordinates from bregma of 6.5 mm posterior, 1.8 mm lateral, 3.5 mm deep and 100 nl of Cre-dependent AAV or AAV-DFO was injected in POM with stereotaxic coordinates from bregma of: 2 mm posterior, 1.25 mm lateral, 2.8 mm deep. To label PrV-targeted VPM, 100 nl of AAV1 transsynaptic virus was injected in PrV with stereotaxic coordinates from bregma of 5 mm posterior, 1.8 mm lateral, 3.2 mm deep and Cre-dependent AAV was injected in VPM with stereotaxic coordinates from bregma of 2 mm posterior, 1.8 mm lateral, 3.25 mm deep. For optogenetic activation of VPM, we used GPR26-Cre animals and injected 50 nl of AAV-DFO in VPM with stereotaxic coordinates from bregma of: 1.7 mm posterior, 1.8 mm lateral and 3.25 mm deep. We kept the pipette at the site of the injection for 5 minutes before retracting it slowly in approximately 5 minutes. We allowed the virus to express 4 weeks before starting experiments.

Brain slicing

We anesthetized mice using a mixture of Ketamine (25 mg/ml) and Xylazine (2mg/ml) and perfused them with dissection buffer containing (in mM): 87 NaCl, 25 $NaHCO_3$, 25 D-glucose, 2.5 KCl, 1.25 NaH_2PO_4, 0.5 $CaCl_2$, 7 $MgCl_2$, 75 Sucrose, aerated with 95% O_2 + 5% CO_2. We cut parasagittal (35° away from vertical for wS1, 40° away from vertical for wS2) acute slices with the same ice-cold dissection buffer in 300-µm-thick sections on a vibratome (Leica; VT1200). After slicing, we transferred the tissue to a chamber with the same solution at room temperature for 25 min. We then transferred the slices to a chamber with standard ACSF containing (in mM): 125 NaCl, 25 $NaHCO_3$, 25 D-glucose, 2.5 KCl, 1.25 NaH_2PO_4, 2 $CaCl_2$, 1 $MgCl_2$, aerated with 95% O_2 + 5% CO_2 at room temperature and maintained them there for at least 1 hour prior to use.

In vitro whole-cell recordings

We recorded membrane potentials of 165 neurons (n=18 mice) in the whole-cell patch-clamp configuration in primary somatosensory barrel cortex (wS1) and secondary somatosensory cortex (wS2) at the age of postnatal day 50 to 60 in both sexes. Patch-clamp recordings of EPSPs were obtained from neurons in the presence of TTX (1 µM), 4-AP (100 µM) and PTX (50 µM). We visualized neurons with a 40x/0.80NA W objective under video microscopy (Olympus BX51WI) coupled with infrared gradient contrast. Patch pipettes with a resistance of 5-7 MΩ were used. The pipettes were filled with intracellular solution containing (in mM): 135 K-gluconate, 4 KCl, 4 Mg-ATP, 10 Na_2-phosphocreatine, 0.3 Na-GTP, and 10 HEPES (pH 7.3, 280 mOsmol/l). We added biocytin to the intracellular solution to give a final concentration of 3-4 mg/ml. We used an Ag/AgCl wire attached to the head-stage, as the recording electrode. We pulled patch pipettes from borosilicate glass capillaries with a tip-resistance of 4-8 MΩ. We filled the pipettes with an internal solution, fixed onto the head stage and lowered into the recording chamber which was superfused with artificial cerebrospinal fluid (ACSF). Another Ag/AgCl electrode connected to the head-stage was dipped into the recording chamber and used as the reference electrode. We applied positive pressure (200 mbar) and lowered the pipette until it touches the slice surface. Then with the same positive pressure, the pipette was advanced to a selected cell. When we touch the cell, we applied negative pressure to

allow the formation of a gigaohm seal. Once the gigaohm seal is formed, we applied brief pulses of suction to break into the cell. We carried out all recordings in current clamp mode. The membrane potential was sampled at 20 kHz in blocks of 2 seconds. Signals were digitized and recorded on an ITC-18 (Instrutech) analog to digital converter board, using custom written routines implemented in IgorPro. Liquid junction potential was not corrected.

Optogenetic stimulation

We used a fiber-optic cable (Thorlabs; NA 0.48; 1 mm) coupled to a 470 nm blue LED (Thorlabs) to deliver the optogenetic stimulus. One end of the fiber was plugged into the LED source and the other end of the fiber was mounted on a manipulator (Luigs and Neumann) and was lowered towards the cortex in the brain slice until the tip of the fiber-optic cable just touched the slice. The light stimulus was a single 1 ms pulse and it was delivered every 5 seconds. The peak light power, below the fiber, was approximately 30 mW.

Histology and cell visualization

At the end of the recording session, we fixed the slices with 4% PFA overnight at 4°C. We incubated the slices in blocking solution containing 5% normal goat serum and 0.3% Triton X for 1 hour. Then we transferred them to the staining solution containing 0.3% Triton X and 1:2000 of Streptavidin conjugated to Alexa 647 (Life Technologies). We incubated the slices for 2-3 hours and then washed them in PBS. We used DAPI as a counterstain. We then mounted the slices and imaged them under a confocal microscope (Leica SP8). All the recovered neurons could be identified and matched to the recording. We measured the cell depth vertically from the pial surface of the slice to the cell body. In the cases where the cell could not be recovered, the manipulator reading was taken as the depth. In the cases where the cell was recovered, we measured on the fixed slice.

Estimation of layer boundaries

Using the combination of DAPI stained sections containing axons with ChR2/YFP expression, wS1, and wS2 layer boundaries were defined by the experimenter.

Analysis of PSP amplitudes

We aligned the membrane potential traces to the onset of the 1 ms ChR2 stimulus of the thalamocortical axons in S1. We averaged individual traces of 20 consecutive sweeps to obtain an average membrane potential trace. Mean EPSP amplitudes were calculated by taking the average peak and subtracting the baseline pre-stimulus membrane potential. The latency of the EPSP was calculated by taking the time at 1% of its maximum peak value. We calculated the resting membrane potentials of each cell during the recordings of light-evoked postsynaptic potentials. We averaged 100 ms of each trace prior to light stimulation. The final resting membrane potential of the cell is computed as an average across 20 consecutive sweeps. All PSP amplitudes were measured from the resting membrane potentials of the neurons (Table 3.4).

Statistical analysis

Data are presented as mean ± SD and median. For each analysis as described throughout in this chapter, values were measured from average responses of 20 consecutive sweeps. To statistically assess the differences between groups, one-way ANOVA combined with Tukey-Kramer posthoc test was used (Matlab implementation).

Results

Anatomy of parallel thalamocortical circuits

In order to characterize parallel sensory thalamocortical circuits, we took advantage of a recently developed transsynaptic virus AAV1.CaMKII-Cre (Zingg et al., 2017). This virus allowed us to label the different parts of the thalamus based on their presynaptic inputs from different brainstem nuclei. We first injected this virus into the principal sensory nucleus (PrV) of the brain stem which allowed us to express Cre-recombinase in its postsynaptic target VPM in the thalamus (Figure 3.1). We then injected a Cre-dependent tdTomato expressing AAV into VPM; thus only the PrV receiving VPM neurons were infected (Figure 3.1B). We could see the typical innervation pattern of VPM in the wS1 with dense patches of axons in L4 barrels and at the L5B/6 border. This result was in agreement with the previous studies showing VPM innervations in wS1 (Bureau et al., 2006; Wimmer et al., 2010; Cruikshank et al., 2010; Oberlaender et al., 2012; Poulet et al., 2012).

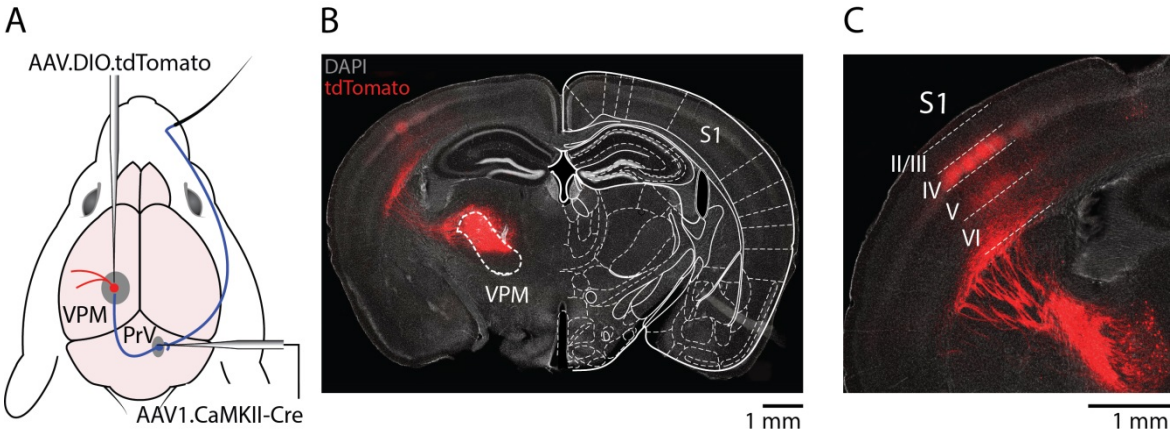

Figure 3.1 Anatomy of first-order thalamic input to S1. (A) Schematic drawing showing the strategy used to label PrV-receiving VPM neurons. Transsynaptic AAV1.CaMKII-Cre was injected into PrV and tdTomato expressing Cre-dependent AAV was injected into VPM. **(B)** Coronal section at the level of VPM showing the expression of the tdTomato in PrV-receiving VPM neurons. **(C)** Coronal section at the level of wS1 showing the innervation pattern of PrV-receiving VPM neurons in wS1. Innervation was in L4 barrels and L5B/L6 border.

We were then interested in investigating the anatomy of the spinal interpolar nucleus (SpVi) targeted thalamus. It has been shown that the POM nucleus is driven by both sensory inputs (via SpVi) and feedback from different sensory and motor cortices (Diamond et al., 1992; Ahissar et al., 2001; Groh et al., 2014; Urbain et al., 2015; Yu et al., 2006, 2015). We hypothesized that maybe POM had different sub-nuclei of which one part might be activated more by the peripheral sensory information and another part that might be activated more by cortical feedback. To test that hypothesis, we again used the transsynaptic virus which expresses Cre-recombinase. We injected this virus into the SpVi which allowed us to have a Cre expression in its postsynaptic target neurons in POM (Figure 3.2). We then injected a Cre-dependent tdTomato expressing AAV into POM, in order to label only the SpVi receiving POM neurons (Figure 3.2B). We observed that, SpVi receiving POM neurons were mainly targeting wS2 in L4 and weaker innervations in L5B/L6 (Figure 3.2C), This result was different from what has been shown about typical POM innervation in wS1 and wS2 in prior studies (Koralek et al., 1988; Chmielowska et al., 1989; Cruikshank et al., 2007; Petreanu et al., 2007; Meyer et al., 2010; Wimmer et al., 2010; Pouchelon et al., 2014). We will call this nucleus “direct-POM (dPOM)”.

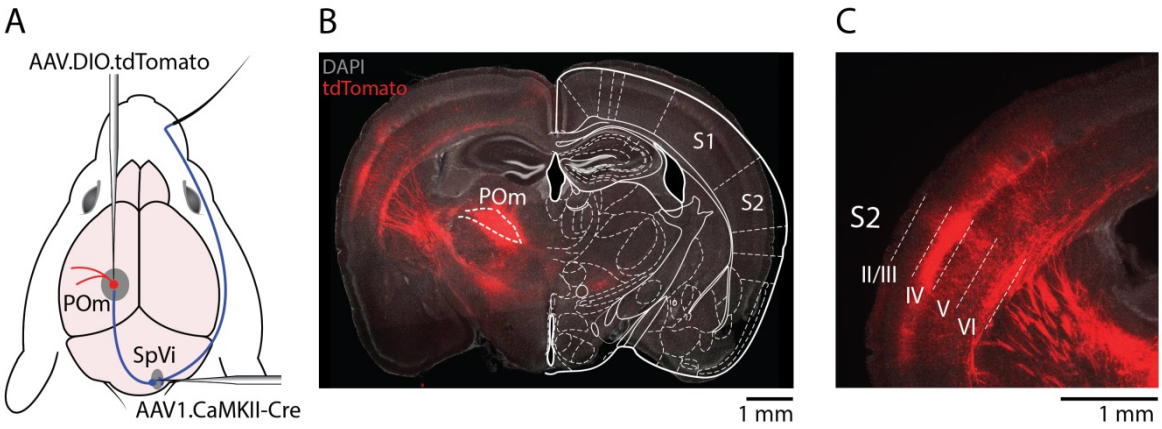

Figure 3.2 Anatomy of first-order thalamic input to S2. (A) Schematic drawing showing the strategy used to label SpVi-receiving POM neurons. Transsynaptic AAV1.CaMKII-Cre was injected into SpVi and tdTomato expressing Cre-dependent AAV was injected into POM. **(B)** Coronal section at the level of POM showing the expression of the tdTomato in SpVi-

receiving POM neurons. **(C)** A magnified coronal section at the level of wS2 showing the innervation pattern of SpVi-receiving POM neurons in wS2.

After visualizing SpVi-targeted POM (dPOM) and its innervations in wS2, we were then interested in the anatomy of the rest of the POM. Since dPOM was innervating mainly wS2 in L4, the rest of the POM must innervate L1 and L5A of wS1 and wS2. To be able to test that, we again used the transsynaptic virus to infect SpVi, however, instead of using a Cre-activated AAV in POM, we used the AAV-DFO virus (AAV.DFO.eYFP) (Figure 3.3), which induces expression in cells without Cre. Using this method, we labeled non-SpVi-receiving POM neurons (Figure 3.3B). We found that these neurons were innervating L1 and L5A of wS1 and wS2. Since this part of POM was not receiving sensory input from SpVi, we will call this nucleus "indirect-POM (iPOM)".

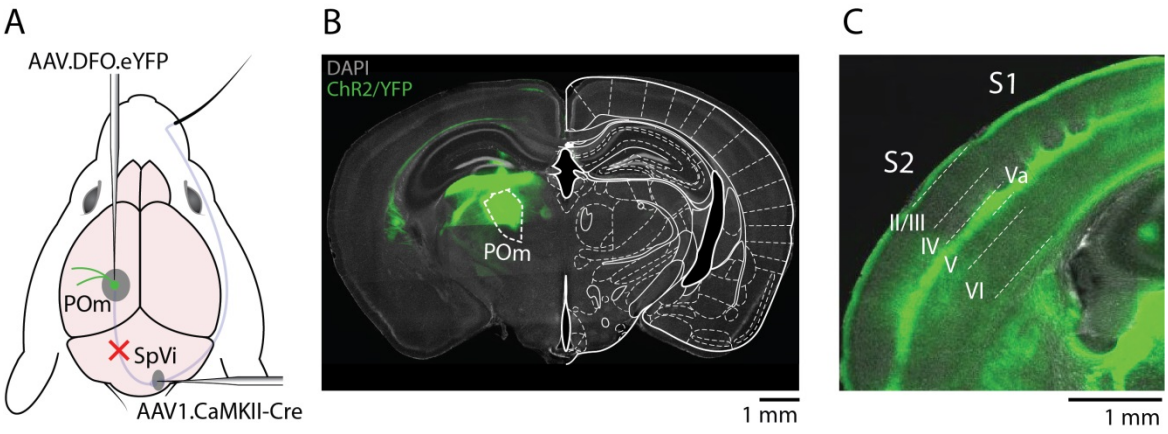

Figure 3.3 Anatomy of higher-order thalamic input to wS1 and wS2. (A) Schematic drawing showing the strategy used to label non-SpVi-receiving POM neurons. Transsynaptic AAV1.CaMKII-Cre was injected into SpVi and eYFP expressing AAV-DFO was injected into POM. **(B)** Coronal section at the level of POM injection site showing the expression of the eYFP in non-SpVi-receiving POM neurons. eYFP signal was amplified by anti-GFP staining **(C)** Magnified coronal section at the level of wS2 and wS1 showing the innervation pattern of non-SpVi-receiving POM neurons in wS1 and wS2.

The first-order thalamic input to wS1

Having characterized the anatomy of VPM, dPOM, and iPOM, we were then interested in their functional input to their target zones. We started looking at the input distribution of VPM in wS1. In order to do that, we performed experiments combining *in vitro* whole-cell patch-clamp recordings with optogenetic activation of thalamocortical axons. We injected ChR2 in VPM of GPR26-Cre mice using AAV-DFO. This gave us a clean expression of ChR2 in VPM and its afferents in wS1 (Figure 3.4).

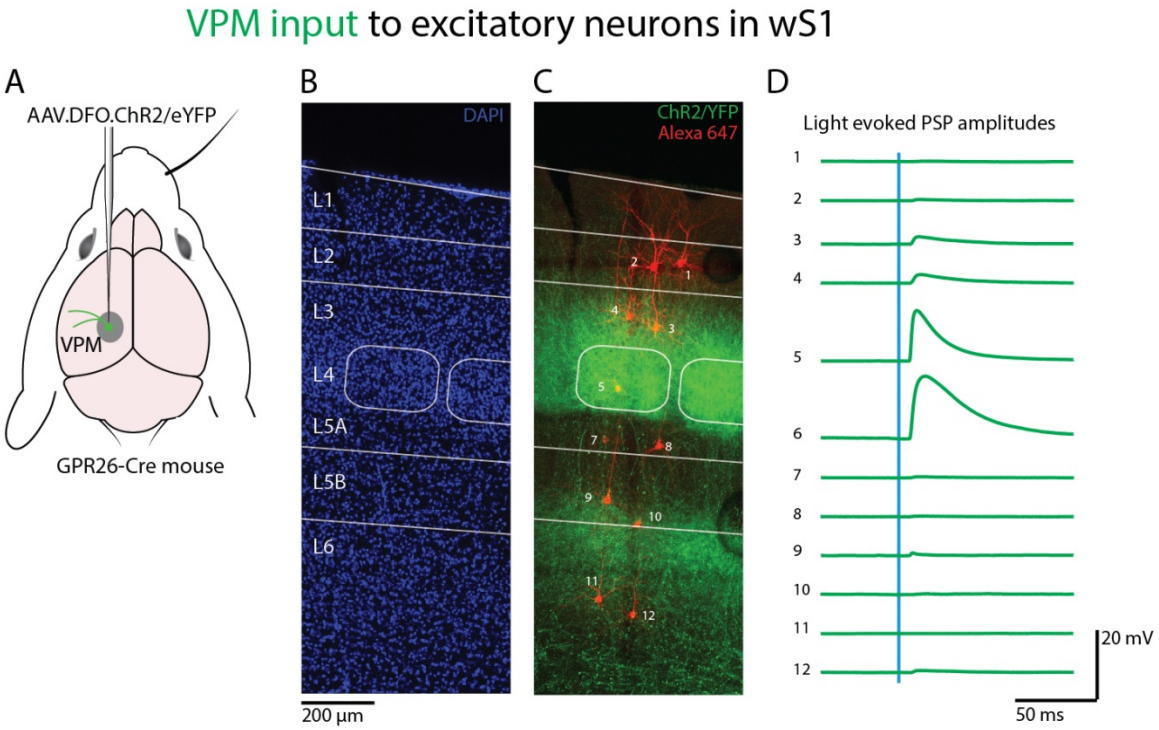

Figure 3.4 VPM-evoked postsynaptic potentials in wS1. (A) Schematic drawing showing the strategy used to inject ChR2 in VPM. **(B)** DAPI staining (blue) and layer structure of wS1. **(C)** Confocal image of a parasagittal slice after fixation with the expression of ChR2/YFP (green) in the VPM axons and recorded neurons with Alexa 647 (red) in wS1. **(D)** Light-evoked postsynaptic potentials from the recorded neurons after 1 ms blue light pulse. Numbers on the left of the PSP traces indicate the recorded neurons in the confocal image (C).

The amplitude of VPM-evoked PSPs in excitatory neurons was recorded across multiple layers of a single slice in the presence of TTX, 4-AP, and PTX. We typically recorded from two nearby neurons simultaneously. 1 ms blue light pulse through a 1 mm optic fiber elicited PSPs in excitatory neurons (Figure 3.4D). We kept the optic fiber position fixed in order to have an accurate comparison across layers.

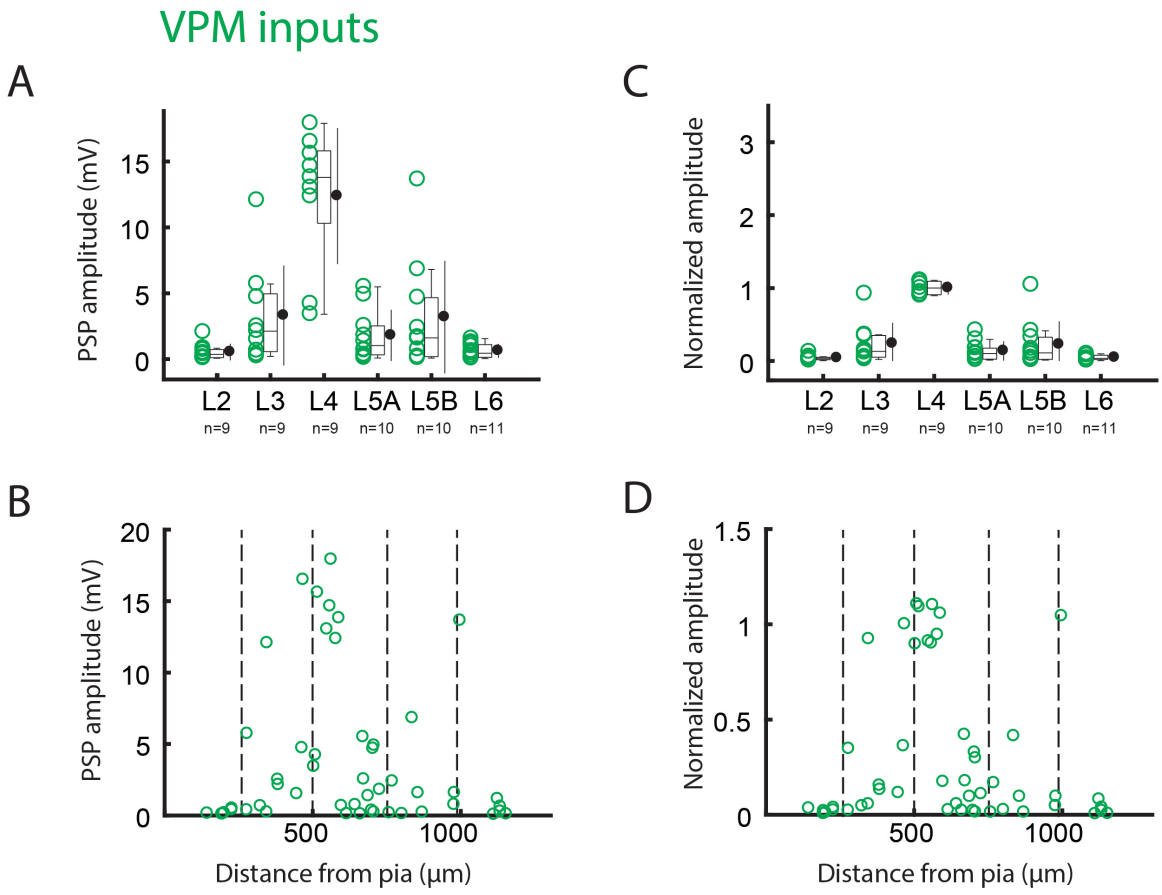

Figure 3.5 Population data of VPM input to excitatory neurons in wS1. (A) VPM-evoked postsynaptic potentials in excitatory neurons across different layers. **(B)** VPM-evoked postsynaptic potentials in excitatory neurons plotted by depth from pia surface. **(C)** VPM-evoked postsynaptic potentials in excitatory neurons across different layers, normalized to the mean strength of input to L4 neurons in the same slice per experiment. **(B)** VPM-evoked postsynaptic potentials in excitatory neurons plotted by depth from pia surface, normalized to the mean strength of input to L4 neurons in the same slice per experiment.

We observed VPM-evoked postsynaptic potentials in excitatory neurons in every layer of the cortical column (Figure 3.5, Table 3.1). In our experiments, we used three different light powers per recording to see responses in different stimulation strengths. We used L4 as a reference layer for VPM experiments since it is considered to be the main input layer. Here we present responses having a maximum of 20 mV PSP amplitude in L4 excitatory neurons within the same slice (Figure 3.5A,B). Maximum mean response was in L4 (12.4 ± 5.2 mV (median: 17.9 mV), mean ± SD) and it was significantly larger than other layers (L4 vs L2: $p < 0.0001$, L4 vs L3: $p < 0.0001$, L4 vs L5A: $p < 0.0001$, L4 vs L5B: $p < 0.0001$, L4 vs L6: $p < 0.0001$).

To be able to compare the input strengths between experiments more accurately, we normalized the responses across layers to the mean strength of L4 neurons (Figure 3.5C,D). The normalized profile of input distribution was similar to that found for the un-normalized data. The normalized mean PSP amplitude was maximum in L4 (1 ± 0.1 mV (median: 1 mV), mean ± SD) and it was also significantly larger than other layers (L4 vs L2: $p < 0.0001$, L4 vs L3: $p < 0.0001$, L4 vs L5A: $p < 0.0001$, L4 vs L5B: $p < 0.0001$, L4 vs L6: $p < 0.0001$).

The first-order thalamic input to wS2

As we found that SpVi receiving POM (dPOM) anatomically targets mainly L4 of wS2, we were then interested in the functionality of that innervation. We performed the same experiments combining *in vitro* whole-cell patch-clamp recordings with optogenetic activation of thalamocortical axons. To have ChR2 expressed in dPOM, we first injected transsynaptic AAV1.CaMKII-Cre in SpVi to have Cre expression in dPOM, then we injected Cre-dependent AAV in POM to express ChR2 (Figure 3.6).

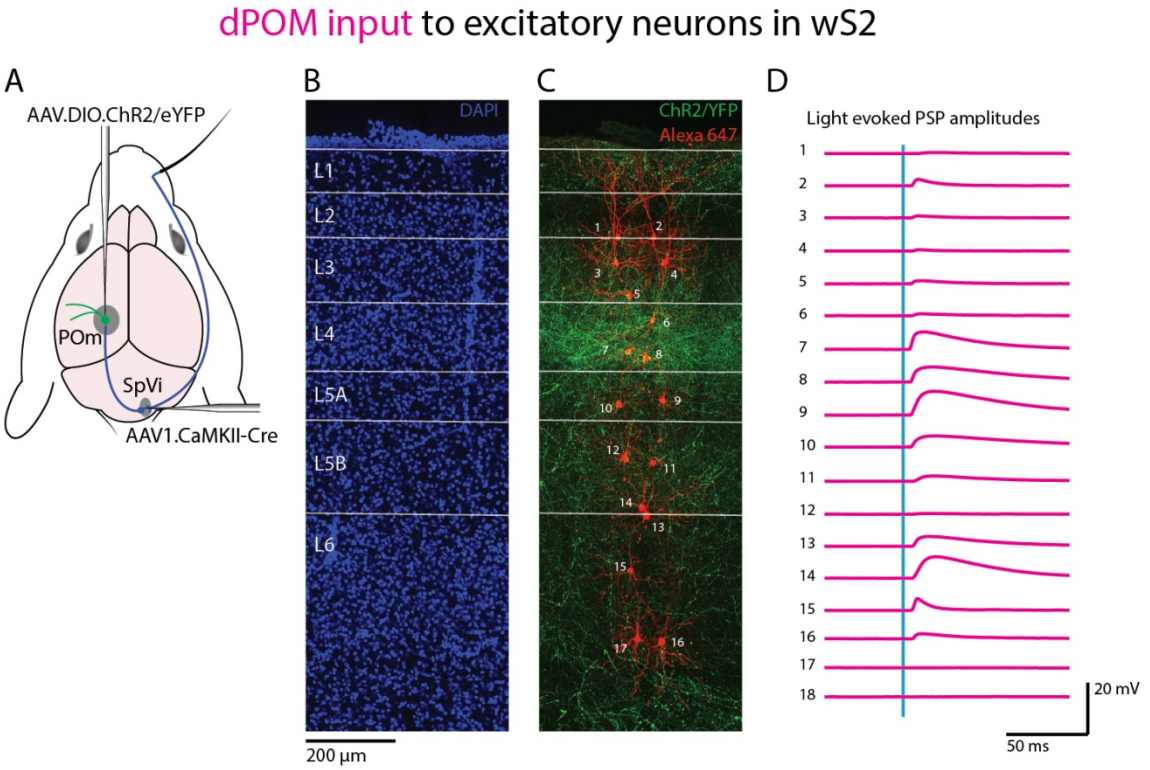

Figure 3.6 dPOM-evoked postsynaptic potentials in wS2. (A) Schematic drawing showing the strategy used to inject ChR2 in dPOM. **(B)** DAPI staining (blue) and layer structure of wS2. **(C)** Confocal image of a parasagittal slice after fixation with the expression of ChR2/YFP (green) in the dPOM axons and recorded neurons with Alexa 647 (red) in wS2. **(D)** Light-evoked postsynaptic potentials from the recorded neurons after 1 ms blue light pulse. Numbers on the left of the PSP traces indicate the recorded neurons in the confocal image (C).

After having ChR2 in the dPOM axons we then recorded VPM-evoked PSPs in excitatory neurons in the presence of TTX, 4-AP and PTX. We used two patch electrodes simultaneously and performed recordings across layers within a single slice. 1 ms blue light pulse through a 1 mm optic fiber elicited PSPs in excitatory neurons (Figure 3.6D). We kept the optic fiber position fixed in order to have an accurate comparison across layers.

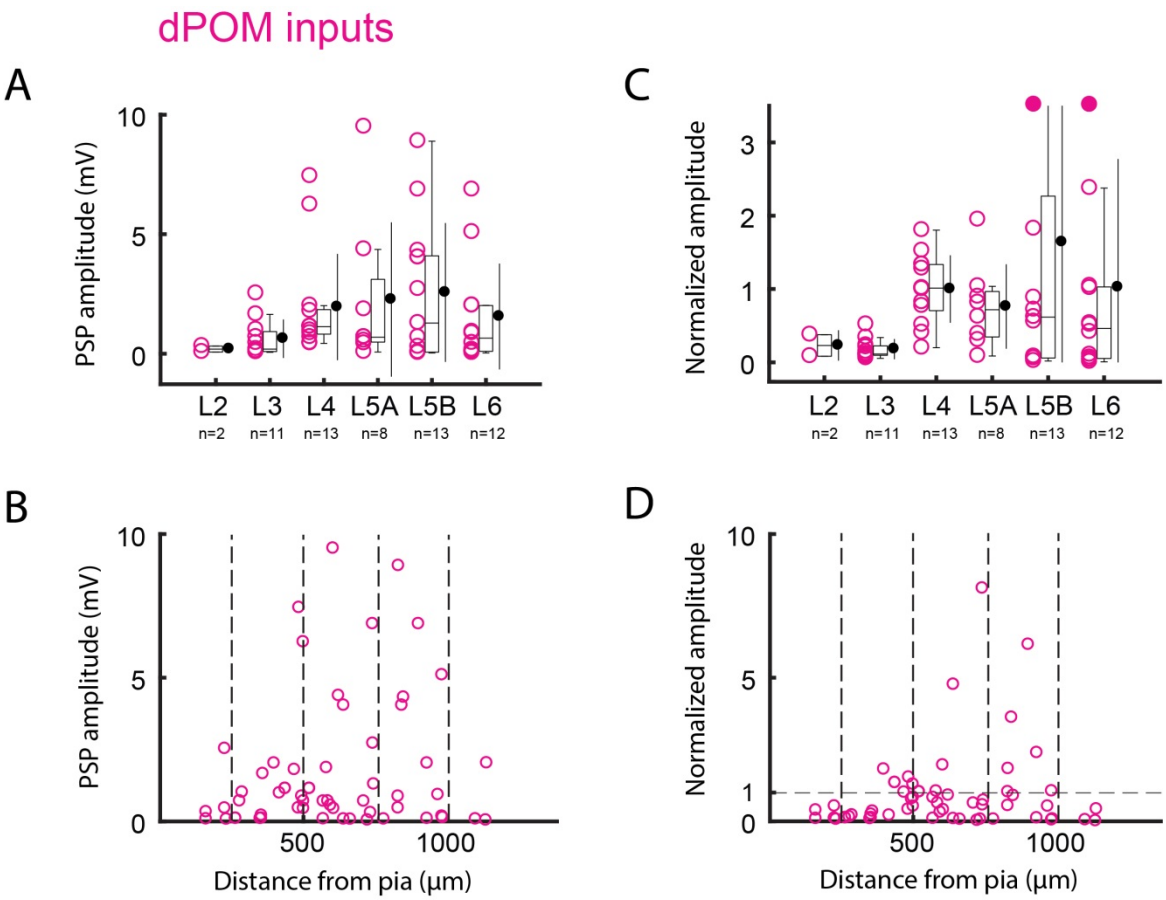

Figure 3.7 Population data of dPOM input to excitatory neurons in wS2. (A) dPOM inputs to excitatory neurons across layers. **(B)** dPOM inputs to excitatory neurons plotted by depth from pia surface. **(C)** dPOM inputs to excitatory neurons across layers, normalized to the mean strength of input to L4 neurons in the same slice per experiment. Filled circles represent outliers in the given scale. **(D)** dPOM inputs to excitatory neurons plotted by depth from pia surface, normalized to the mean strength of input to L4 neurons in the same slice per experiment. The horizontal dashed line indicates normalized amplitude of 1.

We observed dPOM-evoked postsynaptic potentials in excitatory neurons in every layer of the cortical column (Figure 3.7, Table 3.2). As mentioned, in our experiments we used three different light powers per recording session to see responses in different stimulation strengths. We used L4 as a reference layer for dPOM experiments since anatomically it appeared to be the main input layer. Here we present responses having a maximum of 20 mV PSP amplitude in L4 excitatory neurons within the same slice (Figure 3.7A,B). Maximum mean response was in fact in L5A (2.27 ± 3.23 mV (median: 1.13 mV), mean ± SD) however, it was not significantly larger than other layers (L5A vs L2: $p = 0.8735$, L5A vs L3: $p = 0.6678$, L5A vs L4: $p = 0.9997$, L5A vs L5B: $p = 0.9998$, L5A vs L6: $p = 0.9853$).

To be able to compare the input strengths between experiments more accurately, we normalized the responses across layers to the mean strength of L4 neurons (Figure 3.7C,D). After normalization, we saw that the input distribution was different. The normalized mean PSP amplitude was maximum in L4 (1 ± 0.1 mV (median: 1 mV), mean ± SD), however, it was also not significantly larger than other layers (L4 vs L2: $p = 0.9809$, L4 vs L3: $p = 0.7353$, L4 vs L5A: $p = 0.9991$, L4 vs L5B: $p = 0.866$, L4 vs L6: $p = 1$).

In summary, we found that dPOM innervation in wS2 functionally targets cells in every layer. Maximum input strength was in L4, however, this was not significantly different than other layers. This shows no layer dependency of dPOM inputs to wS2, even if the axons are mostly concentrated in L4, however, this could also show the need for more data to confirm the actual organization this input.

The higher-order thalamic input to wS2

After showing the functional inputs of dPOM to wS2, we then investigated the functionality of higher-order POM (iPOM) innervation in wS2. As previously described, in order to test if these axons are functionally connected, we performed *in vitro* whole-cell patch-clamp experiments and combined them with optogenetic stimulation of ChR2 expressing iPOM axons. We first injected transsynaptic AAV1.CaMKII-Cre in SpVi to have Cre expression in dPOM, then we injected AAV-DFO in POM to express ChR2 in non-dPOM cells which is mainly iPOM (Figure 3.8).

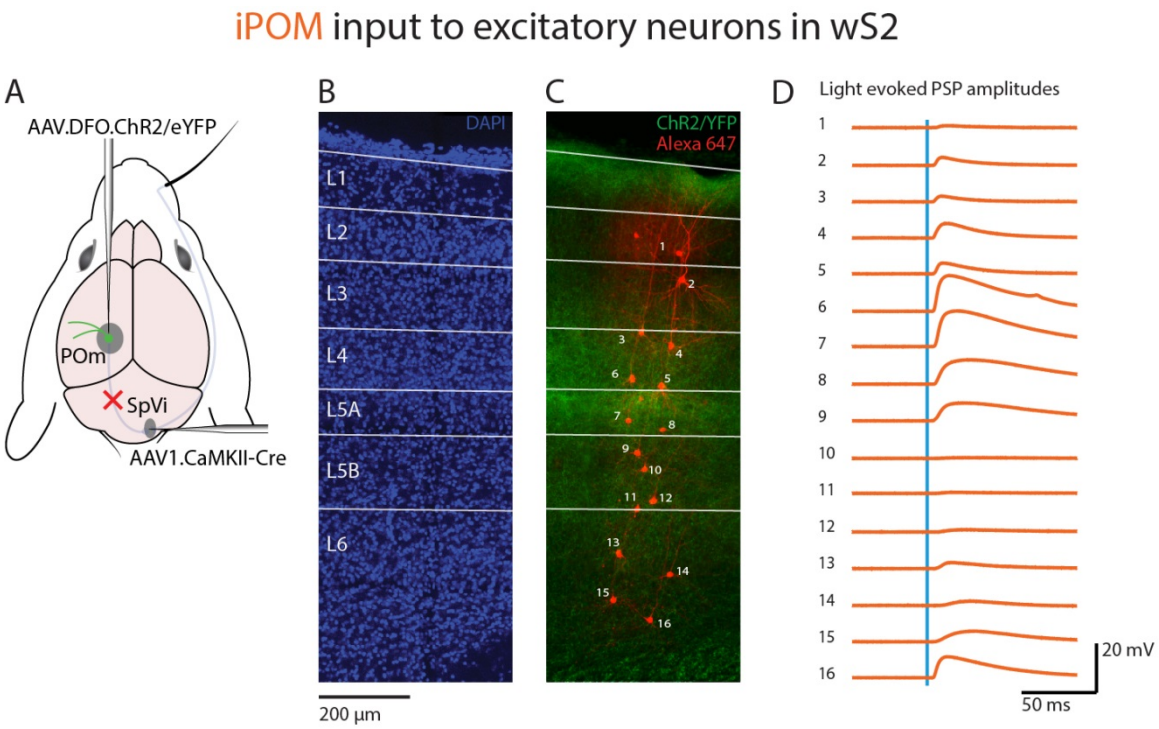

Figure 3.8 iPOM-evoked postsynaptic potentials in wS2. (A) Schematic drawing showing the strategy used to inject ChR2 in iPOM. **(B)** DAPI staining (blue) and layer structure of wS2. **(C)** Confocal image of a parasagittal slice after fixation with the expression of ChR2/YFP (green) in the iPOM axons and recorded neurons with Alexa 647 (red) in wS2. **(D)** Light-evoked postsynaptic potentials from the recorded neurons after 1 ms blue light pulse. Numbers on the left of the PSP traces indicate the recorded neurons in the confocal image (C).

After having ChR2 in the iPOM axons we then recorded VPM-evoked PSPs in excitatory neurons in TTX, 4-AP, and PTX across different layers within the same slice. We used two patch electrodes per one recording session and performed recordings in a sequence. 1 ms blue light pulse through a 1 mm optic fiber elicited PSPs in excitatory neurons (Figure 3.8D). We kept the optic fiber position fixed in order to have an accurate comparison across layers.

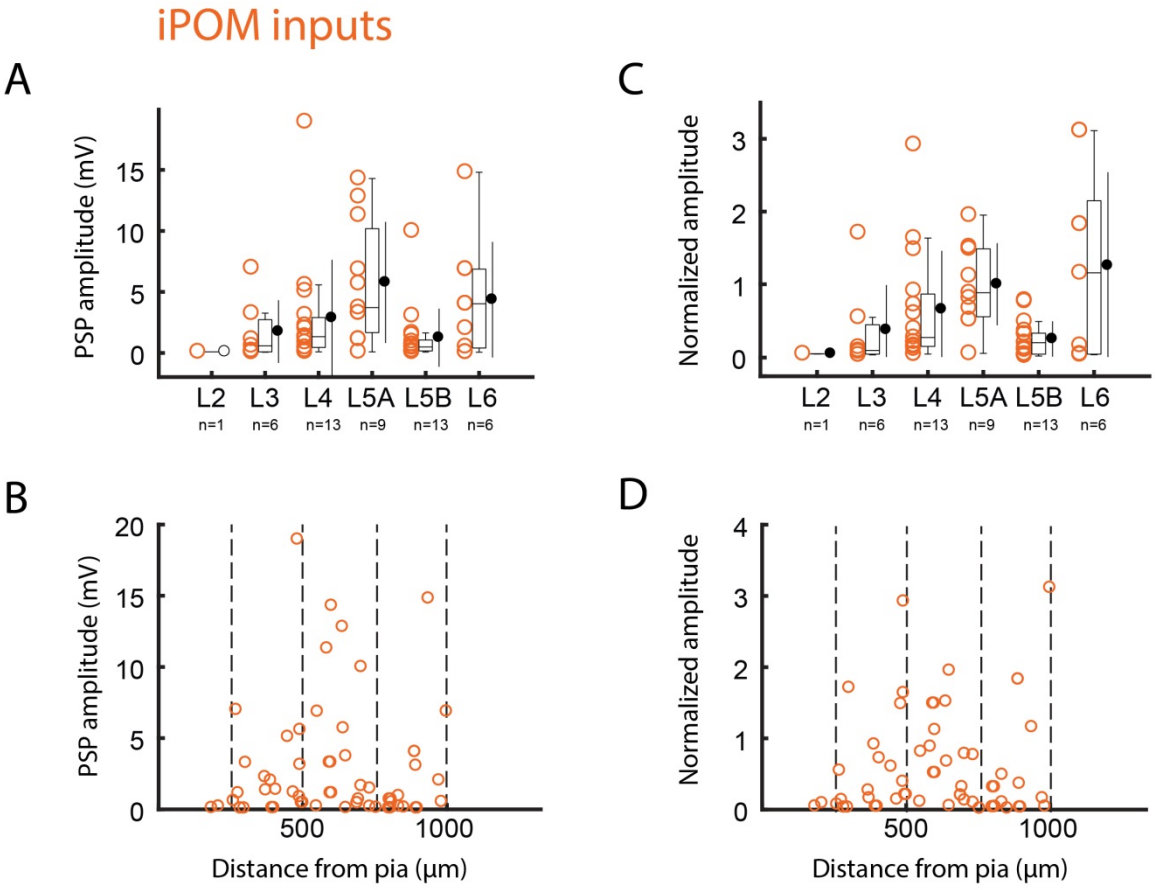

Figure 3.9 Population data of iPOM input to excitatory neurons in wS2. (A) iPOM-evoked responses in excitatory neurons across layers. **(B)** iPOM-evoked responses in excitatory neurons plotted by depth from pia surface. **(C)** iPOM-evoked responses in excitatory neurons across different layers, normalized to the mean strength of input to L5A neurons in the same slice per experiment. **(D)** iPOM evoked responses in excitatory neurons plotted by depth from pia surface, normalized to the mean strength of input to L5A neurons in the same slice per experiment.

iPOM activation induced PSP responses in excitatory neurons in every layer of the cortical column (Figure 3.9, Table 3.3). In our experiments, we used three different light powers per recording session to see responses in different stimulation strengths. We used L5A as a reference layer for iPOM experiments since it anatomically appears to be the main input layer. Here we present responses having a maximum of 20 mV PSP amplitude in L5A excitatory neurons within the same slice. Maximum mean response was in L5A (5.78 ± 4.96 mV (median: 3.72 mV), mean ± SD) however, it was not significantly larger than other layers (L5A vs L2: $p = 0.7535$, L5A vs L3: $p = 0.3171$, L5A vs L4: $p = 0.4592$, L5A vs L5B: $p = 0.0555$, L5A vs L6: $p = 0.9691$).

We normalized the responses across layers to the mean strength of L5A neurons. The profile of the normalized input distribution appeared different from the un-normalised distribution. The normalized mean PSP amplitude was maximum in L6 (1.26 ± 1.29 mV (median: 1.16 mV), mean ± SD), but it was not significantly larger than other layers (L6 vs L2: $p = 0.6172$, L6 vs L3: $p = 0.1732$, L6 vs L4: $p = 0.3832$, L6 vs L5A: $p = 0.97$, L6 vs L5B: $p = 0.0173$).

Parallel thalamocortical pathways

In summary, we found that PrV receiving VPM afferents innervate wS1 in L4 and L5B/6 border. Functionally it gives input to all recorded layers and maximum input was observed in L4 (Figure 3.10A). SpVi receiving POM (dPOM) afferents innervate wS2 mainly in L4 and deeper layers. These afferents also give functional input to all recorded layers of wS2 and maximum input was observed in L4, however, it was not significantly different from other layers (Figure 3.10B). iPOM, which does not receive input from SpVi, innervates L1 and L5A of wS1 and wS2 and it gives functional input to wS2 neurons (Figure 3.10C). Largest iPOM input in wS2 was in L5A, however, it was not significantly different from the rest of the recorded layers.

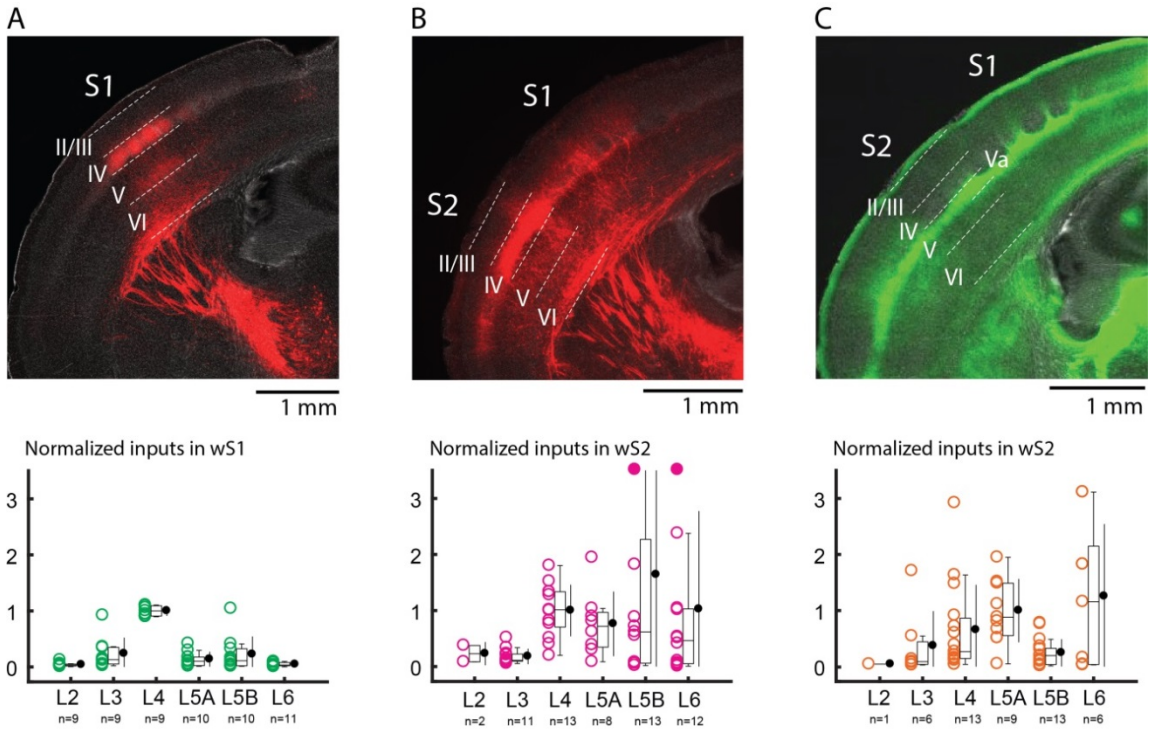

Figure 3.10 Parallel thalamocortical pathways and their functional inputs. (A) Coronal section at the level of wS1 showing the axonal innervation of PrV-receiving VPM neurons in wS1 (top, same image as Figure 3.1C) and VPM-evoked inputs in excitatory neurons across different layers, normalized to the mean strength of input to L4 neurons in the same slice per experiment (bottom, same image as Figure 3.5C) **(B)** Coronal section at the level of wS2 showing the axonal innervation of dPOM neurons in wS2 (top, same image as Figure 3.2C) and dPOM inputs to excitatory neurons across layers, normalized to the mean strength of input to L4 neurons in the same slice per experiment. Filled circles represent outliers in the

given scale (bottom, same image as Figure 3.7C) **(C)** Coronal section at the level of wS2 and wS1 showing the axonal innervation of iPOM neurons in wS1 and wS2 (top, same image as Figure 3.3C) and iPOM-evoked inputs to excitatory neurons across different layers, normalized to the mean strength of input to L5A neurons in the same slice per experiment (bottom, same image as Figure 3.9D).

Discussion

In this chapter, we characterized two distinct sub-nuclei of the POM nucleus of the thalamus. Using transsynaptic AAV, we identified the sensory information receiving (via SpVi) POM (dPOM) and the rest of the POM (iPOM) which does not receive peripheral sensory information from the brain stem. We found that dPOM innervated mainly wS2 in L4. These axons evoked PSP responses in excitatory neurons in all layers confirming functional connectivity. We also observed some weaker innervation in wS1 L4 and L5A, however, we did not investigate whether these axons were functionally connected. We then found that iPOM innervated mainly L5A and L1 of wS1 and wS2, however, we investigated the functional connectivity of these axons only in wS2. We observed also PSP responses in every layer evoked by the stimulation of these axons.

Parallel thalamocortical pathways to somatosensory cortices

dPOM is receiving peripheral sensory input from SpVi and innervates mainly L4 of wS2. This result shows a similarity to the lemniscal pathway where VPM receives peripheral sensory input from PrV and innervates mainly L4 of wS1 (Veinante and Deschênes, 1999; Bureau et al., 2006; Oberlaender et al., 2012). dPOM and VPM could be involved in a parallel sensory processing circuit and could encode different features of the whisker sensory information. Performing in vivo experiments to investigate how whisker sensory information is processed in the dPOM -> wS2 pathway compared to the VPM -> wS1 pathway could reveal more about the functional differences between these two nuclei. The lack of dPOM innervation in wS1 barrel field shows that prior POM studies in wS1 most probably investigated function and connectivity of iPOM.

VPM neurons respond to one principal whisker with a very sharp tuning (Simons and Carvell, 1989; Friedberg et al., 1999; Brecht and Sakmann, 2002). Prior studies have shown that POM neurons have a broad tuning, complex receptive fields and they are activated by both sensory input and cortical feedbacks (Diamond et al., 1992; Ahissar et al., 2001; Groh et al., 2014; Yu et al., 2006, 2015). Moreover, their activities are modulated by whisking (Urbain et al., 2015). Having both higher-order and first-order properties, the role of POM is still not clear (Constantinople and

Bruno, 2013; Yu et al., 2015). Our data suggest that investigating dPOM and iPOM separately could provide a more comprehensive understanding of this nucleus.

Tables

VPM evoked EPSPs	L2	L3	L4	L5A	L5B	L6
Amplitude (mV)	**n=9**	**n=9**	**n=9**	**n=10**	**n=10**	**n=11**
mean ± SD	0.53 ± 0.63	3.31 ± 3.79	12.38 ± 5.15	1.80 ± 1.94	3.19 ± 4.27	0.63 ± 0.53
median	0.36	2.13	13.8	1.03	1.61	0.45
interquartile range	0.73 - 0.11	4.96 - 0.57	15.81 - 10.31	2.52 - 0.33	4.67 - 0.19	1.10 - 0.14
Norm amplitude	**n=9**	**n=9**	**n=9**	**n=10**	**n=10**	**n=11**
mean ± SD	0.04 ± 0.03	0.24 ± 0.28	1 ± 0.09	0.14 ± 0.13	0.22 ± 0.32	0.05 ± 0.32
median	0.03	0.13	1	0.1	0.11	0.03
interquartile range	0.05 - 0.02	0.35 - 0.05	1.09 - 0.91	0.18 - 0.02	0.33 - 0.02	0.08 - 0.02

Table 3.1 VPM-evoked EPSPs in wS1

dPOM evoked EPSPs	L2	L3	L4	L5A	L5B	L6
Amplitude (mV)	**n=2**	**n=11**	**n=13**	**n=8**	**n=13**	**n=12**
mean ± SD	0.19 ± 0.18	0.63 ± 0.80	1.95 ± 2.22	2.27 ± 3.23	2.56 ± 2.90	1.56 ± 2.21
median	0.19	0.2	1.13	0.69	1.28	0.66
interquartile range	0.32 - 0.07	0.93 - 0.09	1.85 - 0.82	3.11 - 0.49	4.09 - 0.07	2.02 - 0.10
Norm amplitude	**n=2**	**n=11**	**n=13**	**n=8**	**n=13**	**n=12**
mean ± SD	0.23 ± 0.21	0.18 ± 0.14	1 ± 0.46	0.76 ± 0.57	1.64 ± 2.44	1.02 ± 1.75
median	0.23	0.11	1.01	0.72	0.62	0.46
interquartile range	0.38 - 0.08	0.22 - 0.09	1.33 - 0.70	0.97 - 0.35	2.27 - 0.06	1.03 - 0.05

Table 3.2 dPOM-evoked EPSPs in wS2

iPOM evoked EPSPs	L2	L3	L4	L5A	L5B	L6
Amplitude (mV)	**n=1**	**n=6**	**n=13**	**n=9**	**n=13**	**n=6**
mean ± SD	0.15 ± 0.07	2.01 ± 2.71	2.87 ± 4.76	5.78 ± 4.96	1.25 ± 2.38	4.36 ± 4.73
median	0.15	0.86	1.33	3.72	0.49	4.03
interquartile range	0.19 - 0.09	3.26 - 0.06	2.91 - 0.45	10.18 - 1.67	1.06 - 0.17	6.87 - 0.41
Norm amplitude	**n=2**	**n=11**	**n=13**	**n=8**	**n=13**	**n=12**
mean ± SD	0.06 ± 0.03	0.42 ± 0.66	0.66 ± 0.80	1 ± 0.57	0.25 ± 0.24	1.26 ± 1.27
median	0.07	0.1	0.27	0.88	0.19	1.16
interquartile range	0.09 - 0.04	0.55 - 0.03	0.86 - 0.14	1.49 - 0.55	0.33 - 0.04	2.15 - 0.04

Table 3.3 iPOM-evoked EPSPs in wS2

VPM in wS1	L2	L3	L4	L5A	L5B	L6
Membrane potential (mV)	**n=9**	**n=9**	**n=9**	**n=10**	**n=10**	**n=11**
mean ± SD	-70.57 ± 9.26	-71.73 ± 4.43	-71.22 ± 4.98	-69.84 ± 2.91	-63.43 ± 7.04	-67.05 ± 7.2
PSP synaptic delay (ms)	**n=1**	**n=6**	**n=9**	**n=5**	**n=6**	**n=3**
median	3.3	3.73	3.3	3.5	3.43	3.35
interquartile range		3.75 - 3.55	3.59 - 3.04	4.38 - 3.09	3.65 - 2.75	3.8 - 2.23
PSP half-width (ms)	**n=1**	**n=6**	**n=9**	**n=5**	**n=6**	**n=3**
median	16.15	20.4	22.2	38.55	31.88	46.9
interquartile range		22.1 - 18.85	32.03 - 17.33	49.29 - 33.05	35.25 - 28.95	49.98 - 25.23
dPOM in wS2	**L2**	**L3**	**L4**	**L5A**	**L5B**	**L6**
Membrane potential (mV)	**n=2**	**n=11**	**n=13**	**n=8**	**n=13**	**n=12**
mean ± SD	-80.47 ± 1.61	-79.89 ± 5.11	-73.7 ± 1.43	-72.47 ± 2.19	-74.52 ± 3.94	-76.45 ± 3.73
PSP synaptic delay (ms)		**n=3**	**n=5**	**n=3**	**n=8**	**n=4**
median		3.4	3.1	3.35	4.1	3.78
interquartile range		3.48 - 3.33	3.33 - 3.05	4.18 - 3.27	4.88 - 3.13	4.13 - 3.53
PSP half-width (ms)		**n=3**	**n=5**	**n=3**	**n=9**	**n=4**
median		15.55	47.22	63.05	34.25	24.55
interquartile range		20.91 - 13.19	54.25 - 37.98	70.78 - 57.24	45.31 - 27.25	31.13 - 15.33
iPOM in wS2	**L2**	**L3**	**L4**	**L5A**	**L5B**	**L6**
Membrane potential (mV)	**n=2**	**n=6**	**n=13**	**n=9**	**n=13**	**n=6**
mean ± SD	-75.02 ± 0.11	-81.33 ± 4.31	-74.68 ± 5.81	-71.25 ± 3.71	-73.45 ± 4.75	-73.97 ± 4.07
PSP synaptic delay (ms)		**n=3**	**n=9**	**n=10**	**n=4**	**n=5**
median		4.1	4.35	3.95	4.18	3.8
interquartile range		4.13 - 3.76	4.55 - 3.95	4.55 - 3.55	4.55 - 3.83	3.9 - 2.9
PSP half-width (ms)		**n=3**	**n=6**	**n=10**	**n=9**	**n=20**
median		21.6	39.65	41.83	28.45	32.53
interquartile range		24.04 - 19.09	57.74 - 22	54.25 - 37.15	43.88 - 22.15	34.25 - 27.25

Table 3.4 Membrane potentials and PSP properties

Chapter 4:

General Discussion and Future Perspectives

VPM and POM input to wS1

In this thesis, we first characterized the inputs from lemniscal and paralemniscal pathways to wS1. Using optogenetics, we achieved enough specificity to activate VPM or POM fibers and measure their inputs in postsynaptic targets.

VPM activation evoked direct inputs in every layer and maximum inputs were mostly in their strongest innervation layer which is L4. Excitatory and PV neurons followed that pattern quite reliably. They both showed the largest responses in L4. PV neurons on average showed larger responses than excitatory neurons, however, compared to a prior study, the difference between PV and excitatory was much smaller in my data compared to previous results (Cruikshank et al., 2010). This could be due to different preparations. We performed our experiments in the presence of TTX, 4-AP, and PTX in parasagittal slices, using a 1 mm fiber activating only VPM in contrast to other experiments activating the whole ventrobasal thalamus in thalamocortical slices using a different light source for stimulation. Moreover, the blockage of inhibition with the presence of PTX abolishes the strong disynaptic inhibition onto excitatory neurons which can increase the PSP amplitudes of excitatory neurons dramatically. SST neurons seemed like following the same pattern, however, their responses were feeble to non-existent compared to excitatory and PV neurons. This result agrees with the previous studies (Staiger et al., 1996; Swadlow and Gusev, 2002; Tan et al., 2008; Lee et al., 2010; Hu and Agmon, 2016). They showed the maximum response in L4 on average, however, it was significantly different only from L5B neurons, which had almost no response. Interestingly, for VIP neurons, the maximum average response was in L3; however, it was not significantly different from any of the other layers. Moreover, despite the low n numbers, we observed direct synaptic inputs to VIP neurons in L1, even though there is no obvious axonal innervation from VPM. Compared to SST neurons, inputs to VIP neurons were larger on average but smaller than PV and excitatory neurons.

Similar to VPM inputs, activating POM axons evoked maximum inputs mostly in their preferred innervation layer which in this case is L5A. Excitatory and PV neurons in L5A responded strongly to POM activation. On average, PV responses were similar to excitatory neurons. This result is different from a prior study

suggesting that PV neurons receiving 2 folds greater responses than excitatory neurons in L5A (Audette et al., 2018). Different results could be due to different preparations. In their experiments, they used coronal brain slices stimulating axons with a light source through their objective which gives limitations to the overall stimulation area and measured EPSCs using voltage-clamp recordings. In our experiments, we used parasagittal brain slices with a 1 mm optic fiber light source and we measured EPSPs using current-clamp recordings. Both experiments were done in the presence of TTX and 4-AP, except our experiments included PTX. In the presence of PTX, we remove the disynaptic inhibition onto excitatory neurons. This could increase the PSP response of the excitatory neurons. Moreover, recording EPSC responses could be different than EPSP responses. PV cells have relatively small membrane resistances which make them harder to excite. The same amount of current entering PV cells could deflect the membrane potential less than excitatory cells. Therefore, even if the recorded EPSC responses of PV cells are larger than excitatory cells, the EPSP responses between them could be similar because of the low membrane resistance of PV neurons. Similar to VPM inputs, SST neurons responded very weakly to POM activation. Maximum inputs were observed in L5A; however, the mean response was not significantly different from other layers except L6 where the responses were reliably weak in every experiment. These weak drives from POM to SST we observed is in agreement with the prior study investigated the same connections (Audette et al., 2018). VIP neurons responded to POM stimulation maximum in L5A, however, it was not significantly different from the other layers. This almost homogeneous distribution of input to VIP neurons could be due to the somato-dendritic morphology of these neurons. Especially bipolar VIP neurons with long dendrites could receive inputs from the layers where their cell bodies are not present.

Overall, thalamic input primarily drives the excitatory and PV neurons in their main innervation layers L4 and L5A (Figure 2.21). SST neurons receive much weaker input which is barely detectable compared to excitatory and PV neurons. VIP neurons, on the other hand, receive bigger inputs than SST and weaker inputs than excitatory and PV neurons. Thalamocortical impact onto VIP neurons is similar across different layers. This could be due to the long dendritic structure of bipolar

VIP neurons, receiving inputs from layers where their cell bodies are not necessarily located in.

Given the low n numbers in some layers for different types of cells, reduces the accuracy of these mapping experiments. To have more statistical strength about the thalamocortical input distribution, more neurons must be recorded to equalize n numbers.

Comparison to in vivo measurements

Targeted *in vivo* whole-cell recordings of different cell types in wS1 and other sensory cortices showed that these different cell types have specific sensory-evoked responses in superficial layers (Gentet, 2012; Sachidhanandam et al., 2013; Mesik et al., 2015). In the study from Gentet et al. in 2012, whisker stimulation evoked depolarization and increase of action potential firing in excitatory neurons, fast-spiking (FS) interneurons and non-fast-spiking (NFS) interneurons, however, SST neurons were hyperpolarized. FS neurons receive the biggest activation after whisker stimulation followed by NFS neurons and excitatory neurons. In our data, we observed that thalamic input to excitatory and PV neurons were similar. VIP neurons receive weaker input than excitatory and PV neurons and SST neurons receive almost no input compared to other cell types. PV neurons in our assay most probably correspond to FS interneurons, and VIP neurons are a sub-population of NFS interneurons. Excitatory neurons show weaker responses *in vivo* due to intact inhibition mainly provided by FS neurons. NFS neurons receive depolarization and we observe thalamic input to VIP interneurons both from VPM and POM. Depolarization of these L2/3 NFS neurons in response to whisker stimulation is as big as FS neurons; however, in our data we observe weaker depolarizations in VIP neurons compared to PV and excitatory neurons. One explanation could be that in our experiments, we measure the responses to either VPM or POM stimulations, whereas *in vivo*, both of these nuclei are actively providing inputs. Both VPM and POM provides input to L2/3 VIP neurons. In chapter 3, we described that the POM input to wS1 is not driven by the brainstem. It is probably activated by wS1 and other cortical areas, which might cause a delayed contribution of POM onto NFS

neurons. If we think about a situation where a whisker is stimulated, VPM afferents could depolarize NFS neurons and then POM afferents contribute a delayed depolarization, which could explain the late time spikes in response to whisker stimulation of NFS neurons. It is known that the SST neurons are inhibited by the VIP neurons in the cortex including wS1 (Lee et al., 2013; Pfeffer et al., 2013; Zhang et al., 2014; Jiang et al., 2015), activation of NFS neurons ultimately could hyperpolarize SST neurons. We observed that SST neurons receive very weak inputs compared to other cell types. Both VPM and POM could depolarize VIP neurons when SST neurons are receiving weak thalamic inputs which could lead to SST hyperpolarization. However, in our experimental conditions using TTX and 4-AP, we might be underestimating the thalamic synaptic strength onto SST neurons. Thalamocortical axons have been shown to be strongly facilitation onto SST neurons (Tan et al., 2008; Hu and Agmon, 2016). We used single 1 ms pulses, and the glutamate release was not mediated by an action potential which means the release was purely depended on ChR2 kinetics. Any burst activity from thalamus *in vivo* might enhance the weak VPM and POM inputs to SST neurons. It is possible that state-dependent enhancements could not be detected in our experiments.

Targeting of the VIP neurons in different layers by VPM and POM could be a signal amplification mechanism. VIP neurons reach different layers with their long dendrites, and inhibit mostly nearby SST neurons. VPM input arrives strongly in L4 and spreads to L2/3 and deep layers, and input to VIP neurons could enhance this overall cortical activation through disinhibition. In future experiments, it will be important to investigate whether the VPM inputs to VIP neurons *in vivo* could be different depending on the behavioural contexts. POM input preferably drives L5A pyramidal neurons and PV neurons. They also give input to VIP neurons in different layers. POM activation of VIP neurons could lead to silencing of SST neurons and enhancing the activation of the barrel cortex. SST neurons inhibit mostly the distal dendrites and silencing them could lead to depolarization of L1 dendrites of pyramidal cells, which could enhance the impact of long range glutamatergic input from for example primary motor cortex (wM1). Again, in the future, it will be important to understand how this POM to VIP connectivity is modulated *in vivo* depending on different behavioral situations.

The sparse coding observed *in vivo* in the L2/3 of the barrel cortex (Crochet and Petersen, 2006; Poulet and Petersen, 2008; O'Connor et al., 2010; Crochet et al., 2011) could be explained by the thalamocortical inputs. In the study from Sachinanandam et al. (2013), the whisker deflection drove membrane potentials of L2/3 excitatory neurons toward a defined potential. Neurons in different resting membrane potentials were reaching a cell-specific reversal potential, which was mostly hyperpolarized relative to the action potential threshold. This keeps most of the cells away from firing action potentials. Cell-specific hyperpolarized reversal potentials could occur due to local GABAergic inhibitory contribution. Indeed, their recordings confirmed that the GABAergic neurons were firing more action potentials in response to whisker stimulation. In our experiments, we observed that VPM gives reliable inputs to PV neurons in different cortical layers including L2/3. Following whisker stimulation, activated PV neurons provide a feedforward inhibition. This recruitment of local PV activation could ultimately give rise to cell-specific reversal potentials.

First and higher-order POM and parallel sensory pathways

After mapping VPM and POM inputs in wS1, we then characterized two-distinct sub-nuclei of POM. As POM was considered to have both first and higher-order properties we investigated if there are sub-compartments of this nucleus. We used a transsynaptic AAV and identified sensory receiving (dPOM) and non-sensory receiving parts (iPOM) of the POM. These different parts turned out to be innervating different regions of the somatosensory cortex. dPOM innervated wS2 specifically, mainly L4. iPOM on the other hand targeted both wS1 and wS2 and innervating L5A and L1 in both cortices. dPOM innervation of wS2 was similar to VPM innervation in wS1. These two nuclei were both receiving input from the trigeminal nuclei of the brain stem SpVi and PrV respectively, suggesting, two parallel sensory pathways to somatosensory cortex. After characterizing these thalamic nuclei, we then investigated that if their axonal innervations were functional in wS2. We found that both dPOM and iPOM evoked inputs in wS2. When we compared dPOM inputs in wS2 and VPM inputs in wS1, we found that VPM had a much more specific input distribution, evoking maximum responses in L4 cells. On

average, dPOM inputs in wS2 were also evoking maximum inputs in L4, however, not significantly different from other layers, showing a different input organization than wS1.

Both wS1 and wS2 are involved heavily in whisker sensory information processing. Since both dPOM and VPM are relaying sensory information to these cortices, this could suggest that they could encode different features of the whisker sensory information. Investigating their function *in vivo* could reveal their actual functional differences. Moreover, since we identified a non-sensory part of POM (iPOM), the actual higher-order properties of POM could be investigated in a more specific manner.

Overall, our data suggest that the paralemniscal pathway actually consists of SpVi and dPOM. Characterizing sub-nuclei of POM, we suggest that there are two main first-order thalamic inputs from VPM and dPOM to somatosensory cortex along with one higher-order thalamic inputs from iPOM (Figure 4.2).

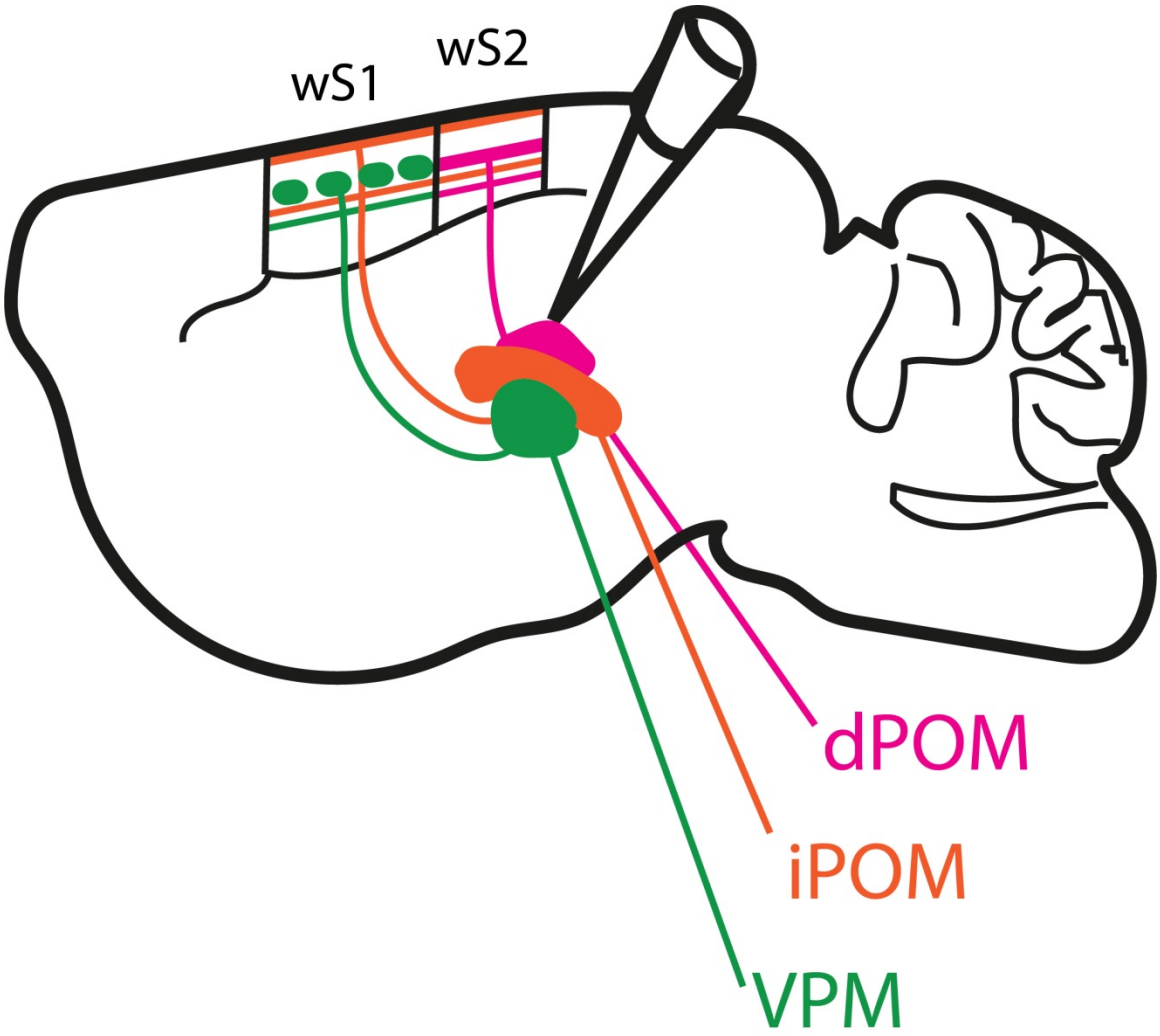

Figure 4.2 Schematic representation of 3 thalamocortical pathways to the primary and secondary whisker somatosensory cortices. Three nuclei innervate primary and secondary somatosensory cortices. VPM innervates L4 and deep L5 of wS1, dPOM innervates L4 and deep L5 of wS2 similar to VPM innervation in wS1 and iPOM innervates L1 and L5A of both wS1 and wS2.

References

Adesnik, H., and Scanziani, M. (2010). Lateral competition for cortical space by layer-specific horizontal circuits. Nature *464*, 1155–1160.

Agmon, A., and Connors, B.W. (1991). Thalamocortical responses of mouse somatosensory (barrel) cortexin vitro. Neuroscience *41*, 365–379.

Agmon, A., and Connors, B.W. (1992). Correlation between intrinsic firing patterns and thalamocortical synaptic responses of neurons in mouse barrel cortex. J. Neurosci. Off. J. Soc. Neurosci. *12*, 319–329.

Ahissar, E., Sosnik, R., Bagdasarian, K., and Haidarliu, S. (2001). Temporal frequency of whisker movement. II. Laminar organization of cortical representations. J. Neurophysiol. *86*, 354–367.

Arenkiel, B.R., Peca, J., Davison, I.G., Feliciano, C., Deisseroth, K., Augustine, G.J., Ehlers, M.D., and Feng, G. (2007). In vivo light-induced activation of neural circuitry in transgenic mice expressing channelrhodopsin-2. Neuron *54*, 205–218.

Aronoff, R., Matyas, F., Mateo, C., Ciron, C., Schneider, B., and Petersen, C.C.H. (2010). Long-range connectivity of mouse primary somatosensory barrel cortex. Eur. J. Neurosci. *31*, 2221–2233.

Audette, N.J., Urban-Ciecko, J., Matsushita, M., and Barth, A.L. (2018). POm Thalamocortical Input Drives Layer-Specific Microcircuits in Somatosensory Cortex. Cereb. Cortex N. Y. N 1991 *28*, 1312–1328.

Beierlein, M., Fall, C.P., Rinzel, J., and Yuste, R. (2002). Thalamocortical bursts trigger recurrent activity in neocortical networks: layer 4 as a frequency-dependent gate. J. Neurosci. Off. J. Soc. Neurosci. *22*, 9885–9894.

Berg, R.W., and Kleinfeld, D. (2003). Rhythmic whisking by rat: retraction as well as protraction of the vibrissae is under active muscular control. J. Neurophysiol. *89*, 104–117.

Bernardo, K.L., and Woolsey, T.A. (1987). Axonal trajectories between mouse somatosensory thalamus and cortex. J. Comp. Neurol. *258*, 542–564.

Bourassa, J., Pinault, D., and Deschênes, M. (1995). Corticothalamic projections from the cortical barrel field to the somatosensory thalamus in rats: a single-fibre study using biocytin as an anterograde tracer. Eur. J. Neurosci. *7*, 19–30.

Boyden, E.S., Zhang, F., Bamberg, E., Nagel, G., and Deisseroth, K. (2005). Millisecond-timescale, genetically targeted optical control of neural activity. Nat. Neurosci. *8*, 1263–1268.

Brecht, M., and Sakmann, B. (2002). Whisker maps of neuronal subclasses of the rat ventral posterior medial thalamus, identified by whole-cell voltage recording and morphological reconstruction. J. Physiol. *538*, 495–515.

Bruno, R.M., and Sakmann, B. (2006). Cortex is driven by weak but synchronously active thalamocortical synapses. Science *312*, 1622–1627.

Bruno, R.M., and Simons, D.J. (2002). Feedforward mechanisms of excitatory and inhibitory cortical receptive fields. J. Neurosci. Off. J. Soc. Neurosci. *22*, 10966–10975.

Bruno, R.M., Hahn, T.T.G., Wallace, D.J., de Kock, C.P.J., and Sakmann, B. (2009). Sensory experience alters specific branches of individual corticocortical axons during development. J. Neurosci. Off. J. Soc. Neurosci. *29*, 3172–3181.

Bureau, I., von Saint Paul, F., and Svoboda, K. (2006). Interdigitated paralemniscal and lemniscal pathways in the mouse barrel cortex. PLoS Biol. *4*, e382.

Burkhalter, A. (2008). Many specialists for suppressing cortical excitation. Front. Neurosci. *2*, 155–167.

Cardin, J.A., Carlén, M., Meletis, K., Knoblich, U., Zhang, F., Deisseroth, K., Tsai, L.-H., and Moore, C.I. (2009). Driving fast-spiking cells induces gamma rhythm and controls sensory responses. Nature *459*, 663–667.

Cauli, B., Audinat, E., Lambolez, B., Angulo, M.C., Ropert, N., Tsuzuki, K., Hestrin, S., and Rossier, J. (1997). Molecular and Physiological Diversity of Cortical Nonpyramidal Cells. J. Neurosci. *17*, 3894–3906.

Chattopadhyaya, B., Di Cristo, G., Higashiyama, H., Knott, G.W., Kuhlman, S.J., Welker, E., and Huang, Z.J. (2004). Experience and activity-dependent maturation of perisomatic GABAergic innervation in primary visual cortex during a postnatal critical period. J. Neurosci. Off. J. Soc. Neurosci. *24*, 9598–9611.

Chen, J.L., Carta, S., Soldado-Magraner, J., Schneider, B.L., and Helmchen, F. (2013). Behaviour-dependent recruitment of long-range projection neurons in somatosensory cortex. Nature *499*, 336–340.

Chmielowska, J., Carvell, G.E., and Simons, D.J. (1989). Spatial organization of thalamocortical and corticothalamic projection systems in the rat SmI barrel cortex. J. Comp. Neurol. *285*, 325–338.

Constantinople, C.M., and Bruno, R.M. (2013). Deep cortical layers are activated directly by thalamus. Science *340*, 1591–1594.

Crochet, S., and Petersen, C.C.H. (2006). Correlating whisker behavior with membrane potential in barrel cortex of awake mice. Nat. Neurosci. *9*, 608–610.

Crochet, S., Poulet, J.F.A., Kremer, Y., and Petersen, C.C.H. (2011). Synaptic mechanisms underlying sparse coding of active touch. Neuron *69*, 1160–1175.

Cruikshank, S.J., Lewis, T.J., and Connors, B.W. (2007). Synaptic basis for intense thalamocortical activation of feedforward inhibitory cells in neocortex. Nat. Neurosci. *10*, 462–468.

Cruikshank, S.J., Urabe, H., Nurmikko, A.V., and Connors, B.W. (2010). Pathway-specific feedforward circuits between thalamus and neocortex revealed by selective optical stimulation of axons. Neuron *65*, 230–245.

DeFelipe, J., Alonso-Nanclares, L., and Arellano, J.I. (2002). Microstructure of the neocortex: comparative aspects. J. Neurocytol. *31*, 299–316.

Diamond, M.E., Armstrong-James, M., and Ebner, F.F. (1992). Somatic sensory responses in the rostral sector of the posterior group (POm) and in the ventral posterior medial nucleus (VPM) of the rat thalamus. J. Comp. Neurol. *318*, 462–476.

Feldmeyer, D., Roth, A., and Sakmann, B. (2005). Monosynaptic connections between pairs of spiny stellate cells in layer 4 and pyramidal cells in layer 5A indicate that lemniscal and paralemniscal afferent pathways converge in the infragranular somatosensory cortex. J. Neurosci. Off. J. Soc. Neurosci. *25*, 3423–3431.

Feldmeyer, D., Brecht, M., Helmchen, F., Petersen, C.C.H., Poulet, J.F.A., Staiger, J.F., Luhmann, H.J., and Schwarz, C. (2013). Barrel cortex function. Prog. Neurobiol. *103*, 3–27.

Ferezou, I., Haiss, F., Gentet, L.J., Aronoff, R., Weber, B., and Petersen, C.C.H. (2007). Spatiotemporal Dynamics of Cortical Sensorimotor Integration in Behaving Mice. Neuron *56*, 907–923.

Fino, E., and Yuste, R. (2011). Dense inhibitory connectivity in neocortex. Neuron *69*, 1188–1203.

Friedberg, M.H., Lee, S.M., and Ebner, F.F. (1999). Modulation of receptive field properties of thalamic somatosensory neurons by the depth of anesthesia. J. Neurophysiol. *81*, 2243–2252.

Gambino, F., Pagès, S., Kehayas, V., Baptista, D., Tatti, R., Carleton, A., and Holtmaat, A. (2014). Sensory-evoked LTP driven by dendritic plateau potentials in vivo. Nature *515*, 116–119.

Gao, P., Bermejo, R., and Zeigler, H.P. (2001). Whisker deafferentation and rodent whisking patterns: behavioral evidence for a central pattern generator. J. Neurosci. Off. J. Soc. Neurosci. *21*, 5374–5380.

Gentet, L.J. (2012). Functional diversity of supragranular GABAergic neurons in the barrel cortex. Front. Neural Circuits *6*, 52.

Gerfen, C.R., Paletzki, R., and Heintz, N. (2013). GENSAT BAC cre-recombinase driver lines to study the functional organization of cerebral cortical and basal ganglia circuits. Neuron *80*, 1368–1383.

Gong, S., Doughty, M., Harbaugh, C.R., Cummins, A., Hatten, M.E., Heintz, N., and Gerfen, C.R. (2007). Targeting Cre recombinase to specific neuron populations with bacterial artificial chromosome constructs. J. Neurosci. Off. J. Soc. Neurosci. *27*, 9817–9823.

Gradinaru, V., Thompson, K.R., Zhang, F., Mogri, M., Kay, K., Schneider, M.B., and Deisseroth, K. (2007). Targeting and readout strategies for fast optical neural control in vitro and in vivo. J. Neurosci. Off. J. Soc. Neurosci. *27*, 14231–14238.

Groh, A., Bokor, H., Mease, R.A., Plattner, V.M., Hangya, B., Stroh, A., Deschenes, M., and Acsády, L. (2014). Convergence of cortical and sensory driver inputs on single thalamocortical cells. Cereb. Cortex N. Y. N 1991 *24*, 3167–3179.

Herculano-Houzel, S. (2009). The human brain in numbers: a linearly scaled-up primate brain. Front. Hum. Neurosci. *3*, 31.

Herkenham, M. (1980). Laminar organization of thalamic projections to the rat neocortex. Science *207*, 532–535.

Hoerder-Suabedissen, A., Hayashi, S., Upton, L., Nolan, Z., Casas-Torremocha, D., Grant, E., Viswanathan, S., Kanold, P.O., Clasca, F., Kim, Y., et al. (2018). Subset of Cortical Layer 6b Neurons Selectively Innervates Higher Order Thalamic Nuclei in Mice. Cereb. Cortex *28*, 1882–1897.

Hoogland, P.V., Welker, E., and Van der Loos, H. (1987). Organization of the projections from barrel cortex to thalamus in mice studied with Phaseolus vulgaris-leucoagglutinin and HRP. Exp. Brain Res. *68*, 73–87.

Hu, H., and Agmon, A. (2016). Differential Excitation of Distally versus Proximally Targeting Cortical Interneurons by Unitary Thalamocortical Bursts. J. Neurosci. Off. J. Soc. Neurosci. *36*, 6906–6916.

Hutson, K.A., and Masterton, R.B. (1986). The sensory contribution of a single vibrissa's cortical barrel. J. Neurophysiol. *56*, 1196–1223.

Jensen, K.F., and Killackey, H.P. (1987). Terminal arbors of axons projecting to the somatosensory cortex of the adult rat. I. The normal morphology of specific thalamocortical afferents. J. Neurosci. Off. J. Soc. Neurosci. *7*, 3529–3543.

Ji, X., Zingg, B., Mesik, L., Xiao, Z., Zhang, L.I., and Tao, H.W. (2016). Thalamocortical Innervation Pattern in Mouse Auditory and Visual Cortex: Laminar and Cell-Type Specificity. Cereb. Cortex *26*, 2612–2625.

Jiang, X., Shen, S., Cadwell, C.R., Berens, P., Sinz, F., Ecker, A.S., Patel, S., and Tolias, A.S. (2015). Principles of connectivity among morphologically defined cell types in adult neocortex. Science *350*, aac9462.

Jouhanneau, J.-S., Ferrarese, L., Estebanez, L., Audette, N.J., Brecht, M., Barth, A.L., and Poulet, J.F.A. (2014). Cortical fosGFP expression reveals broad receptive field excitatory neurons targeted by POm. Neuron *84*, 1065–1078.

Killackey, H.P., and Leshin, S. (1975). The organization of specific thalamocortical projections to the posteromedial barrel subfield of the rat somatic sensory cortex. Brain Res. *86*, 469–472.

Killackey, H.P., and Sherman, S.M. (2003). Corticothalamic projections from the rat primary somatosensory cortex. J. Neurosci. Off. J. Soc. Neurosci. *23*, 7381–7384.

Kim, J., Matney, C.J., Blankenship, A., Hestrin, S., and Brown, S.P. (2014). Layer 6 corticothalamic neurons activate a cortical output layer, layer 5a. J. Neurosci. Off. J. Soc. Neurosci. *34*, 9656–9664.

Koralek, K.A., Jensen, K.F., and Killackey, H.P. (1988). Evidence for two complementary patterns of thalamic input to the rat somatosensory cortex. Brain Res. *463*, 346–351.

Land, P.W., Buffer, S.A., and Yaskosky, J.D. (1995). Barreloids in adult rat thalamus: three-dimensional architecture and relationship to somatosensory cortical barrels. J. Comp. Neurol. *355*, 573–588.

Landisman, C.E., and Connors, B.W. (2007). VPM and PoM nuclei of the rat somatosensory thalamus: intrinsic neuronal properties and corticothalamic feedback. Cereb. Cortex N. Y. N 1991 *17*, 2853–2865.

Larsen, D.D., and Callaway, E.M. (2006). Development of layer-specific axonal arborizations in mouse primary somatosensory cortex. J. Comp. Neurol. *494*, 398–414.

Larsen, D.D., Wickersham, I.R., and Callaway, E.M. (2007). Retrograde tracing with recombinant rabies virus reveals correlations between projection targets and dendritic architecture in layer 5 of mouse barrel cortex. Front. Neural Circuits *1*, 5.

Lavallée, P., Urbain, N., Dufresne, C., Bokor, H., Acsády, L., and Deschênes, M. (2005). Feedforward inhibitory control of sensory information in higher-order thalamic nuclei. J. Neurosci. Off. J. Soc. Neurosci. *25*, 7489–7498.

Lee, S., Hjerling-Leffler, J., Zagha, E., Fishell, G., and Rudy, B. (2010). The largest group of superficial neocortical GABAergic interneurons expresses ionotropic serotonin receptors. J. Neurosci. Off. J. Soc. Neurosci. *30*, 16796–16808.

Lee, S., Kruglikov, I., Huang, Z.J., Fishell, G., and Rudy, B. (2013). A disinhibitory circuit mediates motor integration in the somatosensory cortex. Nat. Neurosci. *16*, 1662–1670.

Lefort, S., Tomm, C., Floyd Sarria, J.-C., and Petersen, C.C.H. (2009). The excitatory neuronal network of the C2 barrel column in mouse primary somatosensory cortex. Neuron *61*, 301–316.

Lu, S.M., and Lin, R.C. (1993). Thalamic afferents of the rat barrel cortex: a light- and electron-microscopic study using Phaseolus vulgaris leucoagglutinin as an anterograde tracer. Somatosens. Mot. Res. *10*, 1–16.

Lui, J.H., Hansen, D.V., and Kriegstein, A.R. (2011). Development and evolution of the human neocortex. Cell *146*, 18–36.

Mao, T., Kusefoglu, D., Hooks, B.M., Huber, D., Petreanu, L., and Svoboda, K. (2011). Long-range neuronal circuits underlying the interaction between sensory and motor cortex. Neuron *72*, 111–123.

Mercier, B.E., Legg, C.R., and Glickstein, M. (1990). Basal ganglia and cerebellum receive different somatosensory information in rats. Proc. Natl. Acad. Sci. U. S. A. *87*, 4388–4392.

Mesik, L., Ma, W., Li, L., Ibrahim, L.A., Huang, Z.J., Zhang, L.I., and Tao, H.W. (2015). Functional response properties of VIP-expressing inhibitory neurons in mouse visual and auditory cortex. Front. Neural Circuits *9*, 22.

Meyer, H.S., Wimmer, V.C., Hemberger, M., Bruno, R.M., de Kock, C.P.J., Frick, A., Sakmann, B., and Helmstaedter, M. (2010). Cell type-specific thalamic innervation in a column of rat vibrissal cortex. Cereb. Cortex N. Y. N 1991 *20*, 2287–2303.

Nagel, G., Szellas, T., Huhn, W., Kateriya, S., Adeishvili, N., Berthold, P., Ollig, D., Hegemann, P., and Bamberg, E. (2003). Channelrhodopsin-2, a directly light-gated cation-selective membrane channel. Proc. Natl. Acad. Sci. U. S. A. *100*, 13940–13945.

Oberlaender, M., de Kock, C.P.J., Bruno, R.M., Ramirez, A., Meyer, H.S., Dercksen, V.J., Helmstaedter, M., and Sakmann, B. (2012). Cell type-specific three-dimensional structure of thalamocortical circuits in a column of rat vibrissal cortex. Cereb. Cortex N. Y. N 1991 *22*, 2375–2391.

O'Connor, D.H., Peron, S.P., Huber, D., and Svoboda, K. (2010). Neural activity in barrel cortex underlying vibrissa-based object localization in mice. Neuron *67*, 1048–1061.

Packer, A.M., and Yuste, R. (2011). Dense, unspecific connectivity of neocortical parvalbumin-positive interneurons: a canonical microcircuit for inhibition? J. Neurosci. Off. J. Soc. Neurosci. *31*, 13260–13271.

Petersen, C.C., and Sakmann, B. (2001). Functionally independent columns of rat somatosensory barrel cortex revealed with voltage-sensitive dye imaging. J. Neurosci. Off. J. Soc. Neurosci. *21*, 8435–8446.

Petreanu, L., Huber, D., Sobczyk, A., and Svoboda, K. (2007). Channelrhodopsin-2-assisted circuit mapping of long-range callosal projections. Nat. Neurosci. *10*, 663–668.

Petreanu, L., Mao, T., Sternson, S.M., and Svoboda, K. (2009). The subcellular organization of neocortical excitatory connections. Nature *457*, 1142–1145.

Pfeffer, C.K., Xue, M., He, M., Huang, Z.J., and Scanziani, M. (2013). Inhibition of inhibition in visual cortex: the logic of connections between molecularly distinct interneurons. Nat. Neurosci. *16*, 1068–1076.

Pierret, T., Lavallée, P., and Deschênes, M. (2000). Parallel streams for the relay of vibrissal information through thalamic barreloids. J. Neurosci. Off. J. Soc. Neurosci. *20*, 7455–7462.

Porter, J.T., Johnson, C.K., and Agmon, A. (2001). Diverse types of interneurons generate thalamus-evoked feedforward inhibition in the mouse barrel cortex. J. Neurosci. Off. J. Soc. Neurosci. *21*, 2699–2710.

Pouchelon, G., Gambino, F., Bellone, C., Telley, L., Vitali, I., Lüscher, C., Holtmaat, A., and Jabaudon, D. (2014). Modality-specific thalamocortical inputs instruct the identity of postsynaptic L4 neurons. Nature *511*, 471–474.

Poulet, J.F.A., and Petersen, C.C.H. (2008). Internal brain state regulates membrane potential synchrony in barrel cortex of behaving mice. Nature *454*, 881–885.

Poulet, J.F.A., Fernandez, L.M.J., Crochet, S., and Petersen, C.C.H. (2012). Thalamic control of cortical states. Nat. Neurosci. *15*, 370–372.

Prönneke, A., Scheuer, B., Wagener, R.J., Möck, M., Witte, M., and Staiger, J.F. (2015). Characterizing VIP Neurons in the Barrel Cortex of VIPcre/tdTomato Mice Reveals Layer-Specific Differences. Cereb. Cortex N. Y. N 1991 *25*, 4854–4868.

Rakic, P. (2009). Evolution of the neocortex: a perspective from developmental biology. Nat. Rev. Neurosci. *10*, 724–735.

Rudy, B., Fishell, G., Lee, S., and Hjerling-Leffler, J. (2011). Three Groups of Interneurons Account for Nearly 100% of Neocortical GABAergic Neurons. Dev. Neurobiol. *71*, 45–61.

Sachidhanandam, S., Sreenivasan, V., Kyriakatos, A., Kremer, Y., and Petersen, C.C.H. (2013). Membrane potential correlates of sensory perception in mouse barrel cortex. Nat. Neurosci. *16*, 1671–1677.

Senft, S.L., and Woolsey, T.A. (1991). Growth of thalamic afferents into mouse barrel cortex. Cereb. Cortex N. Y. N 1991 *1*, 308–335.

Simons, D.J., and Carvell, G.E. (1989). Thalamocortical response transformation in the rat vibrissa/barrel system. J. Neurophysiol. *61*, 311–330.

Sippy, T., Lapray, D., Crochet, S., and Petersen, C.C.H. (2015). Cell-Type-Specific Sensorimotor Processing in Striatal Projection Neurons during Goal-Directed Behavior. Neuron *88*, 298–305.

Staiger, J.F., Zilles, K., and Freund, T.F. (1996). Innervation of VIP-immunoreactive neurons by the ventroposteromedial thalamic nucleus in the barrel cortex of the rat. J. Comp. Neurol. *367*, 194–204.

Staiger, J.F., Flagmeyer, I., Schubert, D., Zilles, K., Kötter, R., and Luhmann, H.J. (2004). Functional diversity of layer IV spiny neurons in rat somatosensory cortex: quantitative morphology of electrophysiologically characterized and biocytin labeled cells. Cereb. Cortex N. Y. N 1991 *14*, 690–701.

Swadlow, H.A., and Gusev, A.G. (2002). Receptive-field construction in cortical inhibitory interneurons. Nat. Neurosci. *5*, 403–404.

Tan, Z., Hu, H., Huang, Z.J., and Agmon, A. (2008). Robust but delayed thalamocortical activation of dendritic-targeting inhibitory interneurons. Proc. Natl. Acad. Sci. U. S. A. *105*, 2187–2192.

Taniguchi, H., He, M., Wu, P., Kim, S., Paik, R., Sugino, K., Kvitsiani, D., Kvitsani, D., Fu, Y., Lu, J., et al. (2011). A resource of Cre driver lines for genetic targeting of GABAergic neurons in cerebral cortex. Neuron *71*, 995–1013.

Tremblay, R., Lee, S., and Rudy, B. (2016). GABAergic Interneurons in the Neocortex: From Cellular Properties to Circuits. Neuron *91*, 260–292.

Urbain, N., Salin, P.A., Libourel, P.-A., Comte, J.-C., Gentet, L.J., and Petersen, C.C.H. (2015). Whisking-Related Changes in Neuronal Firing and Membrane Potential Dynamics in the Somatosensory Thalamus of Awake Mice. Cell Rep. *13*, 647–656.

Varga, C., Sík, A., Lavallée, P., and Deschênes, M. (2002). Dendroarchitecture of relay cells in thalamic barreloids: a substrate for cross-whisker modulation. J. Neurosci. Off. J. Soc. Neurosci. *22*, 6186–6194.

Veinante, P., and Deschênes, M. (1999). Single- and multi-whisker channels in the ascending projections from the principal trigeminal nucleus in the rat. J. Neurosci. Off. J. Soc. Neurosci. *19*, 5085–5095.

Viaene, A.N., Petrof, I., and Sherman, S.M. (2011). Properties of the thalamic projection from the posterior medial nucleus to primary and secondary somatosensory cortices in the mouse. Proc. Natl. Acad. Sci. U. S. A. *108*, 18156–18161.

Wall, N.R., De La Parra, M., Sorokin, J.M., Taniguchi, H., Huang, Z.J., and Callaway, E.M. (2016). Brain-Wide Maps of Synaptic Input to Cortical Interneurons. J. Neurosci. Off. J. Soc. Neurosci. *36*, 4000–4009.

Wang, Y., Toledo-Rodriguez, M., Gupta, A., Wu, C., Silberberg, G., Luo, J., and Markram, H. (2004). Anatomical, physiological and molecular properties of Martinotti cells in the somatosensory cortex of the juvenile rat. J. Physiol. *561*, 65–90.

Welker, E., Hoogland, P.V., and Van der Loos, H. (1988). Organization of feedback and feedforward projections of the barrel cortex: a PHA-L study in the mouse. Exp. Brain Res. *73*, 411–435.

Wimmer, V.C., Bruno, R.M., de Kock, C.P.J., Kuner, T., and Sakmann, B. (2010). Dimensions of a projection column and architecture of VPM and POm axons in rat vibrissal cortex. Cereb. Cortex N. Y. N 1991 *20*, 2265–2276.

Woolsey, T.A., and Van der Loos, H. (1970). The structural organization of layer IV in the somatosensory region (SI) of mouse cerebral cortex. The description of a cortical field composed of discrete cytoarchitectonic units. Brain Res. *17*, 205–242.

Wright, A.K., Norrie, L., Ingham, C.A., Hutton, E.A., and Arbuthnott, G.W. (1999). Double anterograde tracing of outputs from adjacent "barrel columns" of rat somatosensory cortex. Neostriatal projection patterns and terminal ultrastructure. Neuroscience *88*, 119–133.

Yamashita, T., Pala, A., Pedrido, L., Kremer, Y., Welker, E., and Petersen, C.C.H. (2013). Membrane potential dynamics of neocortical projection neurons driving target-specific signals. Neuron *80*, 1477–1490.

Yamashita, T., Vavladeli, A., Pala, A., Galan, K., Crochet, S., Petersen, S.S.A., and Petersen, C.C.H. (2018). Diverse Long-Range Axonal Projections of Excitatory Layer 2/3 Neurons in Mouse Barrel Cortex. Front. Neuroanat. *12*, 33.

Yu, C., Derdikman, D., Haidarliu, S., and Ahissar, E. (2006). Parallel thalamic pathways for whisking and touch signals in the rat. PLoS Biol. *4*, e124.

Yu, C., Horev, G., Rubin, N., Derdikman, D., Haidarliu, S., and Ahissar, E. (2015). Coding of object location in the vibrissal thalamocortical system. Cereb. Cortex N. Y. N 1991 *25*, 563–577.

Zhang, S., Xu, M., Kamigaki, T., Do, J.P.H., Chang, W.-C., Jenvay, S., Miyamichi, K., Luo, L., and Dan, Y. (2014). Long-range and local circuits for top-down modulation of visual cortex processing. Science *345*, 660–665.

Zingg, B., Chou, X., Zhang, Z., Mesik, L., Liang, F., Tao, H.W., and Zhang, L.I. (2017). AAV-mediated Anterograde Transsynaptic Tagging: Mapping Input-Defined Functional Neural Pathways for Defense Behavior. Neuron *93*, 33–47.

Cirriculum Vitae

Berat Semihcan Sermet, MSc.

École Polytechnique Fédérale de Lausanne
EPFL-SV-BMI-LSENS Station 19
CH-1015 Lausanne, Switzerland

Email: berat.sermet@epfl.ch

Phone: +41 21 6931725
Single, 31 years old
Turkish nationality

EDUCATION AND RESEARCH EXPERIENCE

2013–Present **PhD in Neurosciences - École Polytechnique Fédérale de Lausanne**
Brain Mind Institute
Thesis title: Layer, cell-type and pathway-specific thalamocortical input to mouse somatosensory cortex
Supervisor: Carl C. H. Petersen

2010–2013 **Master in Biophysics and Neurosciences**
Marmara University, Department of Biophysics (Istanbul, Turkey) & Universität Bonn, Institut für Zelluläre Neurowissenschaften (Bonn, Germany) Thesis title: Potassium Buffering Properties of Astrocytes in Adult Mouse Hippocampus
Supervisors: Christian Steinhäuser & Ayse Inhan Garip

Summer 2008 **Internship**
International Center for Hydrogen Energy Technologies (UNIDO-ICHET) Fuel-Cell Powered Electrical Engines

Summer 2007 **Internship**
International Center for Hydrogen Energy Technologies (UNIDO-ICHET)

Summer 2005 **Internship**
Koc Sistem Information and Communication Services Inc. MySQL Database and PHP Web Design

2005–2010 **Bachelor in Physics**
Marmara University (Istanbul, Turkey)

TEACHING EXPERIENCE

Summer 2017 **Student Mentoring**
Summer Research Program, Carl Petersen's Laboratory, EPFL (Lausanne, Switzerland)

2016 **Video Course Instructor**
Cellular Mechanisms of Brain Function: Whole-cell recordings, EdX
https://youtu.be/o7RsmRQ1Jps

2013-2016 **Teaching Assistant**
Cellular Mechanisms of Brain Function, EPFL (Lausanne, Switzerland)

2010-2012 **Teaching Assistant**
Biophysics, Marmara University (Istanbul, Turkey)

PROGRAMMING AND LABORATORY SKILLS

Programming: Experience in different programming languages (Igor Pro, ImageJ, MATLAB) to monitor and control hardware and perform data analysis

Techniques: *In vitro* whole-cell patch-clamp recordings, optogenetics and pharmacology in brain slices, confocal and epifluorescence imaging of fixed tissue, intrinsic optical imaging, single-cell RT-PCR, immunohistochemistry

Preparations: Acute brain slice preparations in young and adult rodents, microsurgery on rodents, virus injections

LANGUAGES

Turkish Native speaker

English Fluent

French Proficient

German Conversational

REFERENCES

Dr. Carl Petersen
Full Professor
Head of the Laboratory of Sensory Processing
Neurosciences Brain Mind Institute
Faculty of Life Sciences
École Polytechnique Fédérale de Lausanne
EPFL-SV-BMI-LSENS Station 19
CH-1015 Lausanne, Switzerland
carl.petersen@epfl.ch
Phone: +41 21 6931721, +41 21 6931817

Dr. Christian Steinhäuser
Full Professor
Head of the Institute for Cellular
Universität Bonn
Sigmund Freud Str. 25
53105 Bonn, Germany
Email: christian.steinhaeuser@epfl.ch
Tel: +49 228 287 14669 Email:

Dr. Ayse Inhan Garip
Head of the Biophysics Department
Marmara University
Basibuyuk cad. No.9 Temel Tip Binasi
Basibuyuk, Maltepe, Istanbul, Turkey Email:
agarip@marmara.edu.tr
Tel: +90 542 216 55 95

PUBLICATIONS

El-Boustani S*, **Sermet BS*,** Petersen CC, "Two parallel sensory pathways to the mouse somatosensory cortices" (in preparation)

Sermet BS, Mayrhofer JM, Auffret M, Oram TB, Feyerabend M, Yizhar O, Staiger JF, Petersen CC, "Layer, cell-type and pathway-specific thalamocortical input to mouse primary somatosensory barrel cortex" (in preperation)

Sachidhanandam S**, Sermet BS,** Petersen CC, "Parvalbumin-Expressing GABAergic Neurons in Mouse Barrel Cortex Contribute to Gating a Goal-Directed Sensorimotor Transformation", Cell Reports, S2211-1247(16)30334-5. doi: 10.1016/j.celrep.2016.03.063 (2016)

CONFERENCE PRESENTATIONS

Talks

Sermet BS "Layer, cell-type and pathway-specific thalamocortical input to mouse primary somatosensory barrel cortex", Sensory Lecture, Göttingen (2018)

Sermet BS "Layer, cell-type and pathway-specific thalamocortical input to mouse primary somatosensory barrel cortex", Swisskers Meeting, Geneva (2018)

Poster Presentations

Sermet BS, Mayrhofer JM, Auffret M, Oram TB, Feyerabend M, Yizhar O, Staiger JF, Petersen CC, "Layer, cell-type and pathway-specific thalamocortical input to mouse primary somatosensory barrel cortex", FENS meeting, Berlin (2018)

Sermet BS, Mayrhofer JM, Auffret M, Oram TB, Feyerabend M, Yizhar O, Staiger JF, Petersen CC, "Layer, cell-type and pathway-specific thalamocortical input to mouse primary somatosensory barrel cortex", Barrels and Beyond Meeting, Göttingen (2018)

Sermet BS, Oram TB, Yizhar O, Petersen CC, "Layer, cell-type and pathway-specific thalamocortical input to mouse primary somatosensory barrel cortex", Annual Meeting of the Society for Neuroscience (SfN), Washington, D.C. (2017)

Sermet BS, Oram TB, Yizhar O, Petersen CC, "Layer, cell-type and pathway-specific thalamocortical input to mouse primary somatosensory barrel cortex", 30th Annual Barrels Meeting, Johns Hopkins University, Baltimore (2017)

Sermet BS, Oram TB, Yizhar O, Petersen CC, "Layer-Specific Thalamocortical Input Onto Excitatory Neurons in Mouse Primary Somatosensory Barrel Cortex", FENS Forum of Neuroscience, Kopenhagen (2016)

Sermet BS, Oram TB, Yizhar O, Petersen CC, "Layer-Specific Thalamocortical Input Onto Excitatory Neurons in Mouse Primary Somatosensory Barrel Cortex", Barrel Cortex Function, Amsterdam (2016)